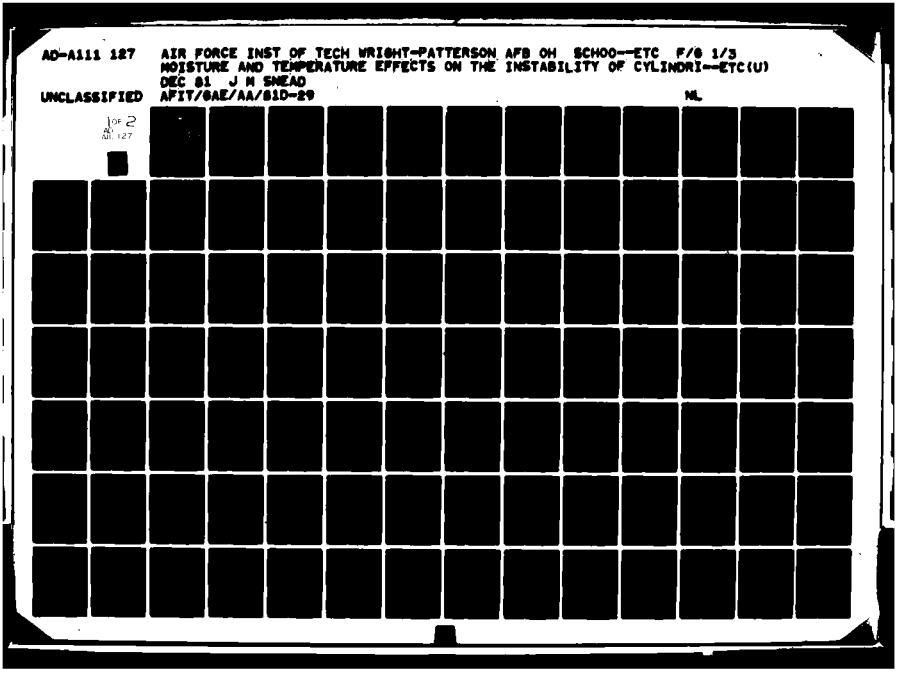
AD-A111 127
AIR FORCE INST OF TECH WRIGHT-PATTERSON AFB OH SCHOO--ETC F/G 1/3
MOISTURE AND TEMPERATURE EFFECTS ON THE INSTABILITY OF CYLINDRI--ETC(U)
DEC 81 J M SMEAD
UNCLASSIFIED
AFIT/GAE/AA/81D-29
NL
1 OF 2
AD A111 127

LEVEL II

1

AD A111127

DTIC
ELECTE
FEB 19 1982
S D
E

DTIC FILE COPY

UNITED STATES AIR FORCE

AIR UNIVERSITY

AIR FORCE INSTITUTE OF TECHNOLOGY

Wright-Patterson Air Force Base, Ohio

This document has been approved for public release and sale; its distribution is unlimited.

82 02 18 126

AFIT/GAE/AA/81D-29

MOISTURE AND TEMPERATURE EFFECTS ON THE INSTABILITY OF CYLINDRICAL COMPOSITE PANELS

THESIS

AFIT/GAE/AA/81D-29 JAMES M. SNEAD

AFIT/GAE/AA/81D-29

MOISTURE AND TEMPERATURE EFFECTS ON THE INSTABILITY OF CYLINDRICAL COMPOSITE PANELS

THESIS

Presented to the Faculty of the School of Engineering

of the Air Force Institute of Technology

Air University (ATC)

in Partial Fulfillment of the

Requirements for the Degree of

Master of Science

by

James M. Snead

Graduate Aeronautical Engineering

December 1981

Preface

A great deal of time and effort went into the development of this thesis. I am extremely grateful to Dr. Anthony Palazotto for his time and advice throughout this thesis effort.

I wish to thank Dr. Khot, of the Air Force Flight Dynamics Laboratory, for sponsoring this work and providing the computer funds necessary to conduct the computer analyses.

To my wife, a very special thank you for her assistance and encouragement during this difficult time.

Contents

List of Figures

List of Tables

Symbols

A_{ij}	Extensional stiffnesses
b	Square plate width
b_1, b_2	Intercept values used in linear curve fit
B_{ij}	Coupling Stiffnesses
C	Moisture concentration
C_0, C_1, C_2	Moisture concentration initial conditions
D_{ij}	Bending stiffnesses
E_1	Longitudinal modulus of elasticity
E_2	Transverse modulus of elasticity
F	Degrees Fahrenheit
G_{12}	Shear modulus of elasticity
h	Laminate thickness
K	Diffusion coefficient
K_x, K_y, K_{xy}	Curvatures
M_x, M_y, M_{xy}	Moment Resultants
m_1, m_2	Slopes of linear function
N_x, N_y, N_{xy}	Force Resultants
$\overline{N}_x$	Bifurcation load
R.H.	Relative humidity
RU, RV, RW	Rotations about the x, y, and z coordinate axes
t	time
T^*	Dimensionless time
T_g	Glass transition temperature
u, v, w U, V, W	Displacements in the x, y, z directions, respectively

x, y, z	Spacial coordinates
X, Y, Z	Structural coordinate directions
α	Angle of intersection of two flat plates
β	Angular rotation
δ	Shear strain
ϵ	Normal strain
θ	Angular rotation at a node
ν	Poisson's ratio
σ	Normal stress
τ	Shear Stress
$(\ )_{,(\ )}$	Comma denotes partial differentiation with respect to the subscript
$(\ )^{o}$	Zero superscript denotes a middle surface value
$[\ ]_{S}$	Denotes a ply orientation that is symmetric with respect to the middle surface

Abstract

An analytical investigation was performed to evaluate the influences of moisture and temperature on the bifurcation load of cylindrical, composite panels subject to axial loading. The composite panels were 8-ply graphite/epoxy (AS/3501-5) laminates. The laminate ply orientations considered were $[0.,45.,-45.,90.]_S$, $[90.,45.,-45.,0.]_S$, and $[45.,-45.,]_{2S}$. The analysis included several different panel radii, two sets of boundary conditions, and three sets of initial moisture conditions. To evaluate the influences of moisture and temperature, the transverse moduli, E_2, and shear moduli, G_{12}, were degraded based on test data for the AS/3501-5 system. Each ply orientation was evaluated at 20 time/temperature conditions that ranged from 80 F to 300 F and moisture concentrations ranging from zero moisture content to an equilibrium moisture concentration distribution. The bifurcation loads were determined using the STAGS-C1 finite element shell analysis program. The bifurcation analysis mode with a pre-buckled linear displacement option was used for the analysis. Moisture and temperature were found to cause a reduction in the panels bifurcation load ranging from 20.6 percent for the $[0.,45.,-45.,90.]_S$ laminate to 42.7 percent for the $[45.,-45.]_{2S}$ laminate.

MOISTURE AND TEMPERATURE EFFECTS ON THE INSTABILITY OF CYLINDRICAL COMPOSITE PANELS

I. Introduction

Background

Advanced composites are a leading candidate in the search for improved aircraft and spacecraft structural efficiency and, thus, improved system performance. In aircraft applications, until very recently, the use of advanced composites has been limited to secondary structural applications or unique primary structural applications. However, the utilization of advanced composites for aircraft primary structure has begun with the new, all-composite, Lear business jet.

The desire to improve the efficiency of the structural design through the application of composites in order to tailor the component's strength and stiffness to match the load and stiffness requirements results in components with unique structural responses. One difficulty in such applications of advanced composites is the inability to use conventional, classical structural design practices to predict the structural response of composite laminates. Attempts to apply isotropic analysis techniques, even for quasi-isotropic laminates, yields questionable results. Often, designers and stress analysts will attempt to compensate with the use of special knock-down factors to

reduce the composite's strength or stiffness so that a "conservative" design is produced. The efficient use of advanced composites in primary structural applications will depend upon the development of suitable design and analysis tools that adequately predict the composite's structural response.

In a semi-monocoque structural design, thin skin panels along with fuselage frames and longerons or wing skins with spars and ribs are used to achieve an efficient structural design. Several all-composite aircraft designs have been proposed which utilize a semi-monocoque design approach in which composite panels are used for the fuselage skins or wing skins and composite members are used for the frames, longerons, etc.

In such a semi-monocoque design, the accurate determination of the buckling load of the curved skin panels is necessary to prevent premature structural failure. This determination of the buckling loads, even for relatively simple isotropic structures, is often complicated by unusual shapes and boundary conditions and/or combinations of loads and moments. Designers and analysts rely upon simple theoretical cases with known solutions or parametric equations based upon laboratory testing to develop buckling allowables. The application of numerical techniques, especially finite difference and finite element techniques, has provided a new method of performing shell stability analyses.

These numerical techniques are of special importance in the evaluation of composite curved panels. Unlike isotropic panels, the uniqueness of the composite panel, due to the design dependent number and orientation of the plies, prevents the development of general design tools. Hence, in most applications, these numerical techniques, in the form of computer programs, provide the only means, besides experimentation, for determining a composite panel's buckling load.

Perhaps because of the current limited applications of composites for thin, structural skin panels, there has been very little published on the stability of curved composite panels. The majority of work has dealt with flat plates or shells-of-revolution. J. D. Wilkins, Ref 1, conducted an experimental investigation of the buckling strength of a cylindrical composite panel subject to axial compression with two sets of boundary conditions. M. L. Becker (2) extended Wilkins' work to more boundary conditions, several panel sizes and aspect ratios, and different ply orientations. Becker also used the finite difference version of the STAGS-C (Structural Analysis of General Shells) program to compare the analytical and experimental buckling results.

An aspect of composite's research receiving considerable attention, is the influence of moisture and temperature on the structural characteristics of the composite system. These influences, sometimes referred to

as hygrothermal effects, fall in the general category of environmental influences. Such environmental effects have been found to significantly degrade the mechanical properties of most organic matrix compounds (3-14).

Purpose

This thesis extends the analytic work of Becker to evaluate the instability of composite cylindrical panels subject to axial compression, using a new finite element version of the STAGS-C shell analysis program. The influence of environmentally-caused reductions in the composite's transverse and shear moduli on the panel's bifurcation load will be investigated using this finite element program.

Scope

The cylindrical panels evaluated in this thesis are 12 in. by 12 in., 8-ply laminates made of Graphite/Epoxy. The panel's thickness, width, and height are held constant while the radius, ply orientations, and boundary conditions are varied. Three radii, three ply orientations, and two boundary conditions are investigated. During the investigation of the environmental influences, four temperatures and three surface moisture conditions at five time values are evaluated.

II. Environmental Influences on Composites

Moisture and Temperature Influences

While composites have many superior properties compared to metals, the commonly used epoxy composite systems are significantly affected by environmental exposure to an agent such as water, which is absorbed by the polymer resin, and to thermal conditions which are near or exceed the polymer's glass transition temperature. The fibers, which are typically graphite or boron, are not affected by either water or the moderate temperatures an aircraft would encounter during normal service. As a consequence, the resin-dominated material properties are affected.

Whitney and Ashton (3) reported that the environmental factors which influence the resin properties were a) increases in temperature, b) absorption by the polymeric resin material of a swelling agent such as water vapor, and c) the sudden expansion of absorbed gases in the resin. It was noted that resin swelling alone, due to moisture and temperature effects, could cause a flat composite plate to buckle.

Temperature and moisture act on the polymeric resin in two ways. Increasing temperatures cause the resin to swell. Absorbed water vapor, which in one study (4) was believed to be due to the water molecules bonding to the hydroxyl groups in the epoxy polymers, also causes the resin to swell. Matrix swelling and rapid heating may eventually lead to

surface crazing and surface cracks which will affect the resin's mechanical properties (12 and 13).

Temperature and moisture also act together to cause reductions in the temperature range over which resin mechanical properties are fairly stable. Moisture absorbed in the resin results in a plasticization of the resin. This plasticization is the result of the lowering of the glass transition temperature T_g. The glass transition temperature is actually a temperature range in which below this range the resin is essentially brittle and above this range it behaves rubbery.

This change in T_g, due to an absorbed agent, is common in polymer science. The polymer's T_g is a function of the free volume in the material. It is accepted theory (14) that 1/40 of the total volume of the material is free volume (total volume less the molecular volume) at and below the material's T_g. As the polymer absorbs an agent, such as water, which contains more free volume, the percentage of free volume of the mixture will increase (12). When the mixture's free volume is above 1/40 of the total volume, the resin begins to soften. Thus, the mixture's temperature must be lowered for the mixture's free volume to return to 1/40 of the total volume. This results in a lower T_g. As increasing concentrations of moisture are absorbed in the resin, the T_g is continually lowered until a moisture equilibrium is reached. Once equilibrium is reached, the T_g remains constant.

These changes in the resin have been found to result in decreases in the tensile properties (6) and reductions in the transverse and shear moduli (7, 8, and 13) of the composite. A slight increase in the longitudinal elastic moduli was reported in Ref 13. As noted in Ref 12, these changes in the composite's mechanical properties may be grouped into two general classifications: (a) those changes due to moisture-induced plasticization which reduces the temperature range over which the material properties are relatively stable and (b) those losses due to mechanical damage from moisure-induced swelling and rapid heating which results in surface crazing and cracking which affect the mechanical properties below the T_g. The reduction in mechanical properties is most significant in the tensile properties. This is primarily because the resin is very brittle below the T_g and the resin is less sensitive in shear to any surface flaws than it is in tension (13).

Prediction of Absorbed Moisture

When the mechanical properties are determined by testing, they are usually measured at known temperatures and moisture concentrations. The absorption of water vapor into the resin is through diffusion. Under certain circumstances, Fick's second law of diffusion (23) has shown good correlation with test data, Fig 1, at predicting the rate of moisture weight gain in a polymeric resin and in the composite. Fick developed this equation in 1855 by drawing

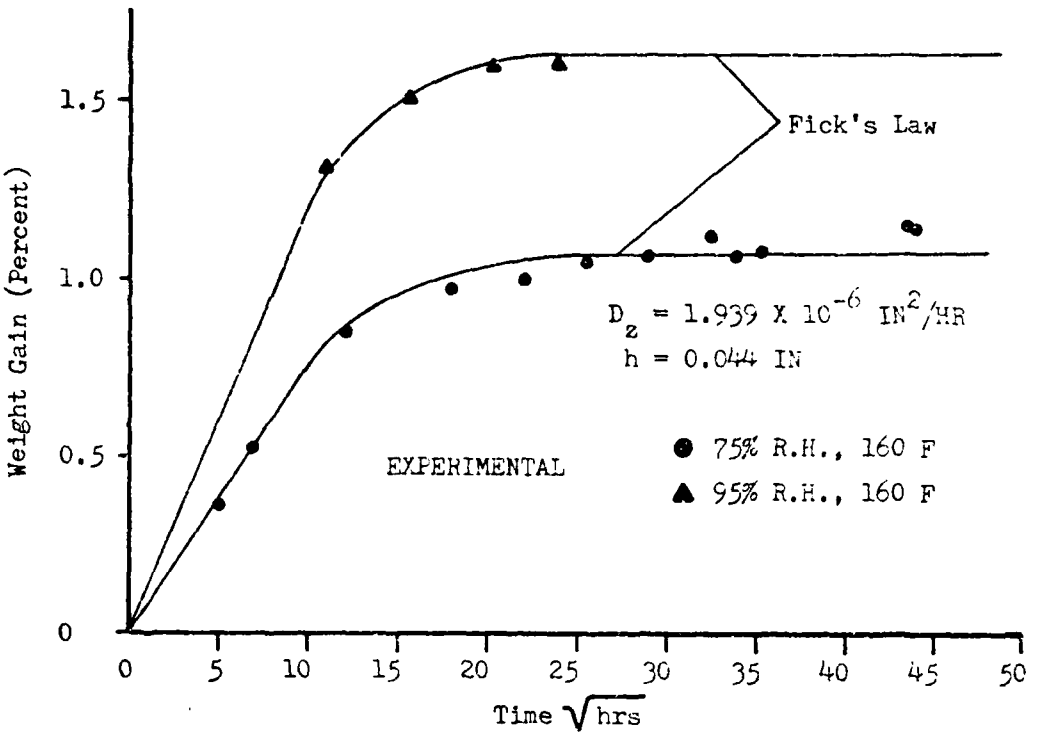

Figure 1. Moisture Gain as a Function of Time for AS/3501-5 Composites (Ref 13)

an analogy between heat conduction in a solid and diffusion through a solid.

The Fick equation is:

$$\frac{\partial C}{\partial t} = K \frac{\partial^2 C}{\partial Z^2}$$

where: C - the concentration of the diffusing substance through the thickness of the laminate as a function of time and distance through the thickness

Z - the space coordinate measured normal to the surface

K - the diffusion constant

t - time

The solution of this partial differential equation with boundary and initial conditions pertinent to the problem is shown below. This series solution in a slightly different form is found in Section 4.3.3 of Ref 23.

$$C(Z,t) = C_1 + (C_2 - C_1)\frac{Z}{h}$$

$$+ \frac{2}{\pi} \sum_{n=1}^{\infty} \frac{C_2 \cos n\pi - C_1}{n} \sin \frac{n\pi Z}{h} \exp \frac{-K n^2 \pi^2 t}{h^2}$$

$$+ \frac{4C_0}{\pi} \sum_{m=1}^{\infty} \frac{1}{2m+1} \sin \frac{(2m+1)\pi Z}{h} \exp \frac{-K(2m+1)^2 \pi^2 t}{h^2}$$

C_0, C_1, and C_2 represent the inital set of moisture conditions for the laminate. C_0 is the initial moisture concentration distribution through the thickness of the laminate. C_1 is the initial moisture condition at the surface of one side of the laminate. C_2 is the initial moisture condition at the surface on the other side of the laminate. The thickness of the laminate is represented by h.

Using this series solution with a known diffusion constant and prescribed initial conditions, the moisture concentration distribution through the thickness can be determined. With the assumption that the effective moisture concentration of each ply can be approximated by the calculated moisture concentration at the middle of the ply, the reduced mechanical properties of each ply can be determined from appropriate test data.

This series solution is seen to represent the summation of a steady state moisture distribution, represented by the first and second terms, and a transient moisture distribution that is a function of time. This is represented by the last two terms. The influence of the transient terms decreases with increasing time. The accuracy of this series approximation is dependent upon the number of terms used during the two summations. This solution was calculated by the computer program shown in Appendix A. To insure an accurate solution the summations were carried out until there was no change from the previous

answer. On the CDC computer this equated to 14 significant digits of accuracy.

There are limitations on the application of Fick's equation. The series solution of Fick's equation assumes that the moisture diffusion coefficient K is constant. The diffusion coefficient is a function of the laminate's temperature. However, since the moisture diffusion is a relatively slow process, with many months or years required before the moisture concentration distribution through the laminate achieves equilibrium, the diffusion process, in simple cases, may be assumed to take place at a constant temperature. Bergmann and Nitsch (4) have noted that K also varies with the laminate's moisture concentration generally increasing with increasing moisture concentration levels.

The accuracy of Fick's equation is also affected by rapid temperature changes. Rapid thermal heating of the laminate (which may be due to flight at supersonic speeds), where the laminate is heated to temperatures near the material's T_g, has been found to increase the rate of moisture weight gain above that predicted by the Fick equation (7, 10, 12, and 13). This increase is believed due to the development of surface crazing and cracking brought about by the rapid heating and resin swelling (13).

With the restrictions of no rapid heating and no surface crazing or cracking, and assuming that K is constant, Fick's equation has been generally accepted as a good initial approximation of the moisture concentration

distribution for simple cases (4, 7, 9, 11, and 13).

AS/3501-5 Mechanical Properties

The STAGS-C1 shell analysis program discussed in Section III requires, as input parameters, the composite's longitudinal moduli E_1, transverse moduli E_2, shear moduli G_{12}, and Poisson's ratio ν_{21}. Poisson's ratio ν_{12} relates the strain in the 2 direction to the strain in the 1 direction when stresed in the 1 direction. Experimentally-measured data for a graphite/epoxy system, AS/3501-5, from Fig 8.18 of Ref 15 was used in the determination of the elastic moduli as a function of temperature and moisture concentration. The units of stress in GPa and temperature in degrees Kelvin are converted to psi and Fahrenheit. The values of E_2 and G_{12} used in this work, from which intermediate values were interpolated, are shown in Table I. The method used for interpolation is described in the next section. Figure 2 shows this data in a graphical form.

The moisture and temperature influences on the transverse and shear moduli are clearly evident in the experimental data for AS/3501-5 shown in Table I and Fig 2. The transverse moduli E_2 shows degradation both at room temperature and at elevated temperatures while the shear moduli G_{12} only shows degradation at elevated temperatures. The moisture caused change in the T_g and the resulting plasticization of the resin is shown by the increased

degradation in the moduli with increasing moisture concentration at each elevated temperature. This is consistent with the previously noted expected changes in elastic moduli. The longitudinal moduli E_1 is dominated by the fiber stiffness and hence is not significantly influeced by changes in moisture and temperature as are the matrix dominated E_2 and G_{12} moduli.

The value of ν_{12} used in this analysis was taken from Table 1.9 of Ref 15. The value of ν_{12} is 0.30 which is a representative value for AS/3501-5 composites. Examination of the test data (13) upon which the material in Ref 15 was based shows that ν_{12} does vary with temperature and moisture concentration. The range of variation was from 0.36 to 0.46. The sensitivity of the analyses to this variation in ν_{12} was found to be very small. This is discussed in more detail in Section IV.

The experimental stress-strain data from Ref 13, reflecting the changes in the shear and transverse moduli as a function of temperature and moisture, are shown in Figs 3 and 4, respectively.

Table I

Values of Transverse and Shear Moduli
for AS/3501-5 (15)

Transverse moduli, E_2 (psi)

Moisture Concentration (percent)	Temperature 80 F	200 F	250 F	300 F
0.0	1.41375E06	1.09475E06	1.015E06	1.015E06
0.050	1.305E06	0.9135E06	0.6235E06	0.522E06
1.050	1.2615E06	0.841E06	0.4785E06	0.290E06

Shear Moduli, G_{12} (psi)

0.0	0.8555E06	0.7830E06	0.6815E06	0.6525E06
1.050	0.8555E06	0.6597E06	0.3915E06	0.15225E06

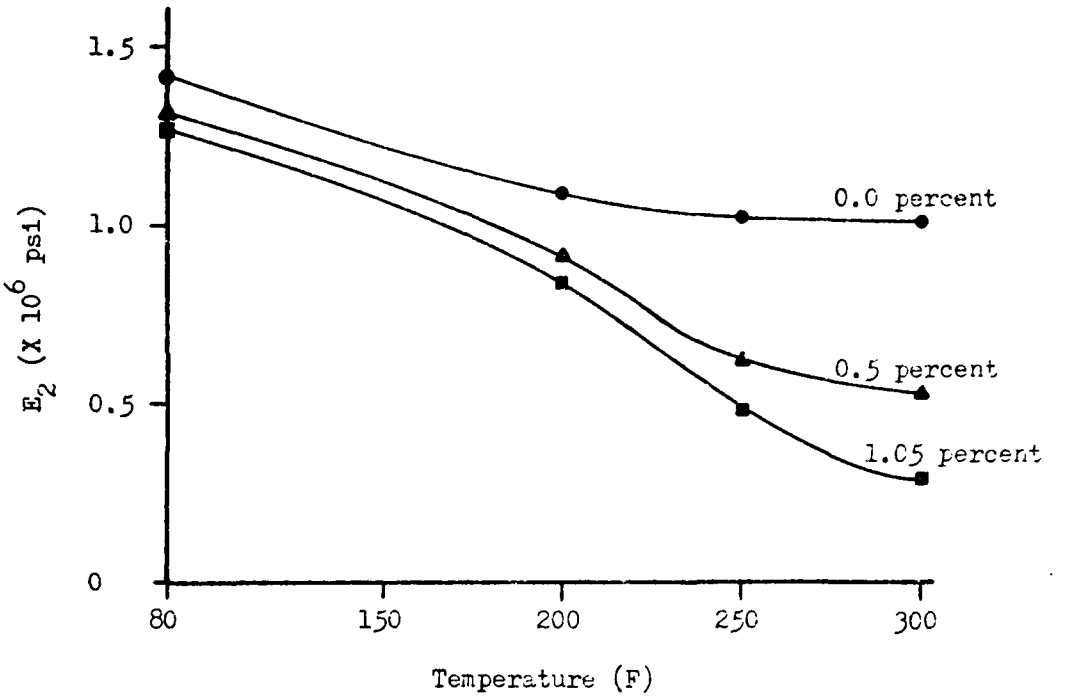

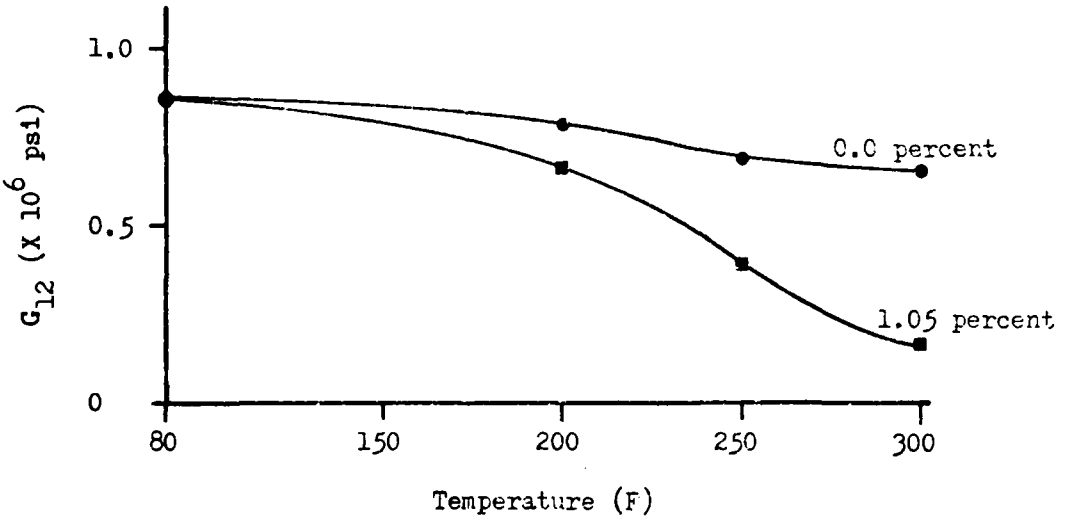

Figure 2. E_2 and G_{12} Degradation vs Temperature at Constant Values of Moisture Concentration

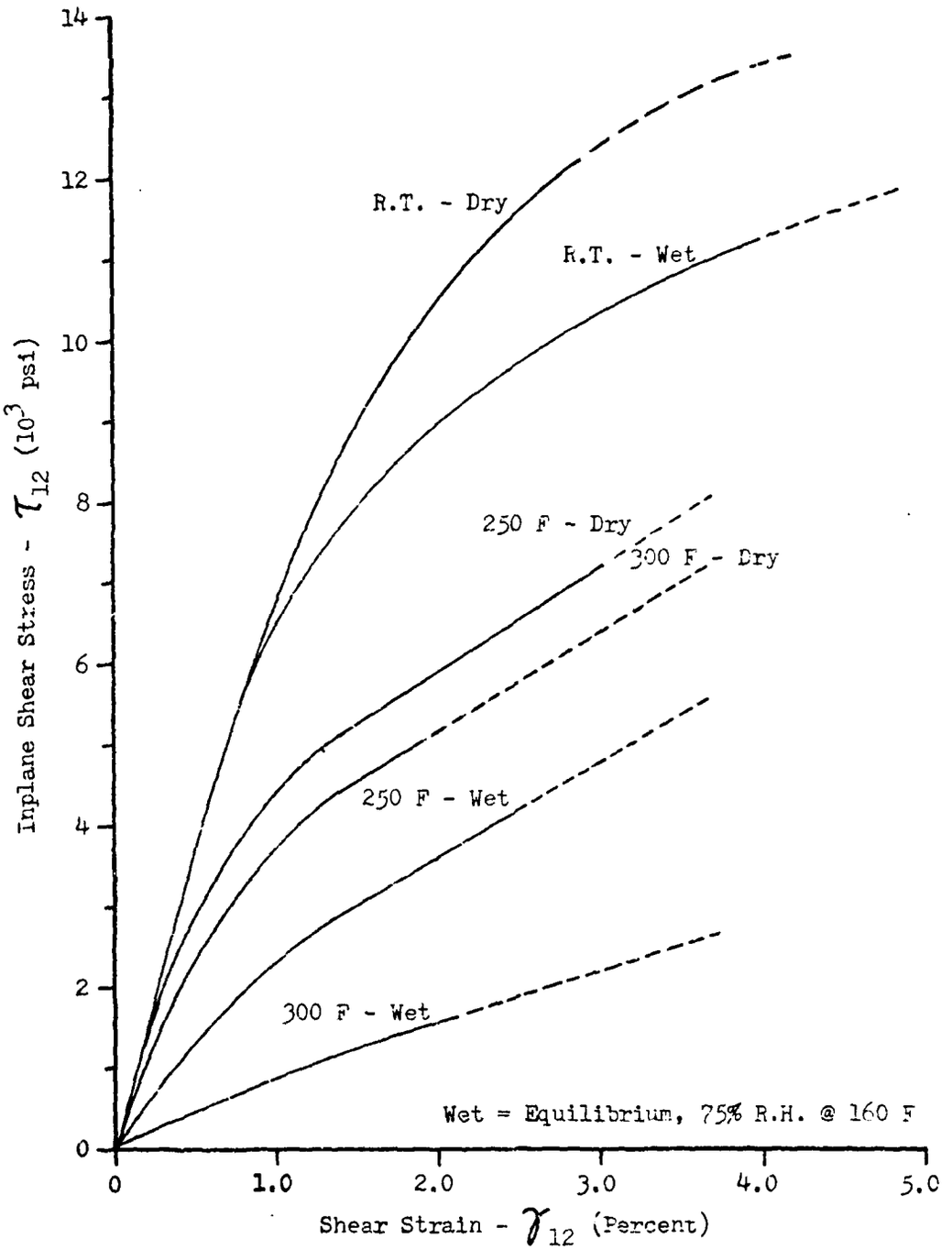

Figure 3. Typical In-plane Shear Stress-strain Curves for AS/3501-5 Unidirectional Composites (Ref 13)

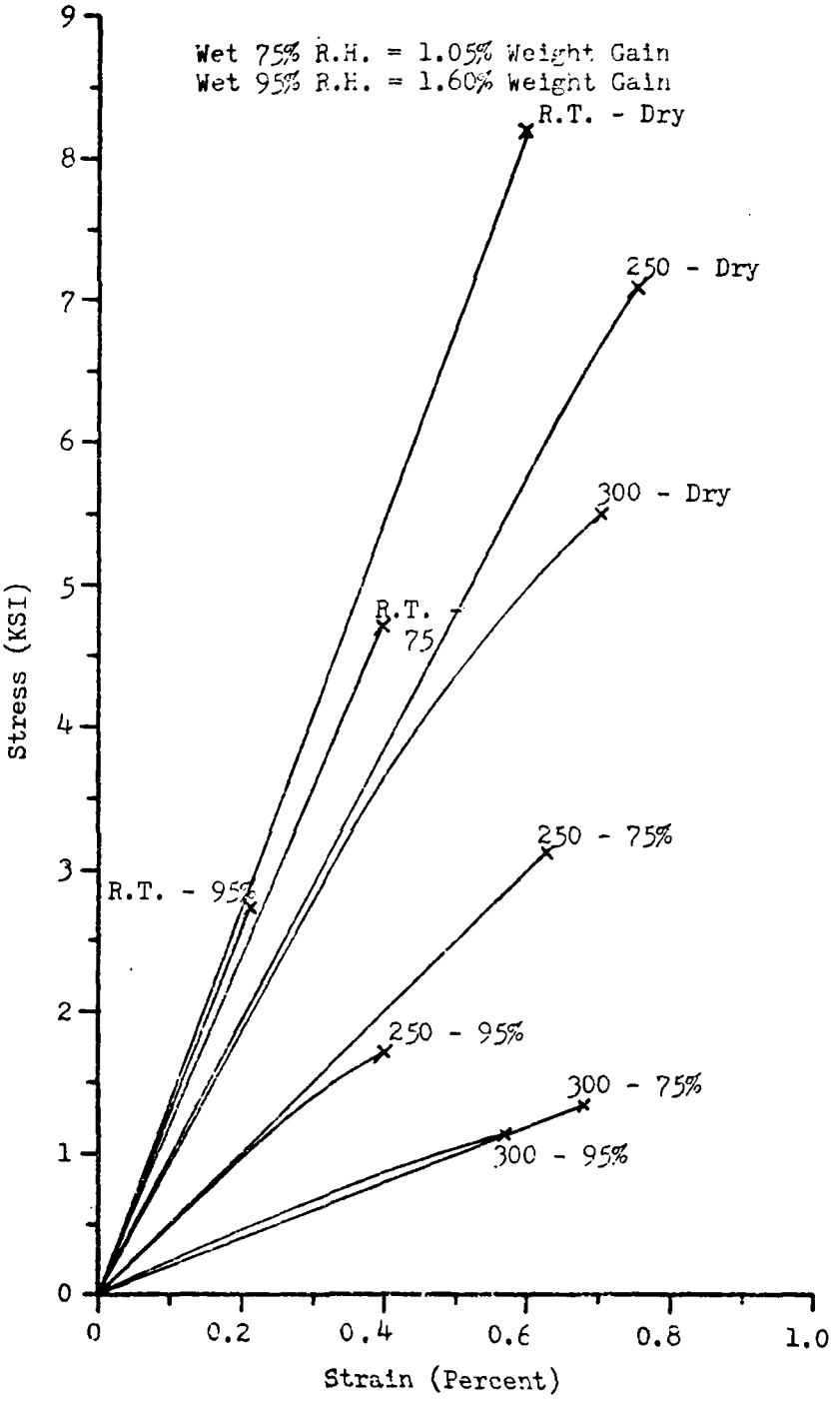

Figure 4. Typical Transverse Stress-strain Curves as a Function of Temperature for AS/3501-5 Unidirectional Composites (Ref 13)

III. Analytical Approach

Background

The cylindrical shell was one of the first shell shapes to be used structurally. From an analytical viewpoint, the analysis of cylindrical shells and, in particular, the analysis of the stability of cylindrical shells was begun in the late 1800s. In the early 1900s, the analytical treatment of cylinders under a variety of loads was developed with the most comprehensive treatment done by Flugge in 1932. In 1933, Donnell (16) proposed a set of simplifications of the non-linear cylindrical shell equilibrium equations. These Donnell equations formed the basis for much of published stability analyses until, in recent years, the availability of high speed computers has led to the development of efficient numerical analytical techniques.

The application of numerical techniques to structural problems began in the 1950s with the advent of matrix analysis. These matrix techniques have evolved through the development of a strong mathematical base into the familiar finite difference and finite element methods now widely used. In the application of these techniques to the study of the stability of shells, a series of programs were developed at the Lockheed Palo Alto Research Laboratory. These programs have generally been known by the name STAGS. The two most recent versions of the program are the finite

difference version, STAGS-C, and the finite element version, STAGS-C1. M. Becker used the finite difference version, STAGS-C, in his comparison of experimental and analytical buckling loads for cylindrical composite panels (2). Since his work, the finite element version, STAGS-C1, has been released and was used in this thesis.

Application to Shell Analysis

The STAGS-C1 program has been specifically developed to perform a collapse analysis of general stiffened and unstiffened shells. The program has several operating modes. Among these are a linear or geometric non-linear static analysis, a bifurcation analysis with a linear or non-linear stress state, and a small vibration analysis with either a stress-free, linear, or nonlinear stress state. The program is capable of handling both isotropic or layered orthotropic materials. The reader is referred to Ref 17 for a comprehensive review of the capabilities of this program and to Ref 18 for an explanation of the program's input parameters.

Both the finite difference and finite element programs are useful in the analysis of shells. While the STAGS-C finite difference program is usually considered better suited for modeling curved surfaces due to the curvilinear fit, it has been found to be less efficient, in certain analysis modes, than the STAGS-C1 finite element program which uses flat elements. Curved finite elements have not

yet been found to be practical because they tend to require large amounts of computer time for the formulation of the stiffness matrix. They also have the problem of self-straining; straining do to rigid body movement associated with the out-of-plane displacement of the shell's surface prior to buckling (19). Until suitable curved elements are developed, modified flat elements are used in STAGS-C1.

The modeling of a cylindrical surface with flat elements is shown in Fig 5. These flat elements have conformity problems which are of importance in their application to nonlinear and stability problems. As seen in Fig 5, both rotational and displacement problems develop at the nodes. The rotational problem is dealt with by assuming that the angle of intersection α is small, and, as a consequence, the normal rotation β_z is ignored and the conformity constraint is met by letting $\beta_y^{(1)} = \beta_y^{(2)}$.

The interelement displacement continuity is more difficult to deal with. Complete displacement compatability along the common boundary requires that

$$(v^{(1)} - v^{(2)}) \cos(\alpha/2) - (w^{(1)} + w^{(2)}) \sin(\alpha/2) = 0$$

$$(w^{(1)} - w^{(2)}) \cos(\alpha/2) + (v^{(1)} + v^{(2)}) \sin(\alpha/2) = 0$$

where v and w are the displacements in the y and z directions, respectively, as shown in Fig 5. If v and w are not represented by polynomials of the same order, then these conditions will not be met. Failure to meet these conditions will allow the individual elements to buckle

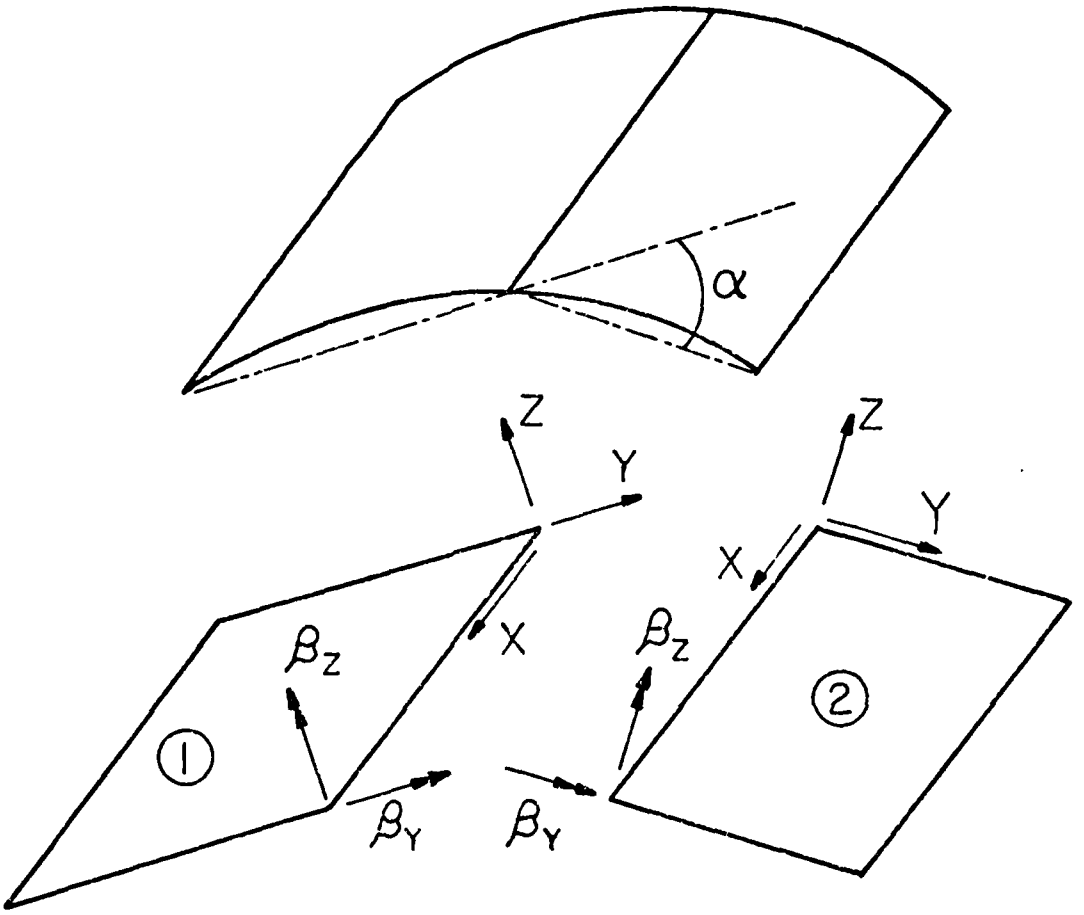

Figure 5. Modeling of Cylindrical Shell with Flat Plates

under axial compression as plates with free edges.

This displacement conformity is met by adding additional freedoms to the element that will raise the order of the polynomials representing inplane deformation. Since w is represented by a cubic polynomial, because the strain energy expression includes second order derivatives of the transverse displacement w, it is necessary that u and v also be represented by cubic polynomials. This is achieved by the use of two rotations at each node, $-v_{,x}$ and $u_{,y}$, and tangential displacements at midside nodes. The difference between these two rotations is the shear strain at each node. This shear strain (γ_1, γ_2, γ_3, γ_4) is introduced as an additional freedom . Thus, each element has 7 degrees-of-freedom at each node and 4 additional displacement freedoms for a total of 32. These additional degrees-of-freedom were added to raise the order of the polynomial representing the inplane deformations. This element is referred to in the STAGS-C1 program as SH411.

A somewhat simpler version of the SH411 element, the SH410 element, is also included for thin shell analysis. This element excludes the midside tangential displacements and uses only an average normal rotation at each of the corner nodes. This restricts u to a linear function in the x-direction and v to a linear function in the y-direction. The shear strain is also suppressed at the nodes.

The freedoms for both these elements are shown in Fig 6. The reader is referred to Refs 19 and 20 for a more

thorough explanation of the development of these elements. Reference 19 contains the derivation of the SH411 element.

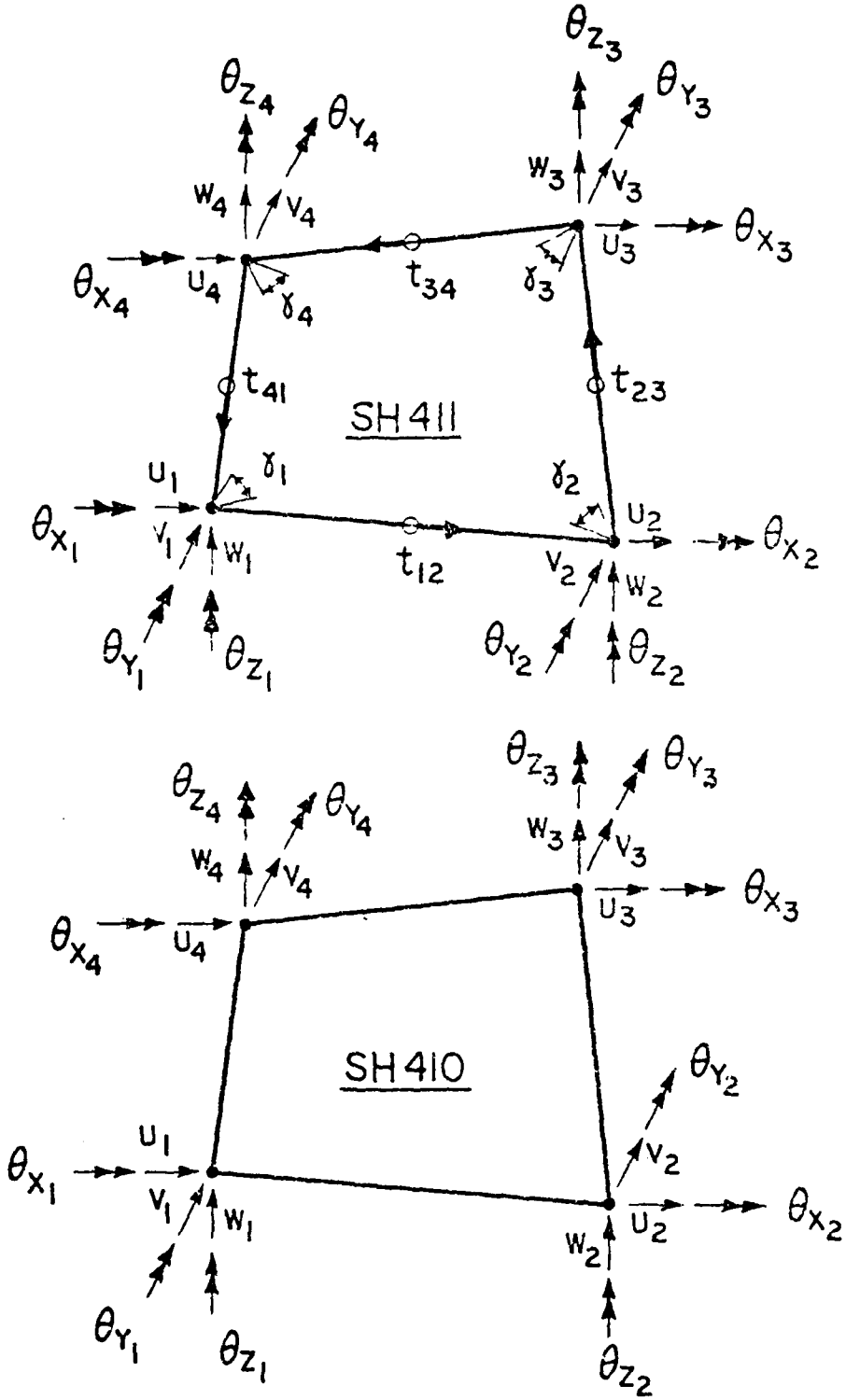

Figure 6. SH411 and SH410 Degrees of Freedom

Classical Laminated Plate Theory

Since this thesis deals with the problem of the buckling of thin, composite panels, a statement of the pertinent assumptions and restrictions is needed. Reference 21 contains a concise statement of restrictions and assumptions applicable to thin plate theory.

Restrictions:

A) Each layer of the laminate is orthotropic, linear elastic, and of constant thickness.

B) The panel thickness is very small compared to its length and width.

C) The radius of curvature of the panel is large insuring that the curved panels may be described as shallow shells or quasi-shallow.

Assumptions:

A) Stresses acting in the xy plane dominate the panel behavior. As a consequence, σ_z, τ_{xz}, and τ_{yz} are assumed to be zero and a state of plane stress exists.

B) The Kirchhoff assumption of negligible transverse shear strains, γ_{xz} and γ_{yz}, and negligible transverse normal strain, ϵ_z, applies.

C) The displacements u, v, and w are small compared to the panel thickness.

D) The square of the rotations are small compared with the linear strains.

E) The strains, ϵ_x, ϵ_y, and γ_{xy}, are small compared to unity.

A diagram of the plate element's geometry and stress resultants is shown in Fig 7.

The assumption that the transverse shear strains may be assumed to be zero results in the transverse shear stresses also being zero. This is a standard assumption in classical laminated plate theory. This is fortunate because the SH411 and SH410 plate elements described previously do not include transverse shear strains in their formulation. However, in addressing the problem of environmental degradation in composites, this assumption may not be valid. Flaggs and Vinson (22) have developed a general buckling theory for flat plates which accounts for the moisture and temperature effects and includes transverse shear, normal deformation, and bending-extensional coupling. The application of this theory to curved panels will require a finite element with transverse shear capability. One such element, referred to as an AHMAD-type element (19), is currently under development but is not yet available in STAGS-C1.

Because of the apparent need for a transverse shear-capable element to totally address the moisture and temperature effects, the study of these effects will be limited to the degradations in elastic moduli due to moisture and temperature. Resin swelling, either due to moisture absorption or temperature expansion, will not be included.

Another restriction needed to use STAGS-C1 is that each

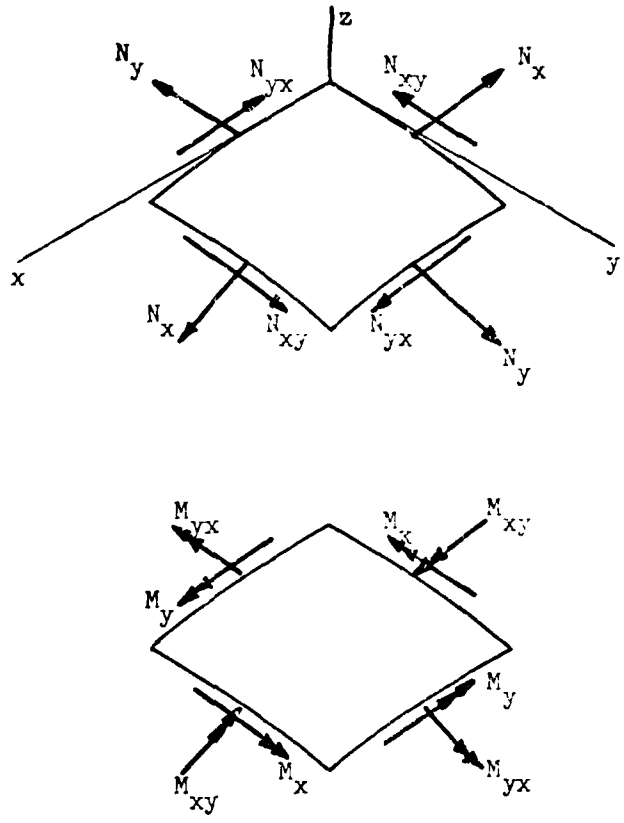

Figure 7. Plate Element Geometry and Stress Resultants

layer's material properties are assumed to be constant across the layer's thickness and throughout that layer. In the calculation of the degraded elastic moduli, each layer was assumed to have a uniform moisture concentration equal to the value calculated at the ply's mid-surface. In the determination of the temperature degradation, the entire laminate was assumed to be at the specified temperature.

With these additional restrictions and assumptions, the STAGS-C1 program should adequately predict the panel's critical load. By limiting the problem to only changes in elastic moduli, the influence of these moduli degradations may be addressed separately. Also, the problem of modeling the laminated plate is simplified.

Because flat elements are being used in the finite element model, the formulation of the stress-strain relationships is straightforward as shown in Ref 21. Since unsymmetric moisture concentration distributions through the laminate's thickness will be investigated, bending-extensional coupling will develop. The equations relating the stress resultants to the mid-surface strains and curvatures are

$$\begin{Bmatrix} N_x \\ N_y \\ N_{xy} \end{Bmatrix} = \begin{bmatrix} A_{11} & A_{12} & A_{16} \\ A_{12} & A_{22} & A_{26} \\ A_{16} & A_{26} & A_{66} \end{bmatrix} \begin{Bmatrix} \epsilon^o_x \\ \epsilon^o_y \\ \gamma^o_{xy} \end{Bmatrix} + \begin{bmatrix} B_{11} & B_{12} & B_{16} \\ B_{12} & B_{22} & B_{26} \\ B_{16} & B_{26} & B_{66} \end{bmatrix} \begin{Bmatrix} K_x \\ K_y \\ K_{xy} \end{Bmatrix}$$

$$\begin{Bmatrix} M_x \\ M_y \\ M_{xy} \end{Bmatrix} = \begin{bmatrix} B_{11} & B_{12} & B_{16} \\ B_{12} & B_{22} & B_{26} \\ B_{16} & B_{26} & B_{66} \end{bmatrix} \begin{Bmatrix} \epsilon^o_x \\ \epsilon^o_y \\ \gamma^o_{xy} \end{Bmatrix} + \begin{bmatrix} D_{11} & D_{12} & D_{16} \\ D_{12} & D_{22} & D_{26} \\ D_{16} & D_{26} & D_{66} \end{bmatrix} \begin{Bmatrix} K_x \\ K_y \\ K_{xy} \end{Bmatrix}$$

where: N_i - membrane stress resultants

M_i - bending stress resultants

A_{ij}, B_{ij}, D_{ij} - stiffnesses

ϵ^o_i - mid-surface extensional strains

γ^o_{xy} - mid-surface shear strains

K_i - mid-surface curvatures

The A_{ij} are called the extensional stiffnesses, the B_{ij} are called the coupling stiffnesses, and the D_{ij} are called the bending stiffnesses. The B_{ij} results in coupling between bending and extension. For symmetric laminates, the B_{ij} vanish and there is no coupling between bending and extension. The influence of the B_{ij} will be evaluated through the appropriate selection of initial moisture conditions that result in symmetric and unsymmetric laminates.

Finite Element Model

This thesis will evaluate the stability of cylindrical composite panels subject to axial compression. A typical composite fuselage skin panel with backup structure is shown in Fig 8. This structural component is used as the basis for the development of the finite element model shown in Fig 10. The STAGS-C1 cylindrical shell geometry is shown in Fig 9.

The panel is square with the panel height and circumferential width being equal. Such a panel is defined to have an aspect ratio of 1. The aspect ratio is defined to be equal to the height divided by the width for both panels and elements. All panels in this thesis have aspect ratios of 1. This panel aspect ratio determination is different from Becker's (2) where the panel's chord dimension was defined as the panel's width. This resulted in the panel's aspect ratio being a function of the panel's radius of curvature. The use of this notation would have made the comparison of panels with different radii difficult because each panel would have a different aspect ratio.

The boundary conditions used in the evaluation of the moisture and temperature effects were selected to represent those of a typical backup structure rather than the standard simple or fixed boundary conditions. Two sets of boundary conditions were chosen. The first set of conditions assumes that the backup structure's ring frames and longerons are

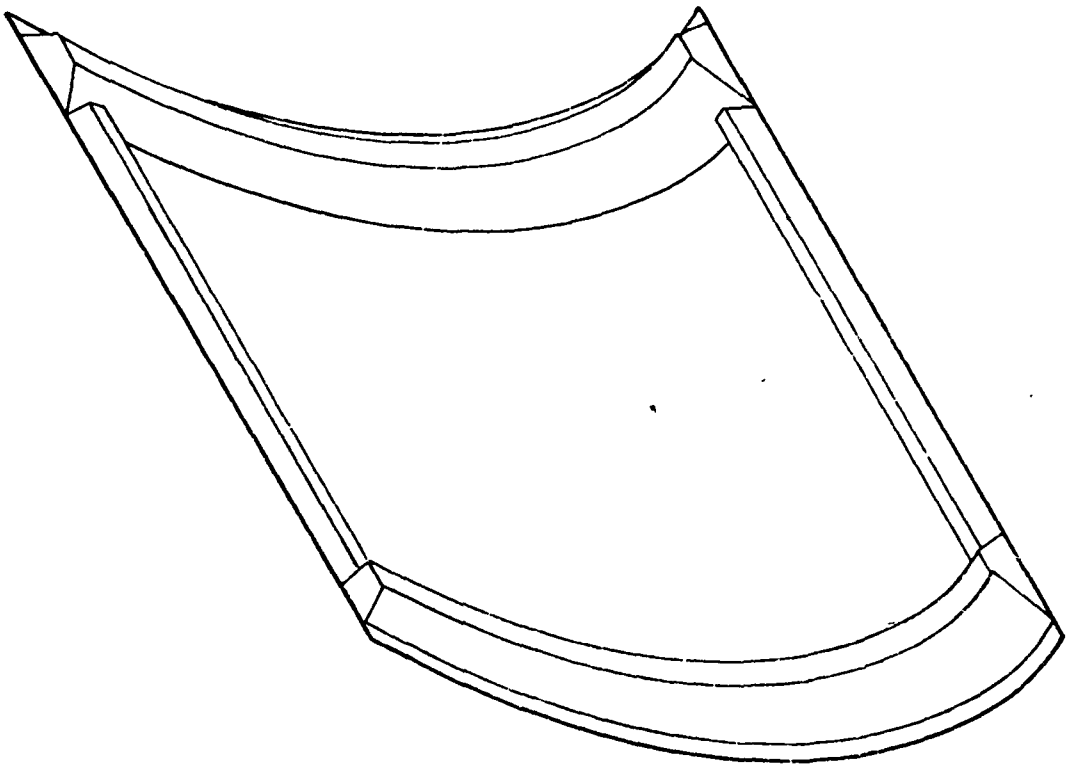

Figure 8. Composite Fuselage Skin Panel with Backup Structure

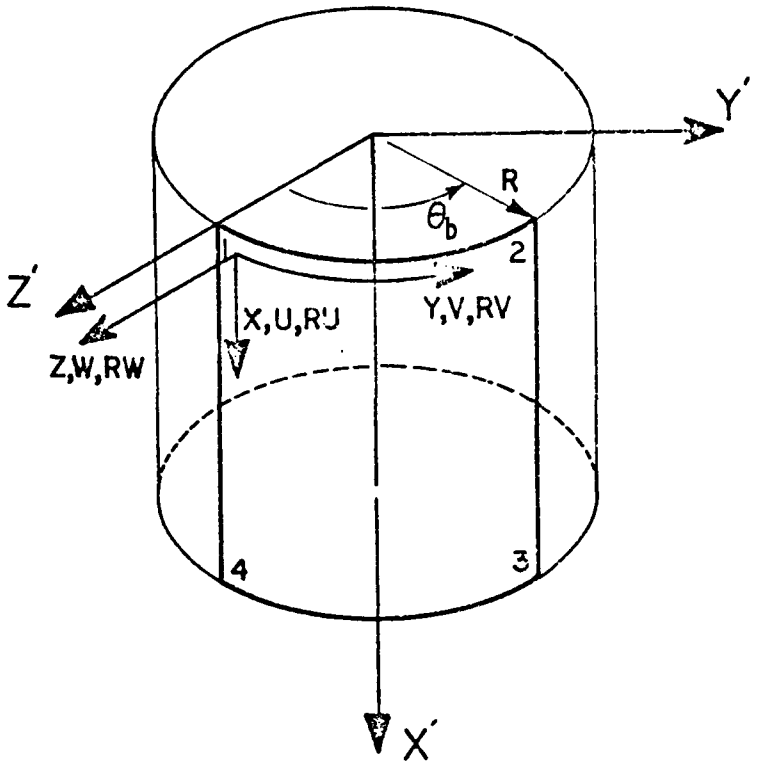

Figure 9. STAGS-C1 Cylindrical Shell Geometry

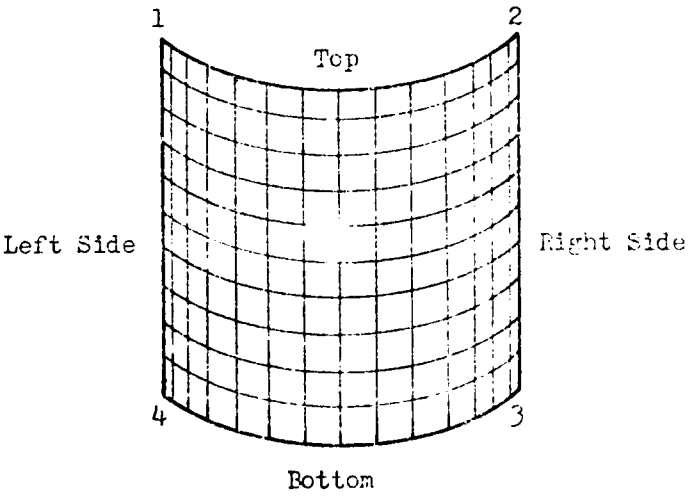

Finite Element Model

Figure 10. Finite Element Model

effective in restraining out-of-plane deflections (W) and rotational movement (RU, RV, RW). The top frame and side longerons are assumed to not be effective in resisting the axial compressive load but do resist in-plane displacements in the circumferential direction (V). The second set of boundary conditions is identical to the first with the exception that the longerons are assumed to have no torsional stiffness and, hence, cannot resist a torsional rotation. In the first set, the longerons were assumed to be closed sections and, hence, effective in torsion. In the second set, the longerons were assumed to be open sections which have little effective torsional resistance. The boundary conditions are summerized in Table II.

Table II

Panel Boundary Conditions

	U	V	W	RU	RV	RW	U	V	W	RU	RV	RW
Top	1	0	0	0	0	0	1	0	0	0	0	0
Right Side	1	0	0	0	0	0	1	0	0	1	0	0
Bottom	0	0	0	0	0	0	0	0	0	0	0	0
Left Side	1	0	0	0	0	0	1	0	0	1	0	0

where 0 represents a fixed displacement and 1 represents a free displacement along the panel's edge.

The loads applied to the panel represent axial compression loading. This load is assumed to act uniformly across the top of the panel and is reacted across the bottom of the panel.

Bifurcation Analysis Method

STAGS-C1 has two buckling analysis modes. One uses a linear, pre-buckling displacement state and is referred to in the STAGS-C1 manual as the bifurcation analysis with a linear stress state. The second method uses a geometric pre-buckling, nonlinear displacement calculation and is referred to as the bifurcation analysis with a non-linear displacement state. As noted in Ref 19, the SH411 and SH410 elements have not produced good results using the nonlinear mode in predicting post-buckling modes. Thus, the bifurcation analysis with a linear displacement state prior to bifurcation will be used. This method will calculate the pre-buckling displacements and rotations, stress resultants, strains, and stresses as desired. It also predicts the bifurcation eigenvalue and the shape of the eigenvector. It does not yield any post-buckling information.

Evaluation of STAGS-C1 Program

A series of comparison runs with the STAGS-C finite difference version of the program and a convergence study to determine the best mesh size was performed. Previously run STAGS-C results for a 12 in. high by 12.567 in. wide cylindrical composite panel (panel aspect ratio of 1 per Becker's notation), with several sets of boundary conditions, were compared with the equivalent STAGS-C1 finite element results. These STAGS-C finite difference runs were done by Becker as a part of the work reported in Ref 4. The STAGS-C runs used the linear bifurcation analysis and the STAGS-C1 runs used the bifurcation analysis with the linear stress state option.

The panel's ply orientation was $[45.,-45.]_{2S}$ with a panel radius of 12 in. The boundary conditions along the vertical, straight side were changed while the boundary conditions along the top and bottom were not changed. The STAGS-C1 results compared well with the STAGS-C results even though the STAGS-C program was using a curved surface formulation and the STAGS-C1 program was using flat plate elements. The results of this comparison study are shown in Table III. These STAGS-C1 runs were made using the simpler SH410 flat plate element with a 24 row by 25 column element mesh.

Table III

Comparison of STAGS-C and STAGS-C1 Results

Bound. Cond.	Case	STAGS-C Bif. Load	STAGS-C1 Bif. Load	Percent Diff.
Free	BF1	116.5	107.2	8.0
CC1	BC1	392.7	399.0	1.6
CC4	BD1	498.0	488.5	1.9
SS1	BS1	391.6	396.1	1.1
SS4	BT1	477.2	452.6	5.2

When using a finite element program, it is important that the convergence characteristics of the elements chosen for use is known. To evaluate the convergence characteristics for the two elements, SH411 and SH410, and to determine the optimum mesh size and element aspect ratio, a series of runs were made on cylindrical panels subject to axial compression. The bifurcation analysis with the linear stress state option was used for all cases. The parameters evaluated were:

1) Convergence characteristics of the SH411 and SH410 elements.

2) Influence of panel ply orientations on the convergence characteristics. Panel ply orientations of $[45.,-45.]_{2S}$ and $[0.,45.,-45.,90.]_{S}$ were evaluated.

3) Influence of panel radius and panel size on the convergence characteristics.

4) Influence of mesh density and element aspect ratio on the convergence characteristics.

In Ref 19, when the convergence characteristics of the two elements were evaluated for a cylindrical shell, the

SH410 element converged very rapidly compared with the SH411 element. It was believed that the rapid convergence was the result of case-dependent cancellation of errors in different directions. The SH410 element also tended to converge more rapidly than the SH411 element in this convergence study. The reason for the better performance of the SH410 element is not evident although it is probably related to the cylindrical panel being curved in only one direction. Figure 11 shows typical convergence results for a $[45.,-45.]_{2S}$ panel using the SH411 element and element aspect ratios of 0.5, 1.0, and 2.0. Figure 12 compares the convergence characteristics of the SH411 and SH410 elements for the $[45.,-45.]_{2S}$ and $[0.,45.,-45.,90.]_{S}$ panels.

The panel's ply orientation had the greatest influence on the rate of convergence with the $[45.,-45.]_{2S}$ panel converging slower than the $[0.,45.,-45.,90.]_{S}$ panel. The element aspect ratio also influenced the rate of convergence. An element aspect ratio (height/width) of 1 had the best rate of convergence followed closely by an aspect ratio of 0.5. The panel radius and panel size (with panel aspect ratio of 1) did not significantly influence the convergence characteristics. Both the SH410 and SH411 elements appeared to be converging monotonically once an element mesh size of 32 elements was reached.

The accuracy of the STAGS-C1 program was evaluated by comparing the bifurcation load of a square $[0.,90.]_{2S}$ flat plate with simple supported edges with the theoretical

solution shown in Ref 21. The theoretical critical load is

$$\overline{N}_x = \frac{13\pi^2 D_{22}}{b^2}$$

These results are shown in Table IV.

Table IV

Comparison of SH410 and SH411 Elements
Bifurcation Loads to Theoretical Results

Element Mesh	SH410	Percert Error	SH411	Percent Error
6 X 6	1.547	4.74	1.529	5.85
10 X 10	1.597	1.79	1.587	2.28
14 X 14	1.611	0.80	1.605	1.17
18 X 18	1.616	0.49	1,613	0.68

The SH410 element required only approximately one-half of the computer time required for the SH411 element. For both flat plates and the cylindrical shells, the SH410 element has better convergence characteristics and a smaller error than the SH411 element.

For the evaluation of the moisture and temperature influences on the bifurcation load, a mesh density of 14 elements by 14 elements was chosen. Comparing the bifurcation load at the 14 by 14 element mesh with an extrapolated bifurcation load shows that for the $[0.,45.,-45.,90.]_S$ panel the SH410 element had an error of 0.64 percent and the SH411 element had an error of 3.38

percent. For the $[45.,-45.]_{2S}$ panel, the SH410 element had an error of 10.45 percent and the SH411 element had an error of 27.44 percent. The extrapolated bifurcation load was calculated using the last three values for the bifurcation load for each case and then applying the Aitken Δ^2 "extrapolation to the limit" method.

The SH410 element will be used in the moisture and temperature evaluation because of its better accuracy and quicker computer run times. The finite element mesh chosen will be 14 by 14 elements (196 elements total) with 225 nodes. The mesh is square with an element aspect ratio of 1.

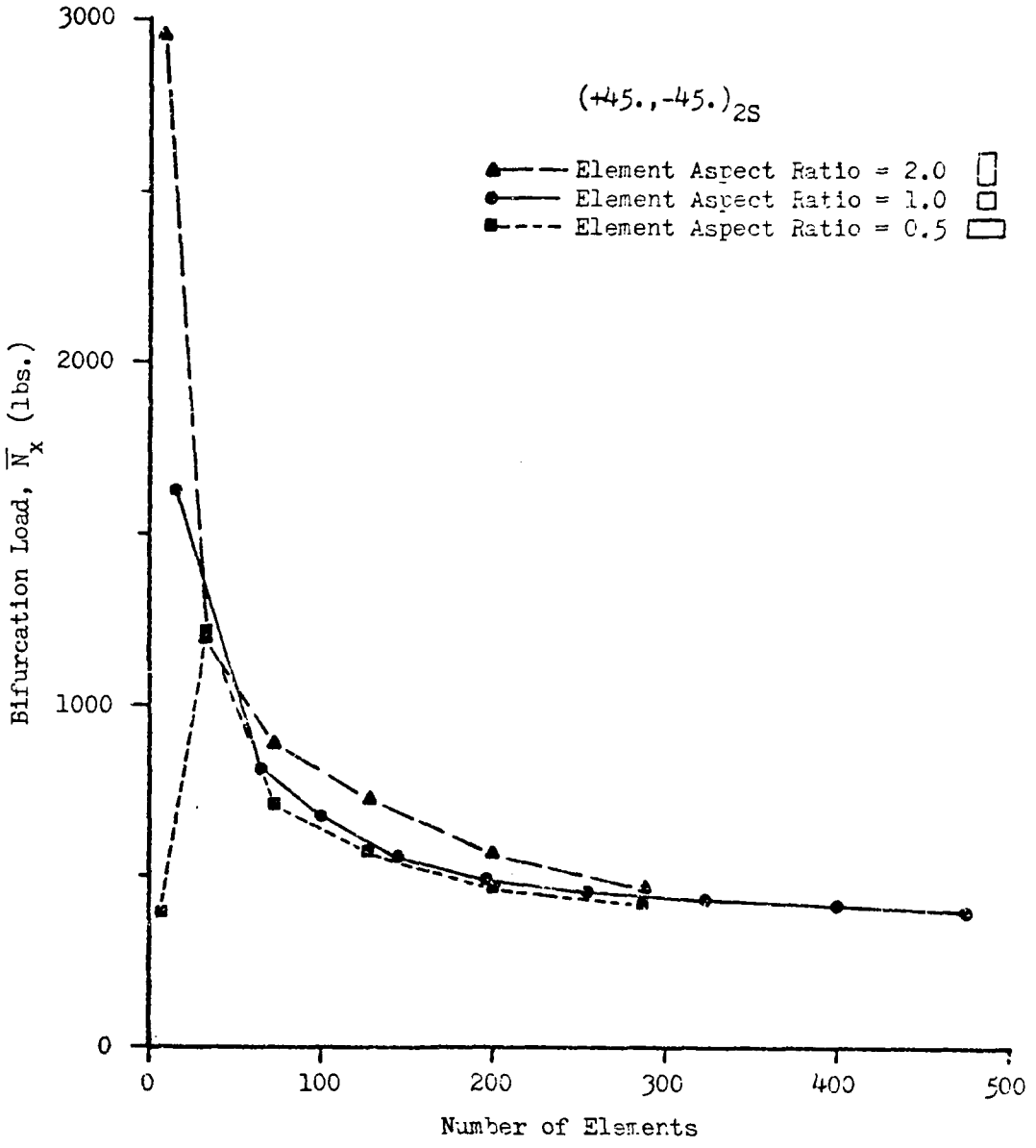

Figure 11. Convergence Characteristics of the SH411 Element

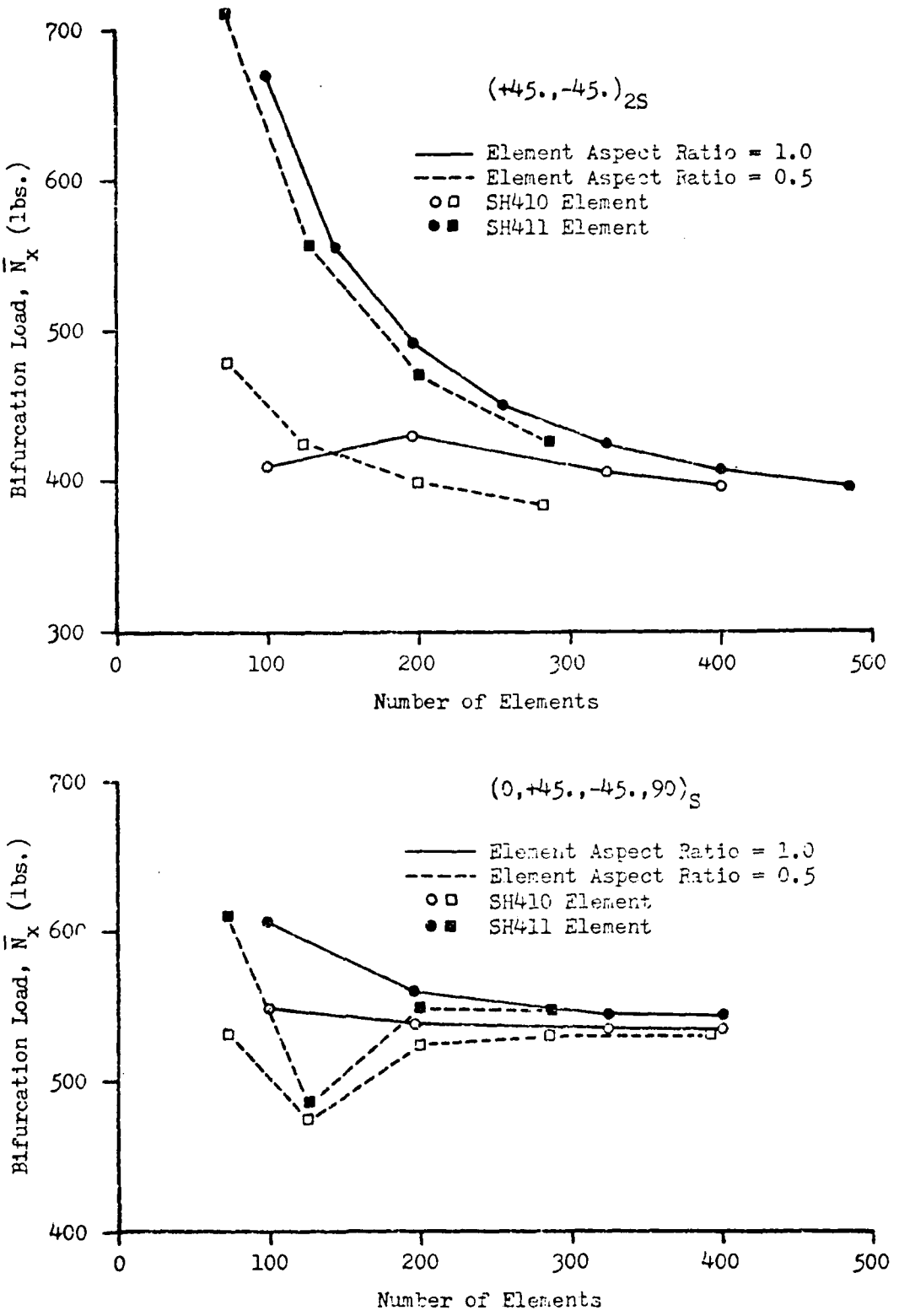

Figure 12. Comparison of Convergence Characteristics for the SH411 and SH410 Elements

IV. Moisture and Temperature Conditions Evaluated

Moisture Conditions

Test data (13) for the AS/3501-5 graphite/epoxy system, which included the degradation in the transverse and shear moduli, was available for a saturation moisture concentration of 1.05 percent. The moisture concentration is measured as a percentage of weight gained. To determine the moisture concentration through the laminate's thickness as a function of time, the series solution to the Fick equation is used. The coefficients, C_1 and C_2, representing the moisture concentration at the surface of the laminate, are selected along with the desired dimensionless time T^* (where $T^* = K(in^2/sec) \times t(sec)/h^2(in)^2$). In the evaluation of the moisture and temperature effects, three moisture concentration conditions were evaluated at each of five time intervals. These moisture conditions are shown in Table V.

Table V

Moisture Conditions

Cond. No.	C_0	C_1	C_2
1	0.00	0.00	0.0105
2	0.00	0.0105	0.00
3	0.00	0.0105	0.0105

The coefficient C_0 represents the initial moisture

concentration in the laminate. For the cylindrical panel, C_1 is the moisture concentration on the inside (-Z) surface and C_2 is the moisture concentration on the outside (+Z) surface. Conditions 1 and 2 will result in an unsymmetric degradation of the E_2 and G_{12} moduli resulting in an unsymmetric laminate. This will introduce bending-extension coupling. Condition 3 is symmetric and will not produce any bending-extension coupling.

The dimensionless times used in this analysis are 0.0, 0.001, 0.01, 0.1, and 0.5. Table VI shows the correspondence between real time and T^*. The moisture distribution through the thickness for moisture conditions 1 and 3 and the five time values are shown in Fig 13. A T^* of 0.5 represents the steady-state distribution. The moisture distribution is shown in Fig 13 as a continuous function. As noted in Section II, the moisture concentration is calculated at the center of each ply and then assumed to be constant through the thickness.

Table VI

Relation Between Real and Dimensionless Time

Real Time (sec)	Real Time (days)	Dimensionless Time T^*
0.0	0.0	0.0
3.045E04	0.35	0.001
3.045E05	3.52	0.01
3.045E06	35.24	0.1
1.527E07	176.24	0.5

Note: These times were calculated using K = 0.52537E-10 (in^2/sec) for an 8-ply, 0.40 thick, AS/3501-5 laminate. The

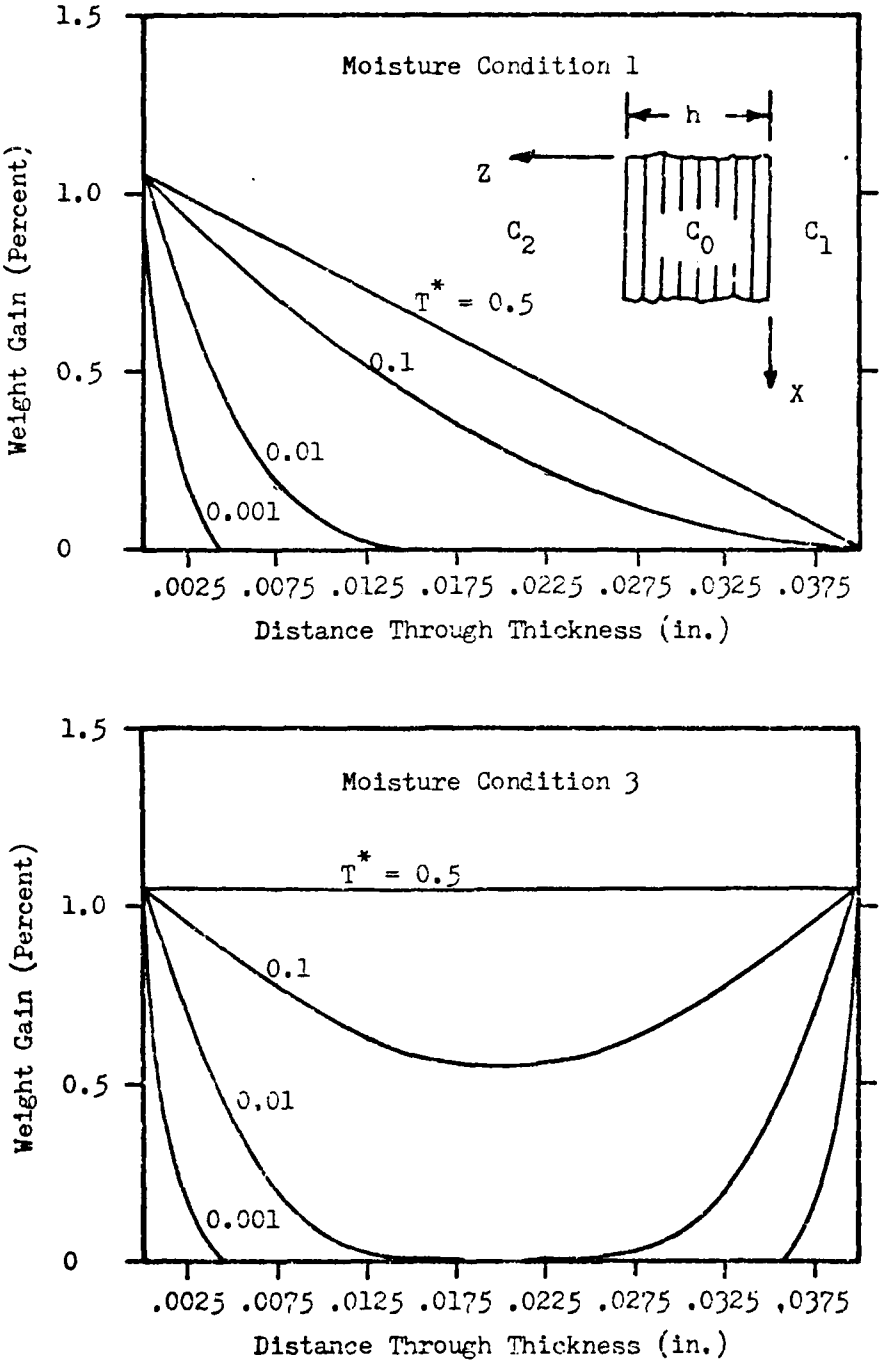

Figure 13. Moisture Concentration Distribution for Moisture Conditions 1 and 3

parametric equation used to determine K was taken from Ref 15. This equation is

$$K = 6.51 \exp\left(\frac{-5722}{T}\right) \times (.03937)^2$$

where: K - diffusion Coefficient in in^2/sec

T - Temperature in degrees Kelvin

Temperature Conditions

The test data for the AS/3501-5 was taken at four temperatures: 80 F, 200 F, 250 F, and 300 F. These four temperatures were used to evaluate the influence of temperature. A thin laminate reaches temperature equilibrium very quickly when compared with the time to reach moisture equilibrium. Thus, the laminate was assumed to be at a constant temperature in this evaluation.

Calculation of Moduli Degradations

For a calculated moisture concentration and at a given temperature, the reduced E_2 and G_{12} values are calculated from the data shown in Table I. This requires an interpolation of the test data at the given temperature. A linear interpolation between the data at the known moisture concentrations was used to calculate intermediate values. In this manner, the E_2 and G_{12} values for each ply were determined. For moisture condition 3, the reduced moduli distribution through the thickness for E_2 and G_{12} are shown

on Figs 14a and 14b, respectively. These two figures represent the general trend in moduli degradation as a function of time and temperature and do not show the degradation of moduli through the thickness.

Laminate Ply Orientations

Three 8-ply laminates will be evaluated. The three ply orientations chosen are $[0.,45.,-45.,90.]_S$, $[90.,45.,-45.,0.]_S$, and $[45.,-45.]_{2S}$. The relationship of these three orientations to the STAGS-C1 coordinate system is shown in Fig 15.

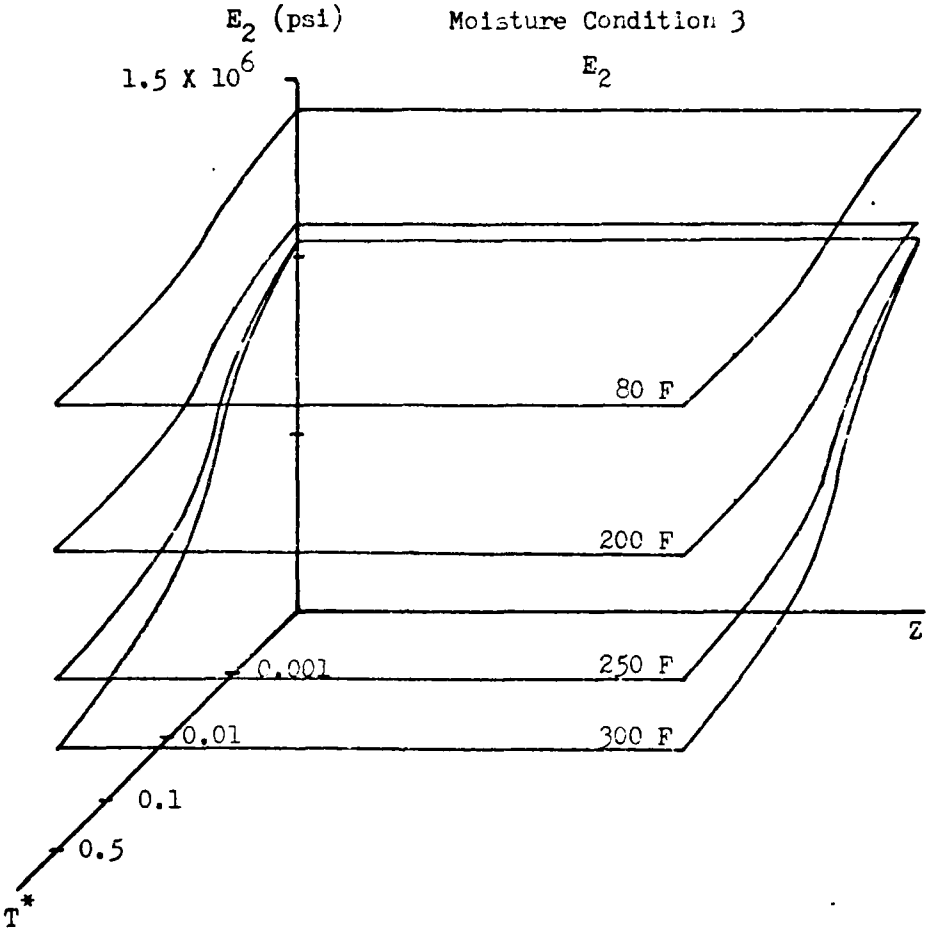

Figure 14a. Degradation in E_2 for Moisture Condition 3

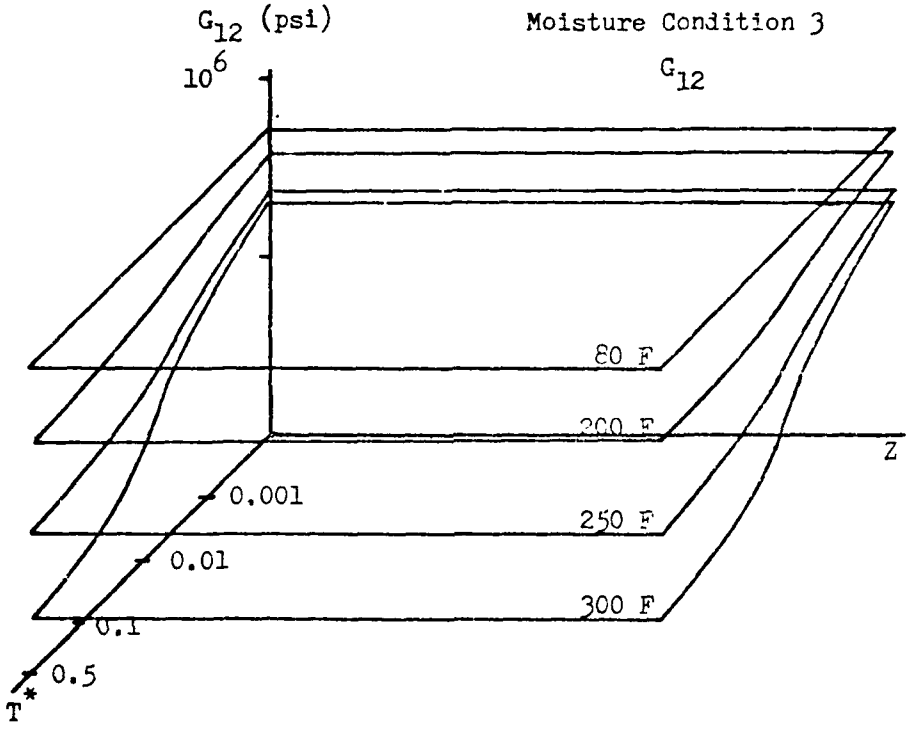

Figure 14b. Degradation in G_{12} for Moisture Condition 3

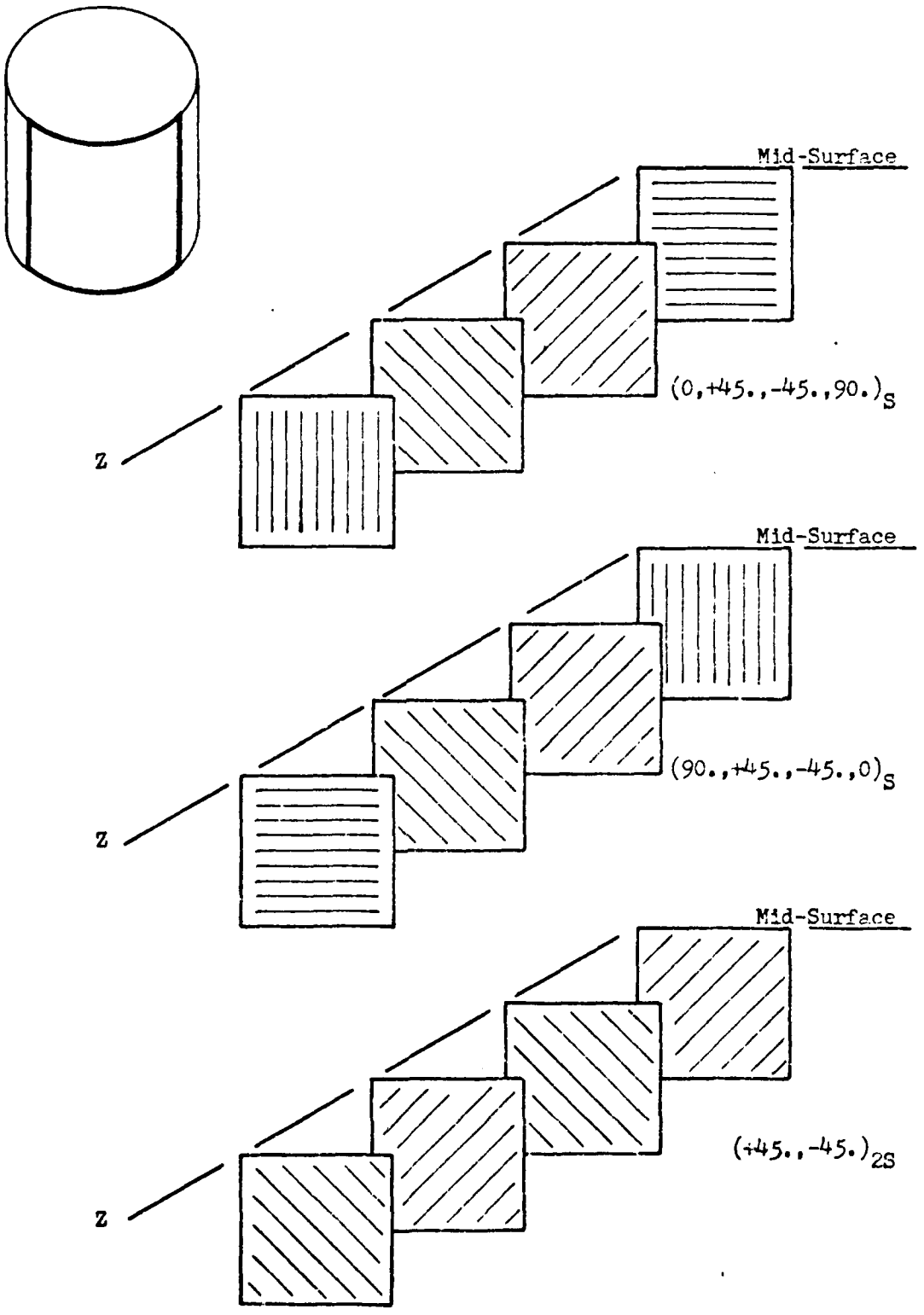

Figure 15. Laminate Ply Orientations

STAGS-C1 Cases

The combination of moisture conditions, temperatures, and times generates a matrix of 60 cases for each laminate per boundary condition. These 60 cases are broken into three sets of 20 cases; 20 cases for each moisture condition. Because of the large number of cases to be evaluated, all 60 cases were run for only the boundary condition with the fixed vertical edges. Only the 20 cases for the first moisture condition were run for the vertical edge's simple-supported boundary condition to evaluate the influence of this change. The matrix of case numbers and the corresponding conditions is shown in Table VII.

Table VII

Moisture and Temperature Conditions Evaluated

Case No.	Moisture Cond.	Boundary Cond.	Laminate	Element Type
1-20	1	Fixed	[0.,45.,-45.,90.]S	410
21-40	1	Fixed	[90.,45.,-45.,0.]S	410
41-60	1	Fixed	[45.,-45.]2S	410
101-120	1	Simple	[0.,45.,-45.,90.]S	410
121-140	1	Simple	[90.,45.,-45.,0.]S	410
141-160	1	Simple	[45.,-45.]2S	410
201-220	2	Fixed	[0.,45.,-45.,90.]S	410
221-240	2	Fixed	[90.,45.,-45.,0.]S	410
240-260	2	Fixed	[45.,-45.]2S	410
401-420	3	Fixed	[0.,45.,-45.,90.]S	410
420-440	3	Fixed	[90.,45.,-45.,0.]S	410
441-460	3	Fixed	[45.,-45.]2S	410

These cases were all run for 12 in. by 12 in. panels with a panel radius of 12 in. Two additional sets, identical to cases 1-20, were run with panel radii of 24 in. and 48 in. to evaluate the influence of panel radius on the degradation characteristics.

The computation of the moisture concentration distribution and the reduction in moduli was done by a computer program. A listing of this computer program is included in Appendix A. This computer program also generated the input deck for the STAGS-C1 program.

Once the value of E_2 was calculated, the corresponding value of ν_{21} was calculated using the relationship

$$\frac{\nu_{12}}{E_1} = \frac{\nu_{21}}{E_2}$$

As noted previously, both E_1 and ν_{12} were assumed to be constant. Actually, both of these material properties vary with moisture concentration and temperature. E_1 increases by about 10 percent and ν_{12} varies from 0.34 to 0.46. Using the STAGS-C1 program, the increase in E_1 resulted in an approximately eight percent increase in the bifurcation load. ν_{12} did not significantly influence the bifurcation load with changes of less than two percent.

Since E_1 caused an increase in the bifurcation load, it was decided not to include this change in the case studies because it would make an evaluation of the effects of reductions in the other two moduli more difficult.

V. Results and Discussion

Reduction in Bifurcation Load

The moisture- and temperature-induced degradations in the E_2 and G_{12} moduli resulted in reductions in the panels' bifurcation load. The results of the STAGS-C1 runs for the three panels with the fixed boundary condition are shown in Figs 16, 17, and 18. In these plots $\bar{N}x_{orig}$ represents the bifurcation load for the room temperature condition at T=0.0. This condition is unaffected by either temperature or moisture degradations. These results are also shown in tabular form, along with individual plots for each time and temperature series, in Appendix B. These results are for 12 in. by 12 in. panels with a radius of 12 in.

As was expected, the panels' bifurcation load decreased with increasing temperature and absorbed moisture. At the higher temperatures and moisture concentrations, this reduction was significant; ranging from 21 percent for the $[0.,45.,-45.,90.]_S$ laminate to 43 percent for the $[45.,-45.]_{2S}$ laminate. These reductions are especially significant considering that the longitudinal moduli was not changed. A summary of the maximum reduction in $\bar{N}_x$ for each laminate and moisture condition is shown in Table VIII. These results are for the fixed boundary condition.

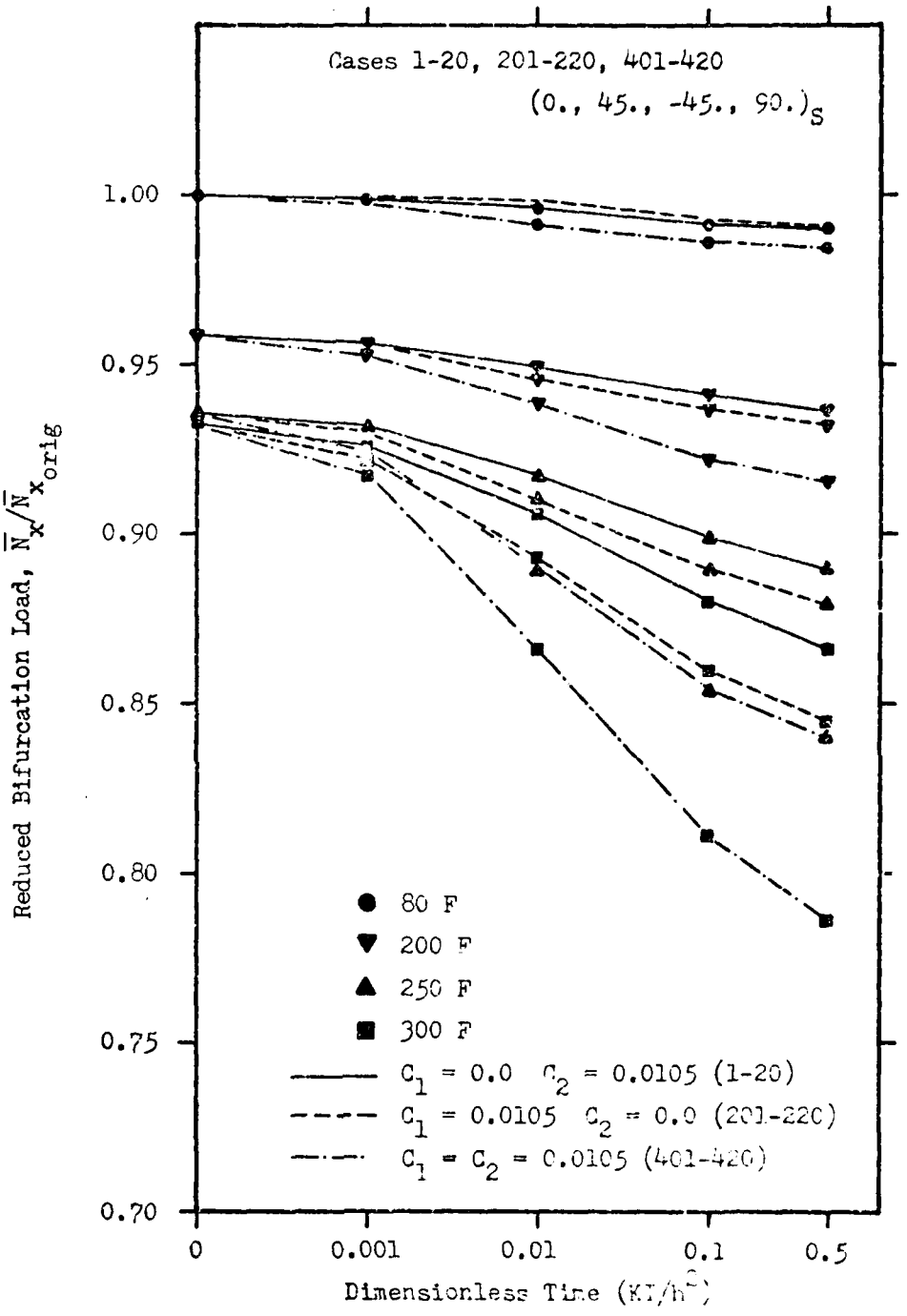

Figure 16. Degradation in $\bar{N}_x$ for the $(0,45.,-45.,90.)_S$ Laminate

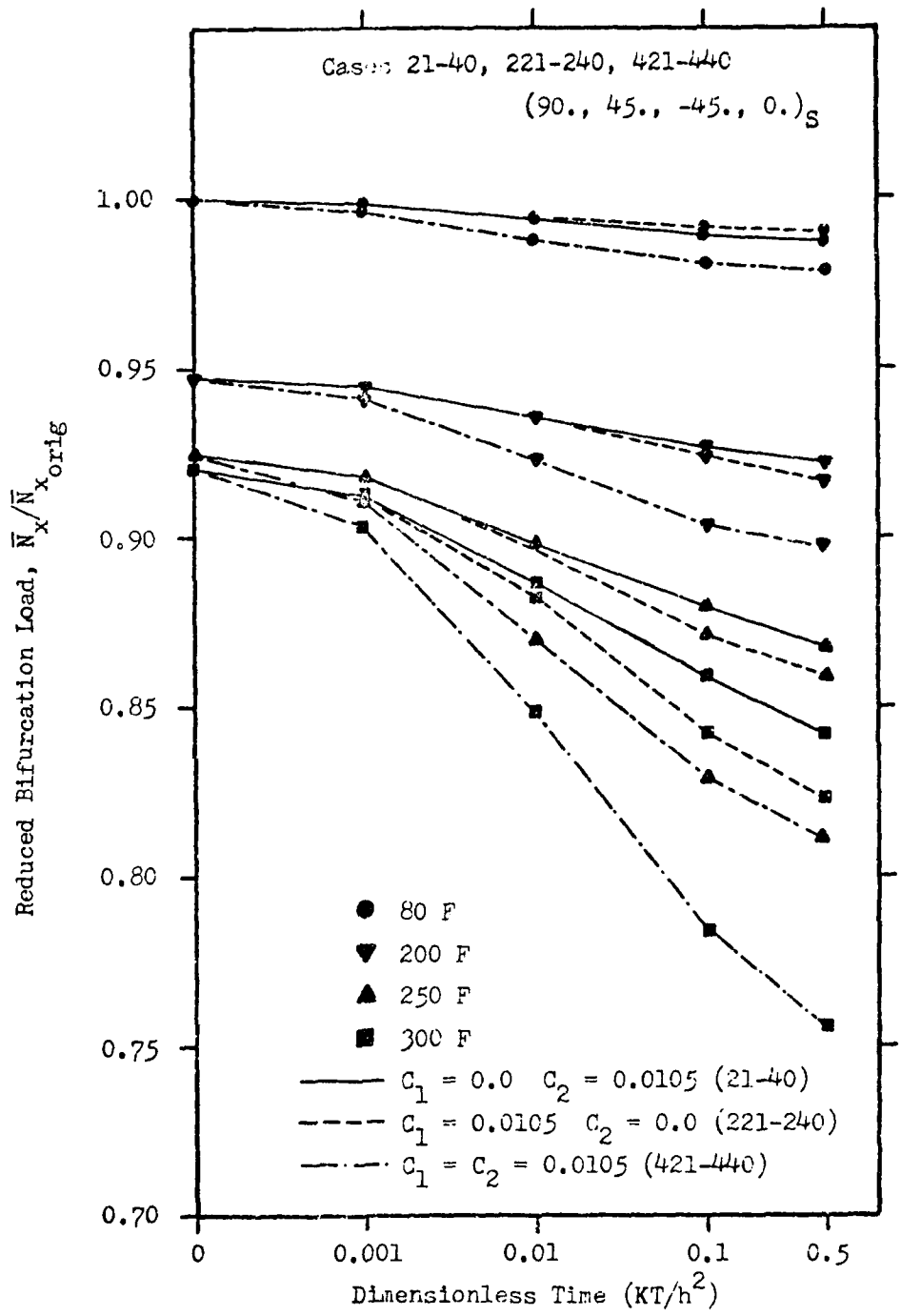

Figure 17. Degradation in $\bar{N}_x$ for the $(90.,45.,-45.,0)_S$

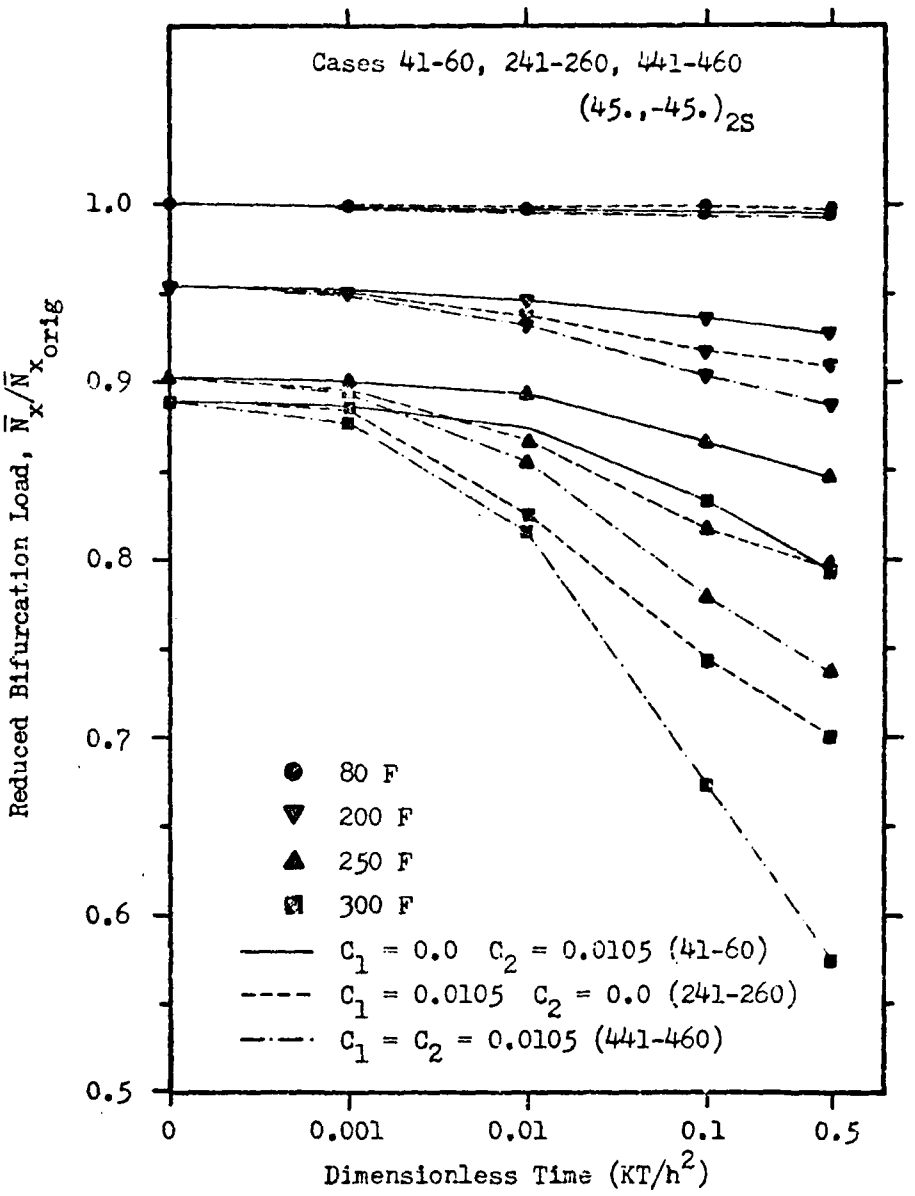

Figure 18. Degradation in $\bar{N}_x$ for the $(45.,-45.)_{2S}$ Laminate

Table VIII

Percent Reduction in Bifurcation Load
at 300 F and T^* = 0.5

Laminate	Moisture Condition 1	2	3
[0.,45.,-45.,90.]S	13.4	15.5	21.3
[90.,45.,-45.,0.]S	15.9	17.7	24.5
[45.,-45.]2S	20.6	29.9	42.7

The change in boundary conditions did not significantly change the panels' bifurcation loads. Comparisons of the calculated $\bar{N}_x$s for the two boundary conditions are shown in Table IX. These results are shown for the original room temperature values and the worst case values at 300 F and T^* = 0.5 for moisture condition 1.

Table IX

Change in $\bar{N}_x$ Due to Changing Boundary Conditions

Moisture Cond. 1, T^* = 0.0, 80 F

Laminate	Boundary Condition Fixed	Simple	Percent Reduction
[0.,45.,-45.,90.]S	514.8	502.8	-2.33
[90.,45.,-45.,0.]S	446.0	444.1	-0.43
[45.,-45.]2S	428.9	421.6	-1.63

Moisture Cond. 1, T^* = 0.5, 300 F

Laminate	Boundary Condition Fixed	Simple	Percent Reduction
[0.,45.,-45.,90.]S	445.9	434.6	-2.53
[90.,45.,-45.,0.]S	375.3	373.5	-0.48
[45.,-45.]2S	340.4	328.9	-3.78

Moisture conditions 1 and 2 cause the initially symmetric laminate to become unsymmetric. This unsymmetry introduces bending-extension coupling. The influence of this coupling can be seen in Figs 16, 17, and 18. For the $[0.,45.,-45.,90.]_S$ laminate and the $[90.,45.,-45.,0.]_S$ laminate, this coupling does not significantly change the panels' $\bar{N}_x$. There is only a three percent difference between the two moisture conditions for these two laminates. The difference between the two conditions for the $[45.,-45.]_{2S}$ laminate is 10 percent at 300 F and a time of 0.5. The influence of the coupling stiffnesses is greater for this laminate because the magnitude of the B_{ij} terms are larger than they were for the other two laminates while the magnitude of this laminate's A_{ij} and D_{ij} terms are generally smaller.

To evaluate the influence of panel radius on the moisture- and temperature-caused reductions, the 20 cases for moisture condition 1 for the $[0.,45.,-45.,90.]_S$ panel were rerun with radii of 24 in. (Cases 601-620) and 48 in. (Cases 701-720). As expected, the panel's original $\bar{N}_x$ reduced with increasing radii. $\bar{N}_x$ changed from 514.8 lbs. at a 12 in. radius to 290.8 lbs. at a 24 in. radius to 170.3 lbs. at a 46 in. radius. The percentage of reduction from this original $\bar{N}_x$ did not significantly vary from those for the 12 in. radius panel. This indicates that the moisture- and temperature-caused reductions are not significantly influenced by panel radius; hence, the results obtained for

the 12 in. radius panel should be valid for any radius within the limits of a shallow shell.

Pre-Buckled Displacement Characteristics

Unlike flat plates and straight columns, the cylindrical shell experiences normal displacements and rotations prior to buckling. The pre-buckled displacements for the three panels were very similar with the differences being one of magnitude. For the $[0.,45.,-45.,90.]_S$ and $[90.,45.,-45.,0.]_S$ panels, the displacements were small and within the limits of the small displacement assumptions. The displacements for the $[45.,-45.]_{2S}$ panel were an order of magnitude larger. A typical plot of the pre-buckled displacement geometry for the $[0.,45.,-45.,90.]_S$ panel is shown in Fig 19. This is a plot for Case No. 20 of the U, V, W resultant component displacements. The scale factor is 20,000. Contour plots representing lines of constant displacement or rotations for the U, V, W, RU, and RV displacements and rotations for this case are shown in Figs 20-24. The numbers adjacent to the contour lines signify the percentage of maximum displacement that that contour line represents. The influence of the fixed boundary conditions are clearly shown in the contour plots. Additional displacement and contour plots for representative cases for each ply orientation and boundary condition are included in Appendix C.

The ply orientation and boundary conditions controlled

the overall shape of the pre-buckled displacement. The moduli degradations due to moisture and temperature did not change the displacement shape, but did influence the magnitude of the displacements. Figure 25 shows the W displacements along row 8, which is in the circumferential direction. Comparison plots for several cases representing both fixed and simple boundary conditions for the $[0.,45.,-45.,90.]_S$ laminate are shown. Similar plots for the $[90.,45.,-45.,0.]_S$ laminate are shown in Fig 26.

CASE NO. 20
PLOT NO. 1, UNIT 0, STEP 0
DISPLACEMENT GEOMETRY
UVW COMPONENT
MODEL SCALE = .5000E+00, ORIENT. = 0.00, 60.00,
SOLUTION SCALE = .2000E+05

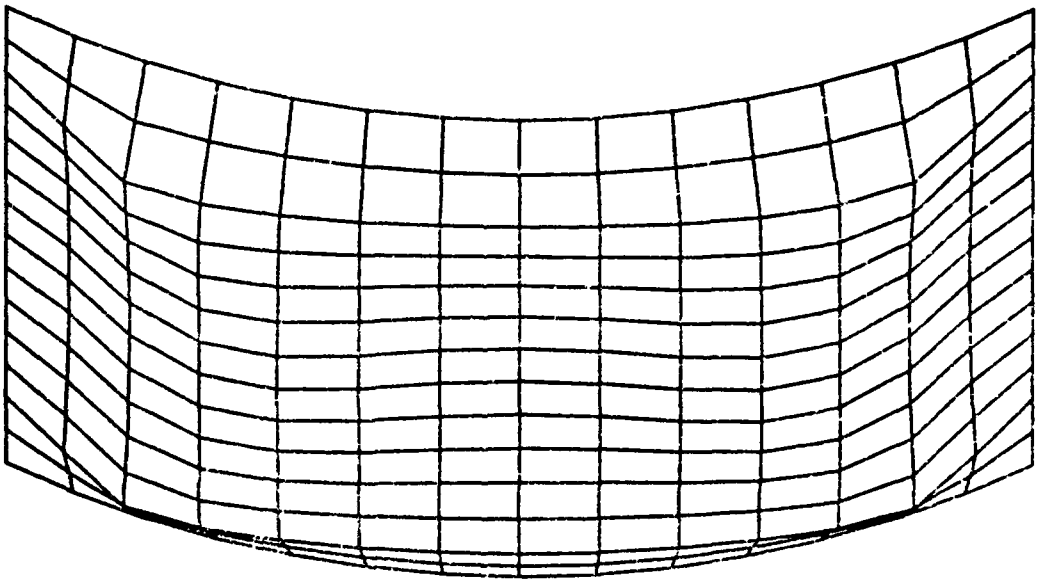

Figure 19. Pre-Buckled Displacement Geometry for $(0.,45.,-45.,90.)_S$ Laminate

CASE NO. 20
PLOT NO. 3, UNIT 1, STEP 0
DISPLACEMENT CONTOURS
U COMPONENT

MODEL SCALE = .5000E+00. ORIENT. = 0.00, 0.00,
SOLUTION SCALE = .2273E+07

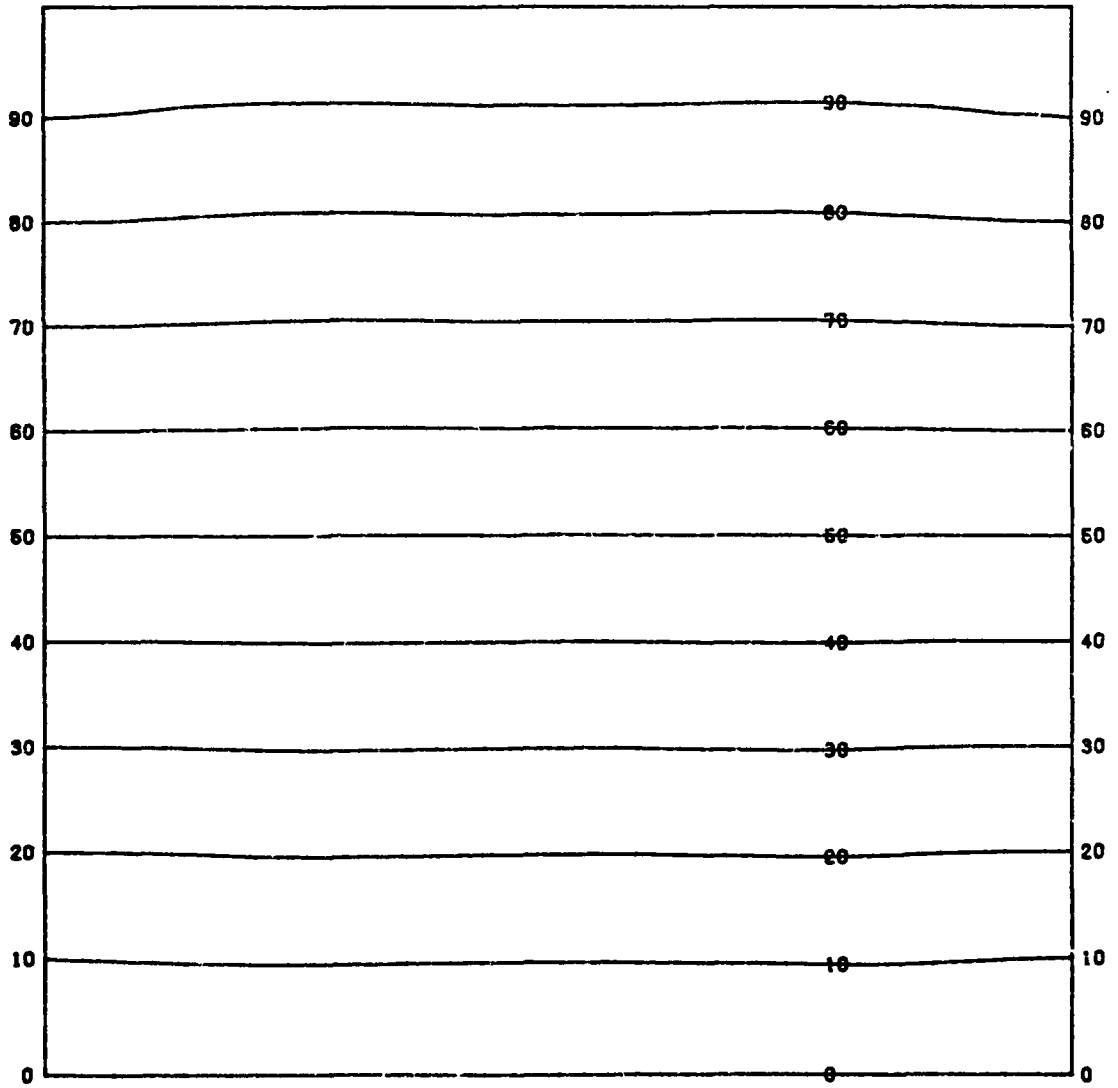

Figure 20. U Component Displacement Contour Plot for $(0.,45.,-45.,90.)_S$

CASE NO. 20
PLOT NO. 4. UNIT 1. STEP 0
DISPLACEMENT CONTOURS
V COMPONENT
MODEL SCALE = .5000E+00. ORIENT. = 0.00. 0.00.
SOLUTION SCALE = .9486E+08

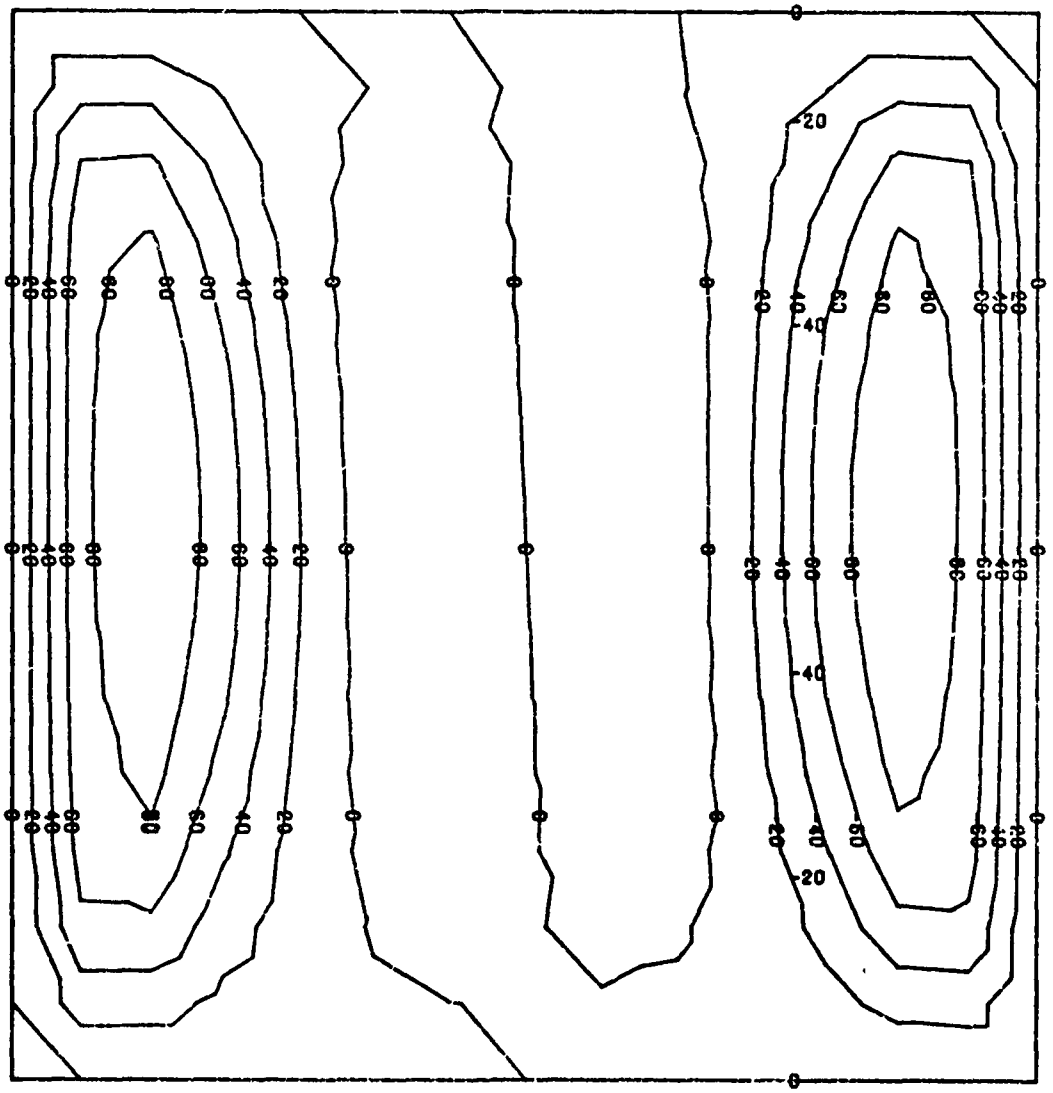

Figure 21. V Component Displacement Contour Plot for $(0.,45.,-45.,90.)_S$

CASE NO. 20
PLOT NO. 5, UNIT 1, STEP 0
DISPLACEMENT CONTOURS
W COMPONENT

MODEL SCALE = .5000E+00, ORIENT. = 0.00, 0.00,
SOLUTION SCALE = .4701E+07

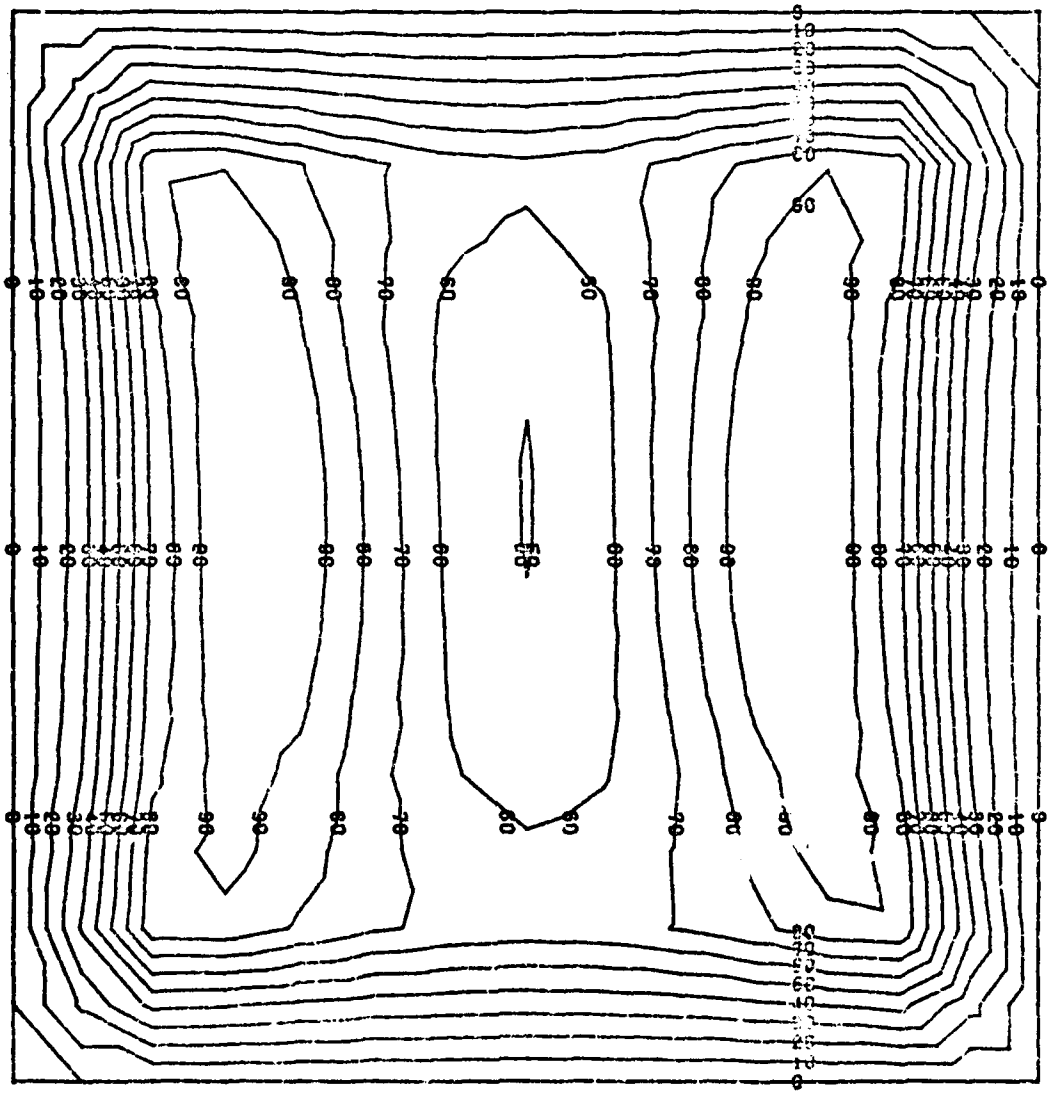

Figure 22. W Component Displacement Contour Plot for $(0.,45.,-45.,90.)_S$

CASE NO. 20
PLOT NO. 6, UNIT 1, STEP 0
DISPLACEMENT CONTOURS
RU COMPONENT

MODEL SCALE = .5000E+00, ORIENT. = 0.00, 0.00,
SOLUTION SCALE = .4767E+07

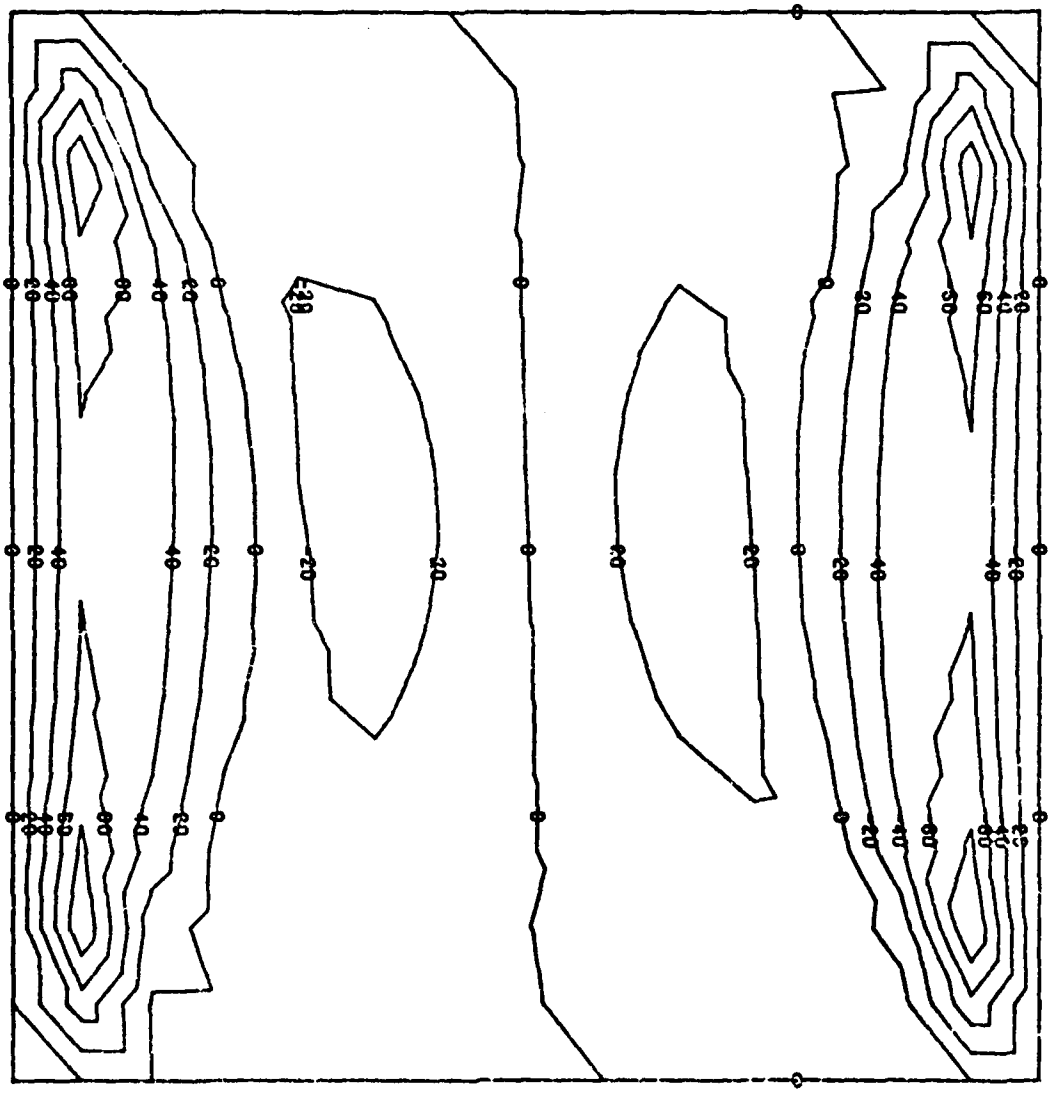

Figure 23. RU Component Displacement Contour Plot for $(0.,45.,-45.,90.)_S$

CASE NO. 20
PLOT NO. 7, UNIT 1, STEP 0
DISPLACEMENT CONTOURS
RV COMPONENT

MODEL SCALE = .5000E+00, ORIENT. = 0.00, 0.00,
SOLUTION SCALE = .4790E+07

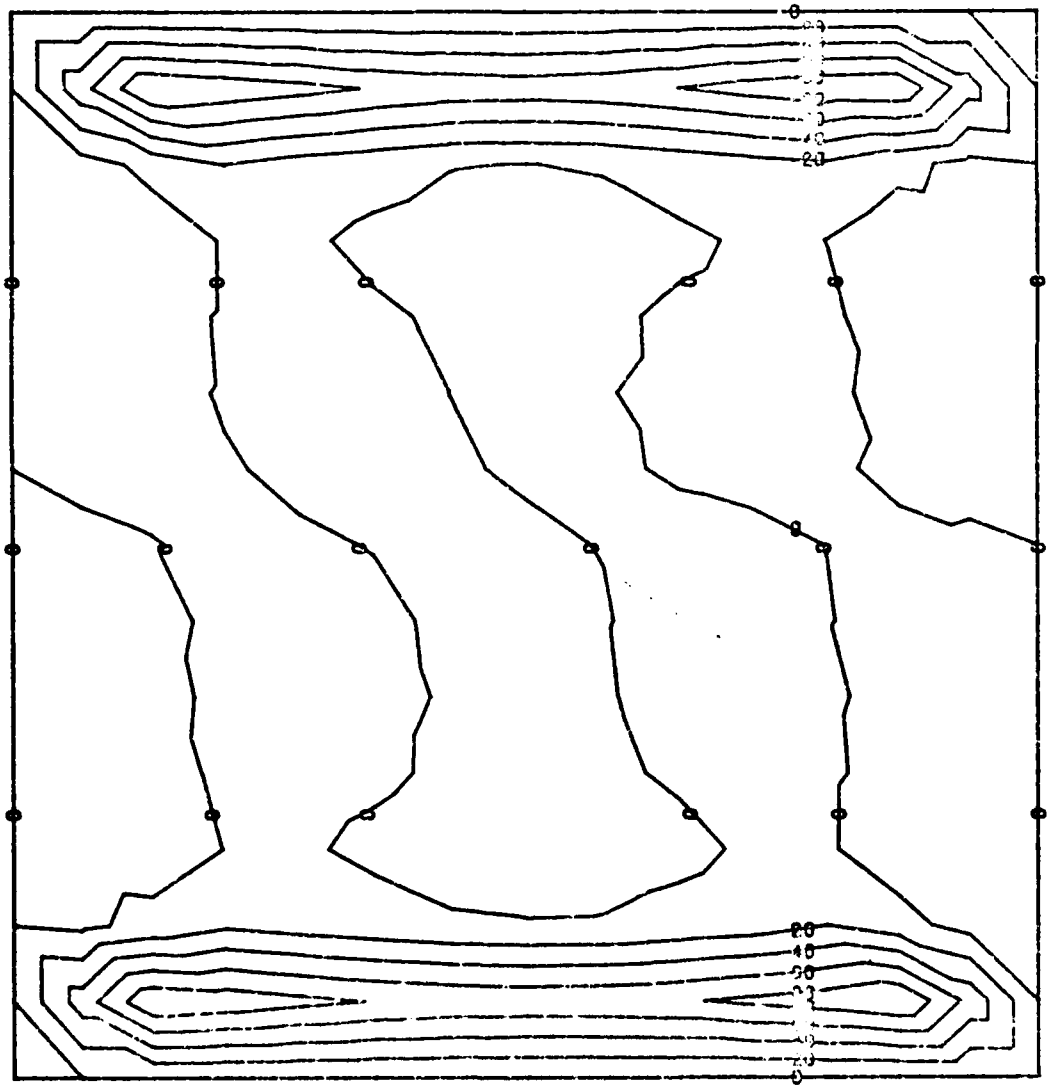

Figure 24. RV Component Displacement Contour Plot for $(0.,45.,-45.,90.)_S$

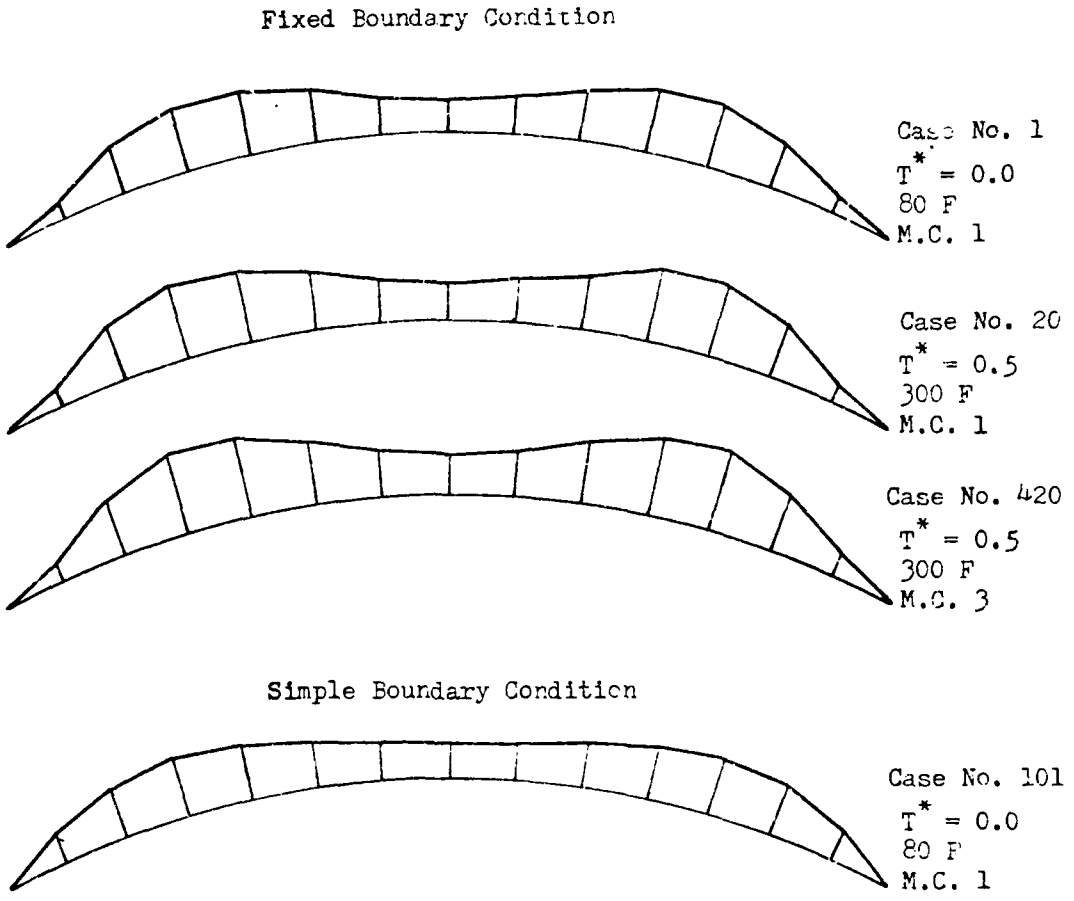

Note: Displacements are of magnitude 10^{-4} (in.) for a unit axial load; M.C. is the moisture condition.

Figure 25. Comparison of Pre-buckled W Displacements for $(0.,45.,-45.,90.)_S$ Laminate

$(0.,45.,-45.,90.)_S$ Fixed Boundary Condition

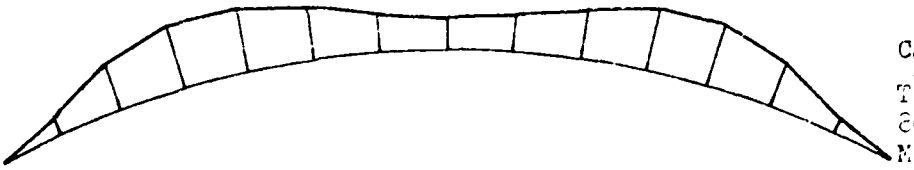

Case No. 1
T^* = 0.0
80 F
M.C. 1

$(90.,45.,-45.,0.)_S$ Fixed Boundary Condition

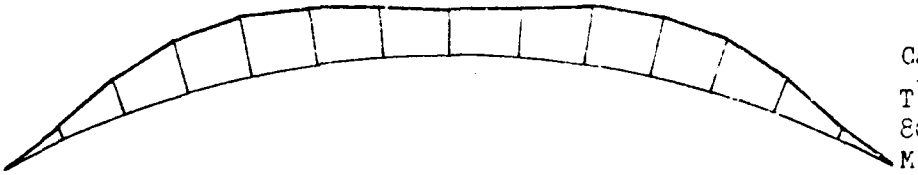

Case No. 21
T^* = 0.0
80 F
M.C. 1

$(90.,45.,-45.,0.)_S$ Simple Boundary Condition

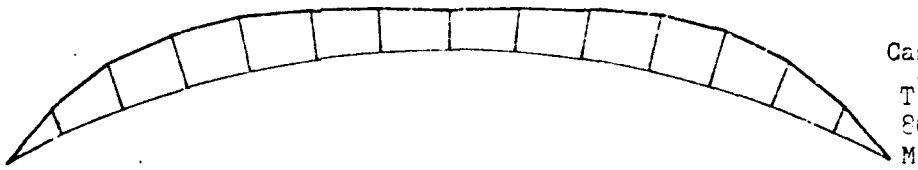

Case No. 121
T^* = 0.0
80 F
M.C. 1

$(90.,45.,-45.,0.)_S$ Fixed Boundary Condition

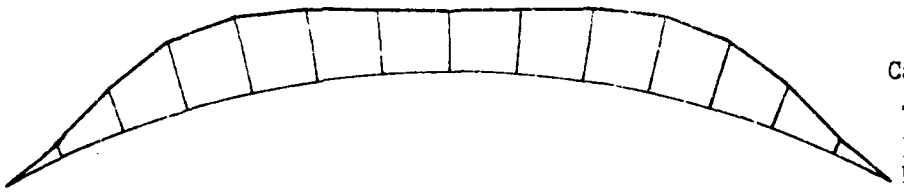

Case No. 440
T^* = 0.5
300 F
M.C. 3

Note: Displacements are of magnitude 10^{-4} (in.) for a unit axial load; M.C. is the moisture condition.

Figure 26. Comparison of Pre-buckled W Displacements for $(0.,45.,-45.,90.)_S$ and $(90.,45.,-45.,0.)_S$ Laminates

In comparing the plots for the two laminates, it is seen that the $[0.,45.,-45.,90.]_S$ laminate develops a moderate but significant hump along the vertical edge for the fixed boundary condition. In Table X, the D_{ij} bending stiffnesses for these two laminates are shown.

Table X

Bending Stiffnesses for the $[0.,45.,-45.,90.]_S$ and $[90.,45.,-45.,0.]_S$ Laminates at 80 F and $T^* = 0.0$

	$[0.,45.,-45.,90.]_S$	$[90.,45.,-45.,0.]_S$
D_{11}	0.72001E02	0.19337E02
D_{12}	0.11012E02	0.11012E02
D_{16}	0.43887E01	0.43887E01
D_{22}	0.19337E02	0.72001E02
D_{26}	0.43887E01	0.43887E01
D_{66}	0.13297E02	0.13297E02

The only difference between the two laminates is the D_{11} and D_{22} values. Since the A_{ij} values are the same and the B_{ij} values are zero for this case, it appears that the larger hump in the $[0.,45.,-45.,90.]_S$ laminate is because its D_{22} stiffness is smaller than the $[90.,45.,-45.,0.]_S$ laminate. It is possible that these two humps may be acting as two connected cylindrical panels with a smaller effective radius which, along with the larger D_{11} stiffness [illegible] laminate, provides the additional [illegible] the $[0.,45.,-45.,90.]_S$

laminate to have a higher bifurcation load.

The simple supported boundary condition does not provide rotational restraint along the vertical edges. The plots for Case No. 101 and 121 in Figs 25 and 26 show these boundary conditions. The simple supported edge reduces the size of the hump in each case but the $[0.,45.,-45.,90.]_S$ laminate appears to have a slightly smaller effective radii which results in a higher bifurcation load.

The shape of the pre-buckled displacement for the $[45.,-45.]_{2S}$ laminate is similar to those for the other two laminates. However, the displacements are an order of magnitude larger. Figure 27 shows the displacement plot of the U, V, W displacement component at the same scale factor as the previous plot. Figure 28 shows the plots of the W displacement in the circumferential direction. The drastic change in magnitude of the W displacement is clearly seen by comparing Case No. 460 with Case No. 41.

In order to determine which of the reductions in moduli is causing the large deflections for the $[45.,-45.]_{2S}$ laminate, two STAGS-C1 runs were made in which, separately, the E_2 and G_{12} moduli were reduced to 20 percent of the original values. Plots for the W displacement in the circumferential direction for both fixed and simple boundary conditions are shown in Fig 29. The reduction in the G_{12} moduli causes significantly larger displacements than a reduction in E_2 does. This rapid increase in displacement with reduced moduli explains the large reductions in $\bar{N}_x$

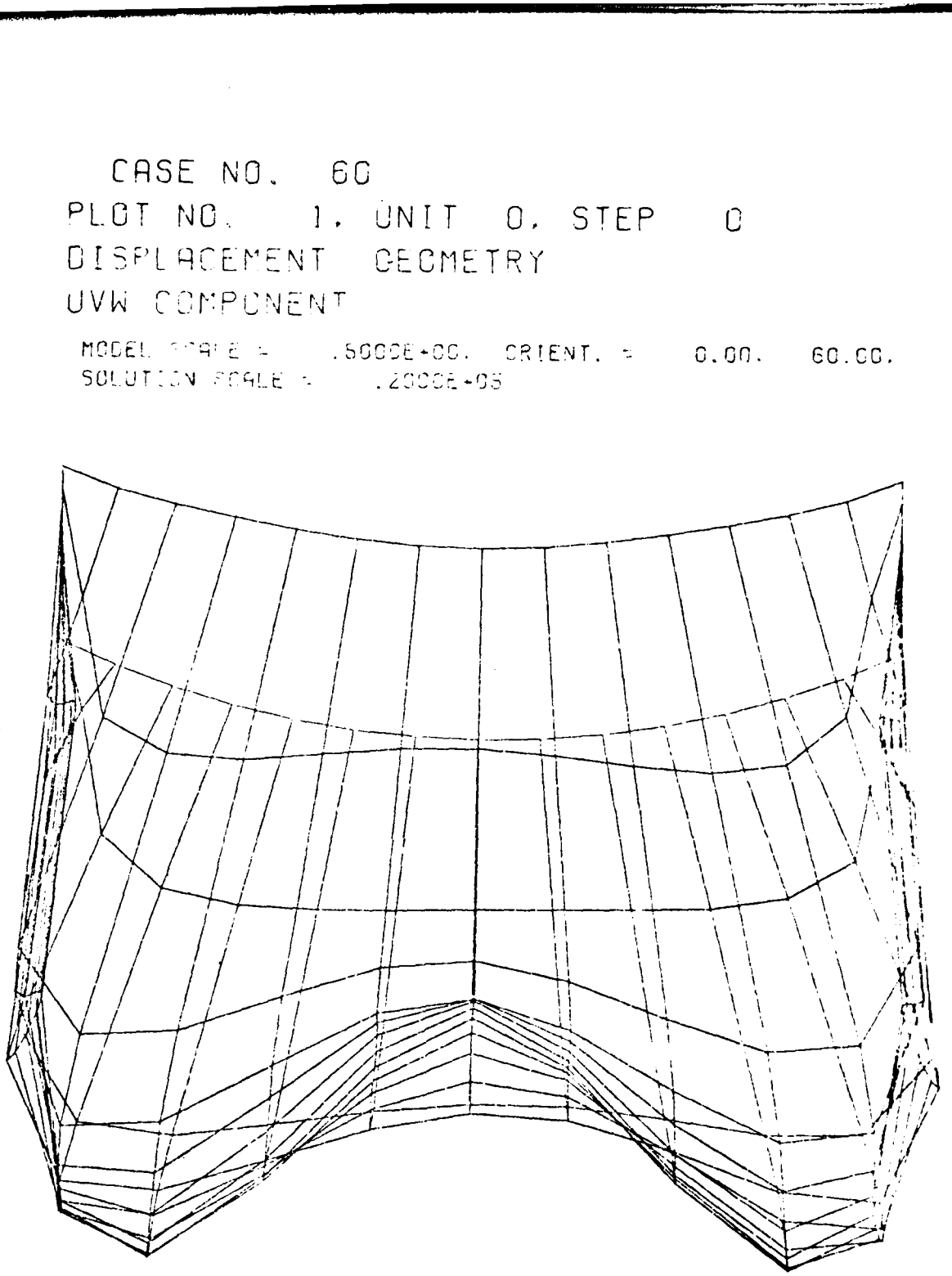

Figure 27. Pre-buckled Displacement Geometry for $(+45.,-45.)_{2S}$ Laminate

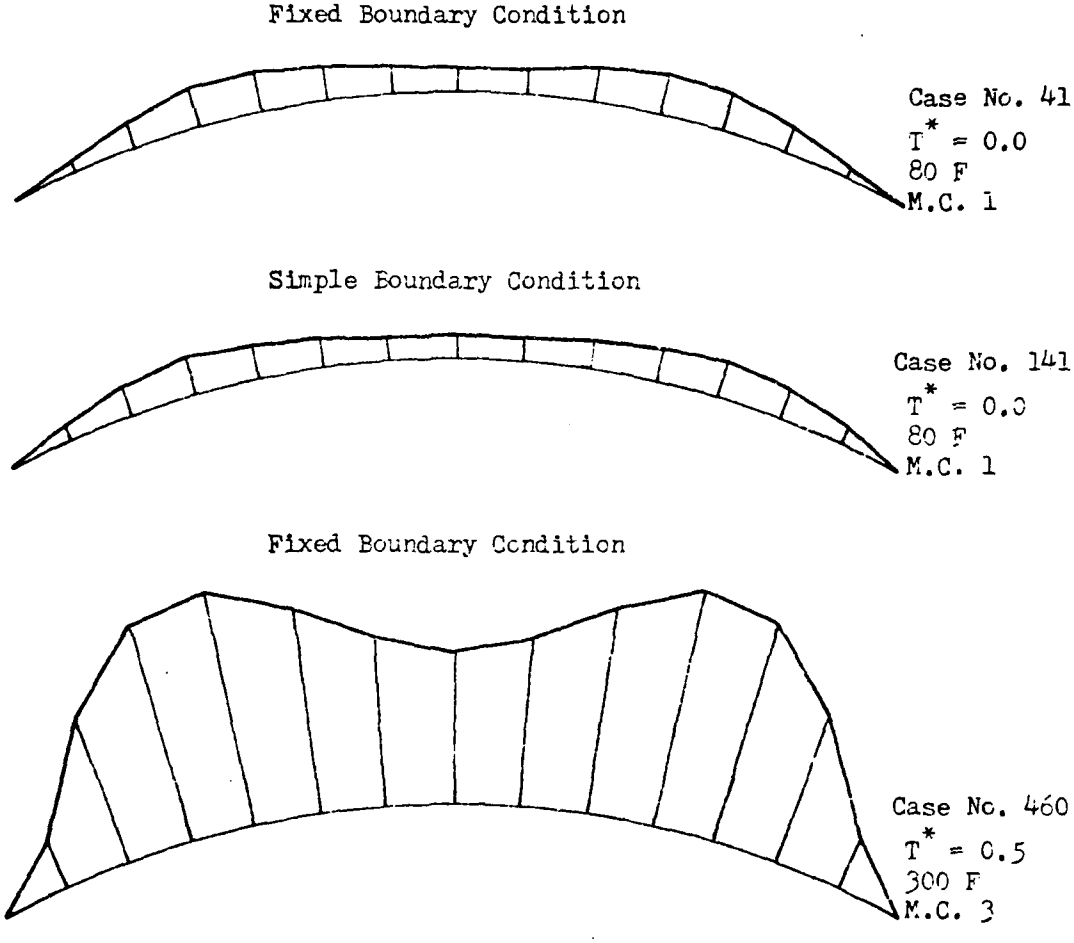

Note: Displacements are of magnitude 10^{-3} (in.) for a unit axial load; M.C. is the moisture condition.

Figure 28. Comparison of Pre-buckled W Displacements for $(45. -45.)_{2S}$ Laminate

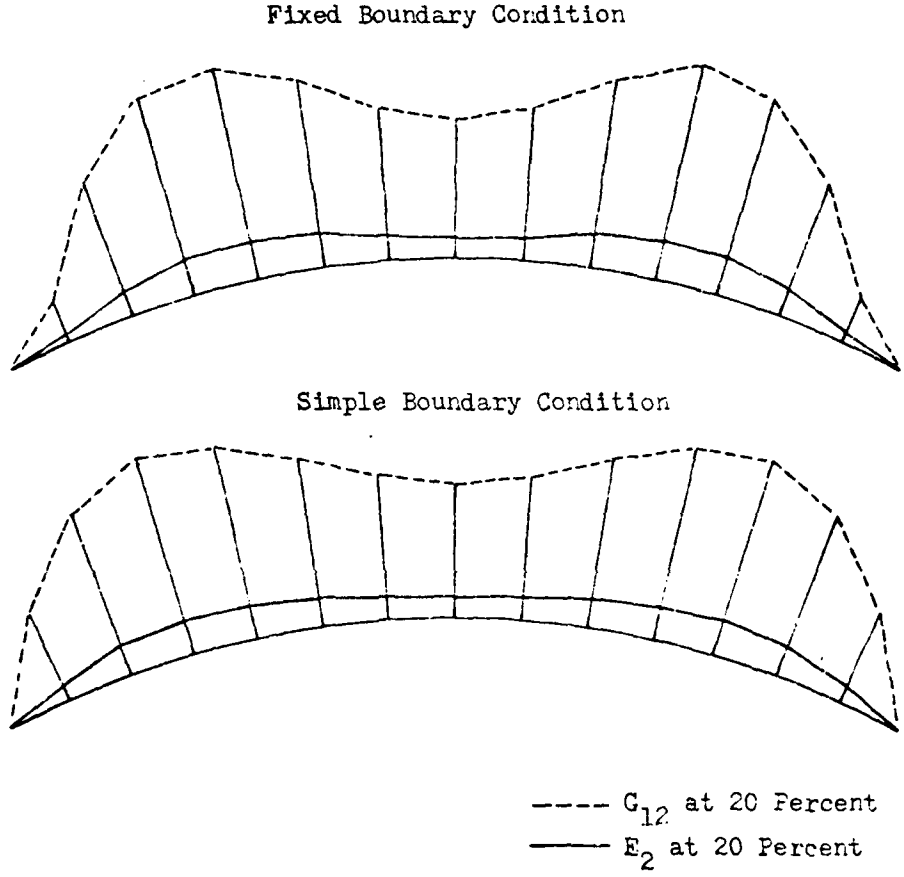

Note: Displacements are of magnitude 10^{-3} (in.) for a unit axial load.

Figure 29. Comparison of Pre-Buckled W Displacements with E_2 and G_{12} Reduced to 20 Percent for the $(45.,-45.)_{2S}$ Laminate

noted above.

The maximum displacements for the $[45.,-45.]_{2S}$ laminate, at the bifurcation load, are of the order of 10^{-1} with extensional strains of the order of 10^{-2} and rotations approaching 5 degrees. These large displacements are approaching the limits of small displacement theory associated with the choice of the bifurcation analysis used in this analysis displacement. A more rigorous analysis using the STAGS-C finite difference program with a non-linear buckling analysis would be appropriate for this laminate.

Eigenvector

Each of the three laminates has a distinctive eigenvector. Displacement and contour plots for each laminate's eigenvector are shown in Figs 30-35. The amplitude of the eigenvector in the displacement plots has been exagerated to show the shape.

The $[0.,45.,-45.,90.]_S$ laminate develops a series of waves that are oriented with the direction of the outer 45 degree plies. The amplitude of the waves increases to a maximum near the center of the panel. Moisture and temperature changes and the boundary conditions do not alter the shape of the eigenvector. The $[90.,45.,-45.,0.]_S$ and $[45.,-45.]_{2S}$ laminates develop a series of axial waves. Again, neither the temperature and moisture changes or the boundary conditions alter the shape of the eigenvector.

CASE NO. 20
PLOT NO. 2. UNIT 0. STEP 0
EIGENVECTOR GEOMETRY
UVW COMPONENT , MODE 1
MODEL SCALE = .5000E+00. ORIENT. = 0.00. 60.00.
SOLUTION SCALE = .5000E+00

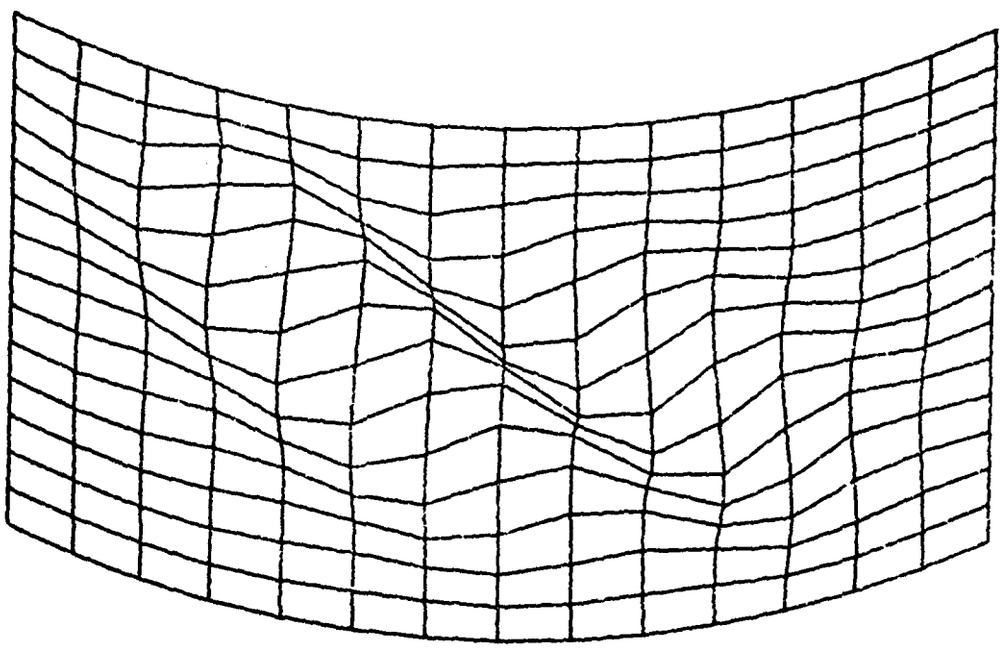

Figure 30. Eigenvector Geometry for $(0.,45.,-45.,90.)_S$ Laminate

CASE NO. 20
PLOT NO. 10, UNIT 1, STEP 0
EIGENVECTOR CONTOURS
W COMPONENT , MODE 1
MODEL SCALE = .5000E+00, ORIENT. = 0.00, 0.00,
SOLUTION SCALE = .3497E+02

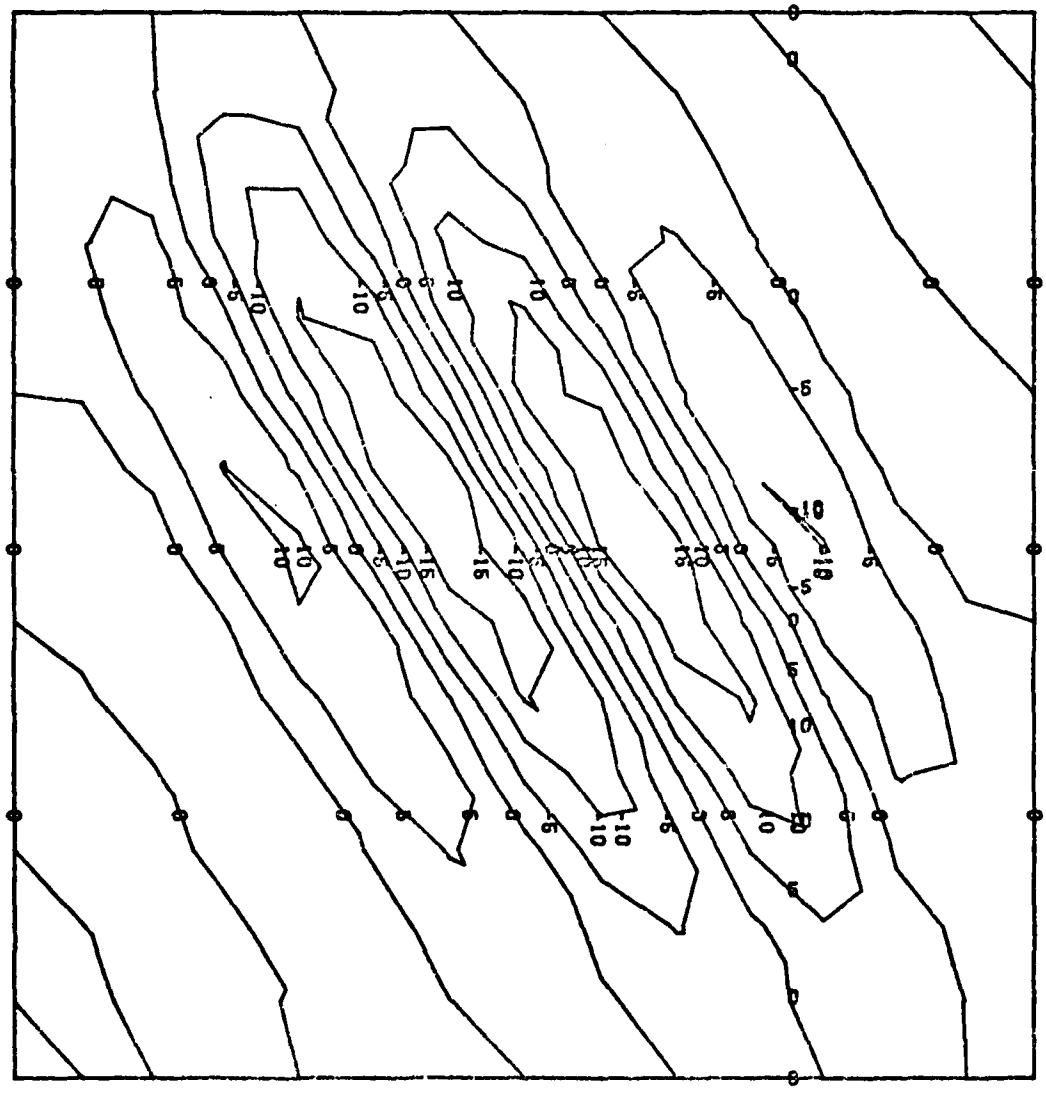

Figure 31. Contour Plot of W Component of the Eigenvector for the $(0.,45.,-45.,90.)_S$ Laminate

CASE NO. 21
PLOT NO. 2. UNIT 0. STEP 0
EIGENVECTOR GEOMETRY
UVW COMPONENT , MODE 1
MODEL SCALE = .5000E+00, ORIENT. = 0.00, 60.00,
SOLUTION SCALE = .5000E+00

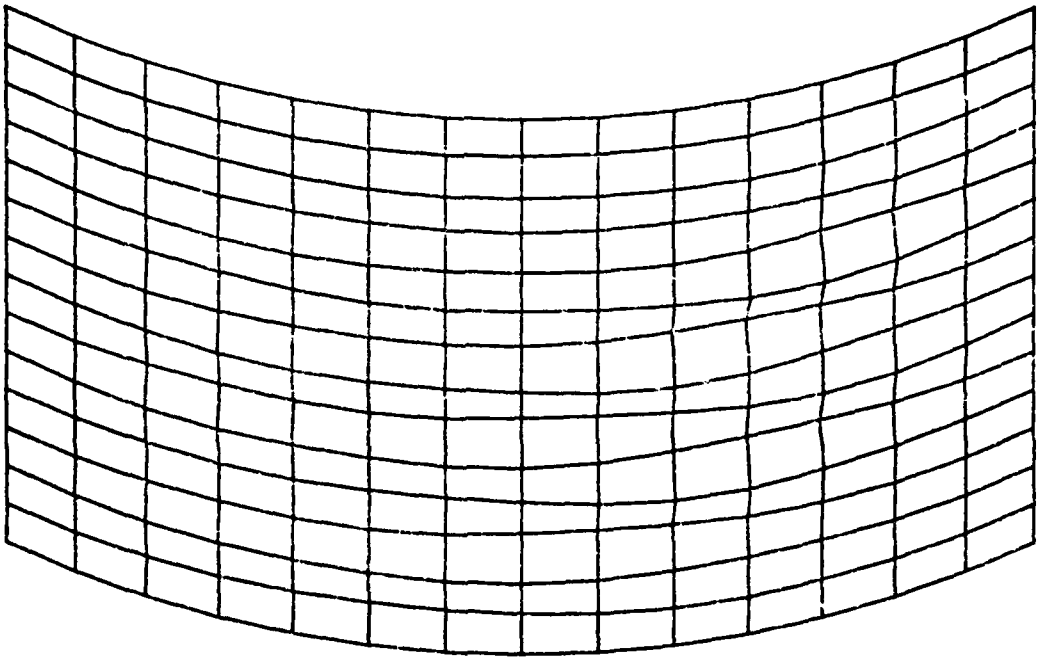

Figure 32. Eigenvector Geometry for $(90.,45.,-45.,0.)_S$ Laminate

CASE NO. 21
PLOT NO. 10, UNIT 1, STEP 0
EIGENVECTOR CONTOURS
W COMPONENT , MODE 1
MODEL SCALE = .5000E+00, ORIENT. = 0.00, 0.00,
SOLUTION SCALE = .1529E+03

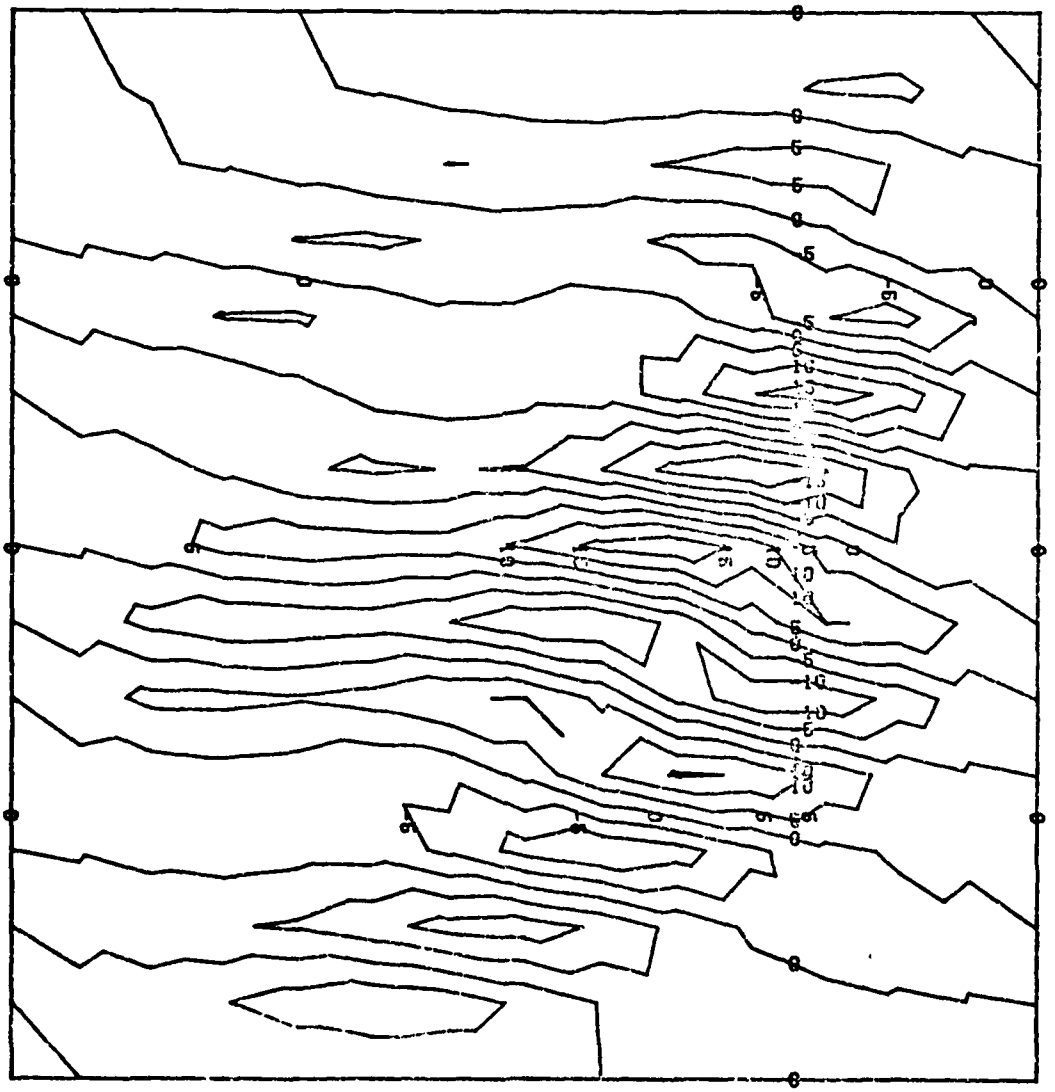

Figure 33. Contour Plot of W Component of the Eigenvector for the $(90.,45.,-45.,0.)_S$ Laminate

CASE NO. 41
PLOT NO. 2, UNIT 0, STEP 0
EIGENVECTOR GEOMETRY
UVW COMPONENT , MODE 1
MODEL SCALE = .5000E+00. ORIENT. = 0.00. 60.00.
SOLUTION SCALE = .8000E+00

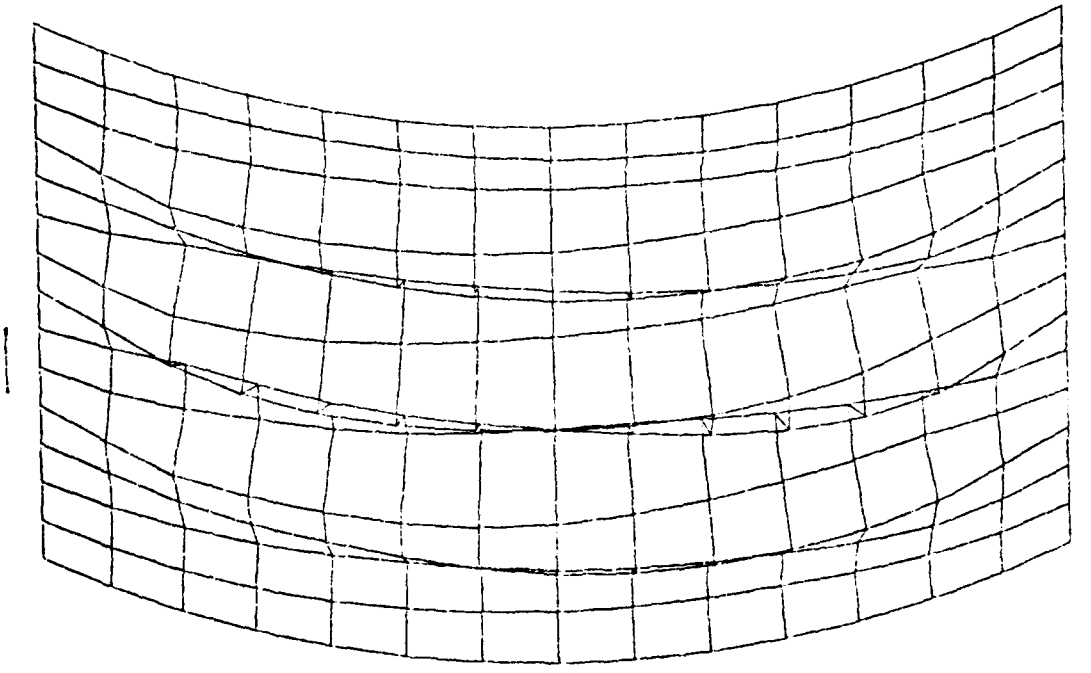

Figure 34. Eigenvector Geometry for $(45.,-45.)_{2S}$ Laminate

CASE NO. 41
PLOT NO. 10, UNIT 1, STEP 0
EIGENVECTOR CONTOURS
W COMPONENT , MODE 1

MODEL SCALE = .5000E+00. ORIENT. = 0.00. 0.00.
SOLUTION SCALE = .5511E+02

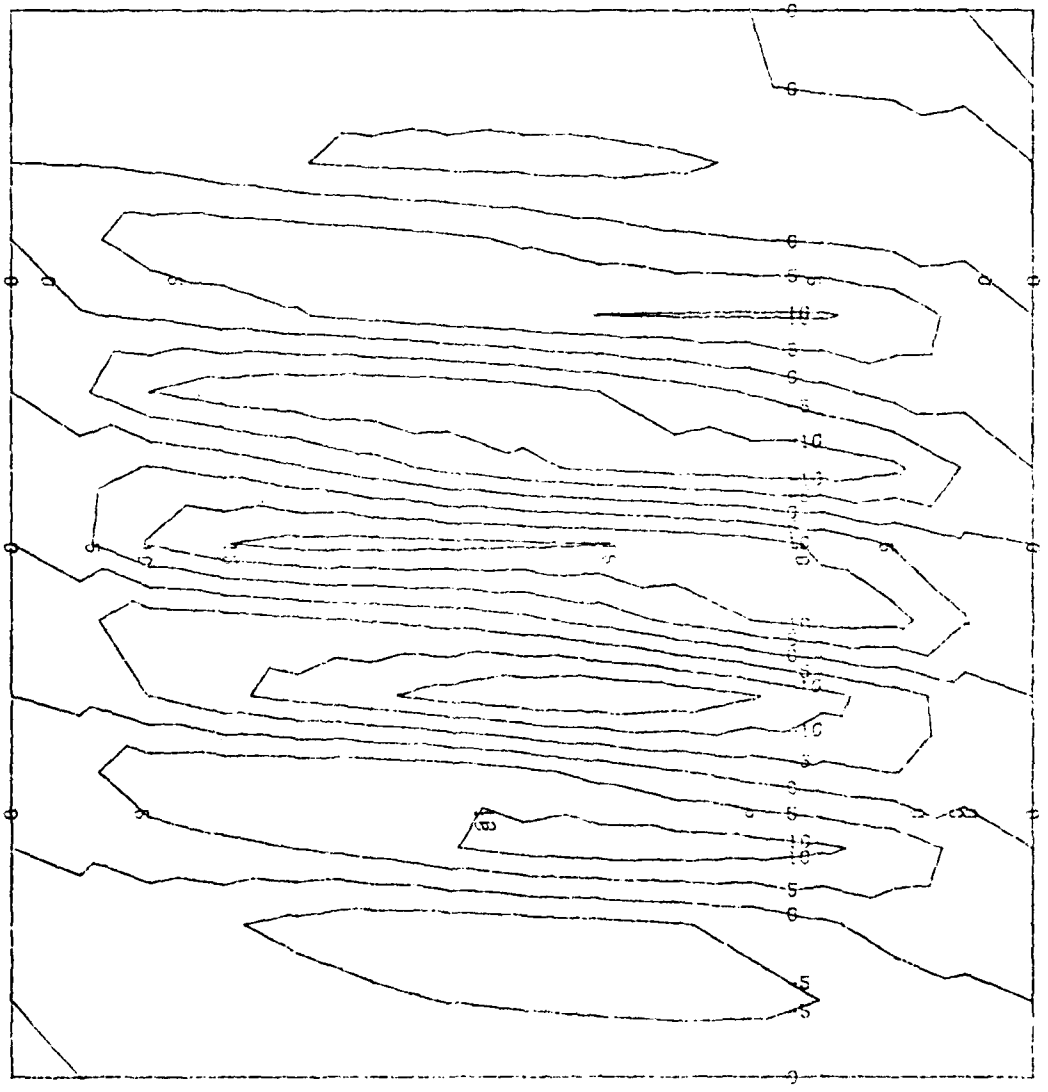

Figure 35. Contour Plot of W Component of the Eigenvector for the $(45.,-45.)_{2S}$ Laminate

Linear Approximation of Reductions in the Bifurcation Load

The W and U displacements for the $[0.,45.,-45.,90.]_S$ and $[90.,45.,-45.,0.]_S$ laminates were found to vary approximately linearly with the changes in $\bar{N}_x$ due to moisture and temperature. Figure 36 shows plots of W, measured at the middle of the panel, and U, measured at the middle of the top edge, vs the $\bar{N}_x$ for the $[0.,45.,-45.,90.]_S$ laminate. The closed symbols represent the fixed boundary conditions and the open symbols represent the simple boundary conditions. The lines connect the symmetric cases, represented by circles, while the triangle represents the unsymmetric moisture condition 1 and the square represents moisture condition 2.

The linear behavior of these plots indicated that the changes in $\bar{N}_x$ due to moisture and temperature could be approximated by a linear function. It was noted previously that several additional STAGS-C1 runs were made with the E_2 and G_{12} moduli individually reduced for the $[45.,-45.]_{2S}$ laminate. Similar runs were also made for the $[0.,45.,-45.,90.]_S$ and $[90.,45.,-45.,0.]_S$ laminates. A plot of the results, Fig 37, showed that $\bar{N}_x$ was almost a linear function of the reductions in moduli. Linear relationships between the reduced E_2 and G_{12} moduli and $\bar{N}_x$ were developed. In these equations, the $\bar{N}_x$ is calculated as a function of the reduced moduli which is represented as a percentage of the original moduli value. By combining these two linear functions, one equation relating the $\bar{N}_x$ to the reduced

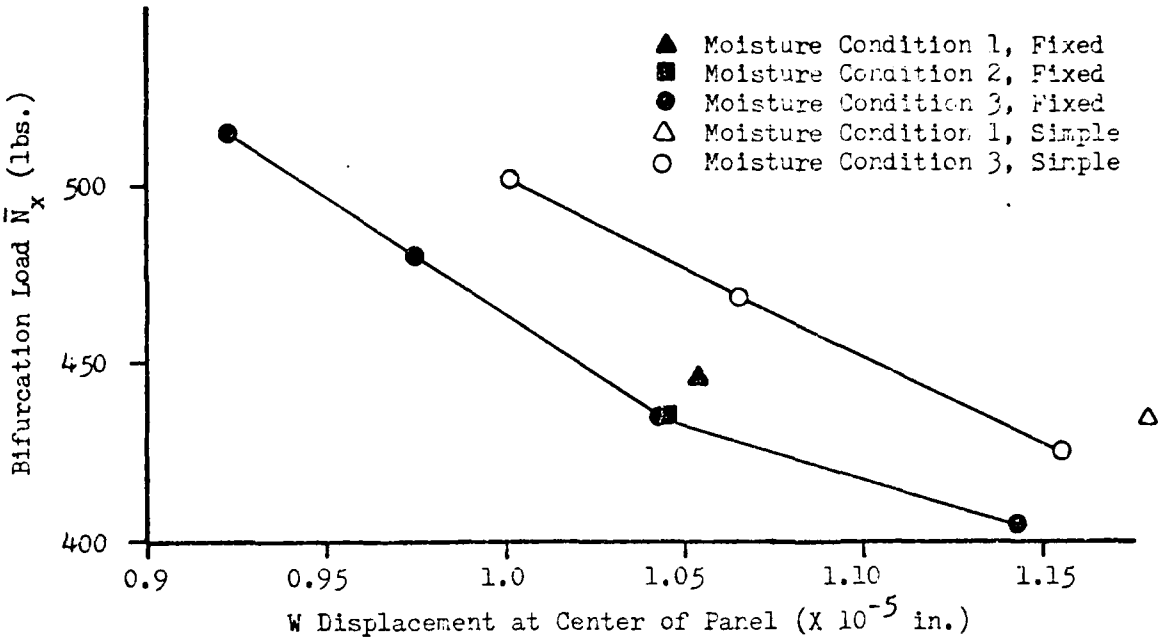

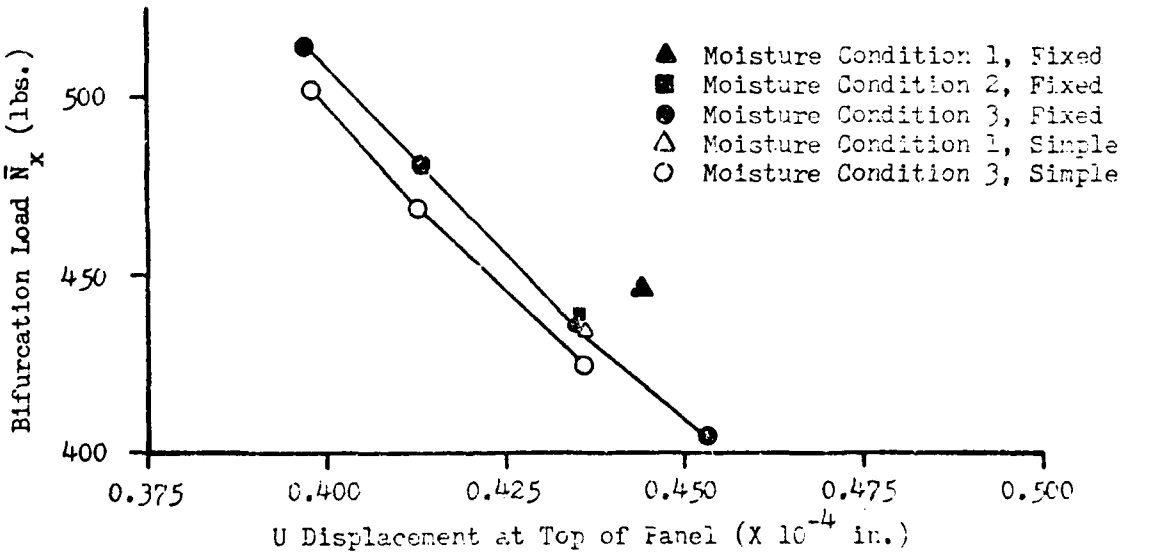

Figure 36. Bifurcation Load vs Axial and Radial Displacements for $(0.,+45.,-45.,90.)_S$ Laminate

AD-A111 127 AIR FORCE INST OF TECH WRIGHT-PATTERSON AFB OH SCHOO--ETC F/G 1/3
MOISTURE AND TEMPERATURE EFFECTS ON THE INSTABILITY OF CYLINDRI--ETC(U)
DEC 81 J M SNEAD

UNCLASSIFIED AFIT/GAE/AA/81D-29 NL

2 OF 2
AD A111 127

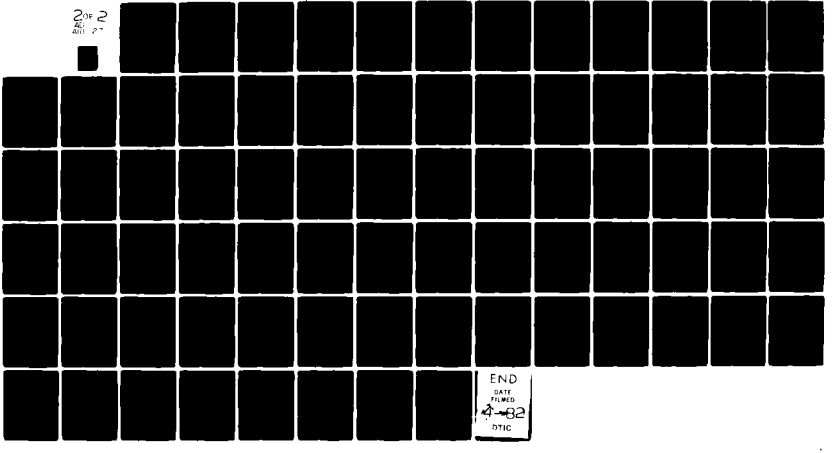

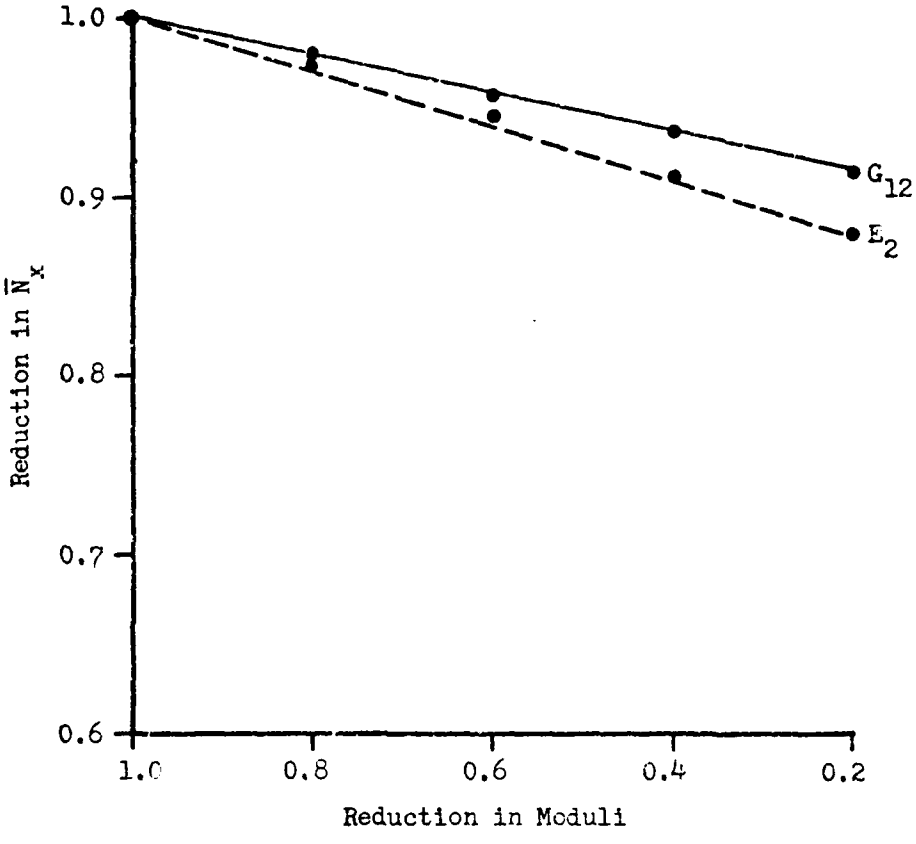

Figure 37. Influence of E_2 and G_{12} Degradation on N_x for $(0.,45.,-45.,90.)_S$ Laminate

moduli was developed. This equation is dependent upon the ply orientations and boundary conditions, but independent of the time, temperature, moisture concentrations, or panel radius within the limits discussed above.

To calculate the $\bar{N}_x$ at a particular time and temperature, the Fick equation is used to calculate the moisture concentration distribution through the thickness. Using these values and the temperature, the reduced moduli are determined from the test data. An average reduced moduli value, represented as a percentage of the original moduli, is calculated for the laminate for both E_2 and G_{12}. These values are input into the equation for the particular laminate ply orientations and boundary conditions. The panel's $\bar{N}_x$, as a percentage of the original $\bar{N}_x$, is calculated.

The three ply orientations and two boundary conditions used in this thesis require six equations to predict the $\bar{N}_x$. The general form of the equation is shown below along with a table of the slope and intercept values for each of the six cases.

$$\bar{N}_x = m_1 E_2 + b_1 + m_2 G_{12} + b_2 - 100$$

where: $\bar{N}_x$ - reduced bifurcation load expressed as percentage of the original $\bar{N}_x$

E_2 - reduced transverse moduli expressed as percentage of the original E_2

G_{12} - reduced shear moduli expressed as a percentage of the original G_{12}

For the reasons discussed previously, this equation does not include the effects of any change in E_1 or ν_{12}. However, the equation could be modified to include these changes.

Table XI

Slope and Intercept Values

Laminate	E_2		G_{12}	
	m_1	b_1	m_2	b_2
$[0.,45.,-45.,90.]_S$				
Fixed	0.1532	84.68	0.1094	89.06
Simple	0.1554	84.46	0.1099	89.01
$[90.,45.,-45.,0.]_S$				
Fixed	0.2099	79.01	0.1031	89.69
Simple	0.2097	79.03	0.1044	89.56
$[45.,-45.]_{2S}$				
Fixed	0.0772	92.28	0.4616	53.84
Simple	0.0759	92.41	0.4776	52.24

The values of m_1 and m_2 allow comparisons to be made of how equal changes in the values of E_2 and G_{12} influence the change in $\bar{N}_x$. It was noted above that the $[90.,45.,-45.,0.]_S$ laminate loses more buckling strength than the $[0.,45.,-45.,90.]_S$ laminate does for each moisture and temperature conditions. From the above values of m_1 and m_2 for these two laminates, the apparent reason for this is that the m_1 for the $[90.,45.,-45.,0.]_S$ laminate is about 30 percent larger than the m_1 value for the $[0.,45.,-45.,90.]_S$

laminate. Thus for equal changes in E_1, the $[90.,45.,-45.,0.]_S$ laminate's bifurcation load degrades more rapidly.

The comparison between the m_1 and m_2 values for the $[45.,-45.]_{2S}$ laminate supports the conclusion reached above that the change in G_{12} is the major cause of the large reductions in this panel's $\bar{N}_x$.

Comparisons of the $\bar{N}_x$ values calculated using this equation and the STAGS-C1 calculated $\bar{N}_x$ values for Cases 1-20 are shown below. Additional tables of comparisons for other cases are shown in Appendix D. In most cases, the maximum error was less than 5 percent. However, in some of the $[45.,-45.]_{2S}$ cases, the error reached 10 percent. This may be because, at the higher temperatures and moisture conditions, the resulting large displacements and rotations are influencing the accuracy of the STAGS-C1 program.

Table XII

Comparison of Predicted and Calculated $\bar{N}_x$ Values

Case No.	STAGS-C1 $\bar{N}_x$ Value	Predicted $\bar{N}_x$ Value	Percent Error
1	514.8	514.80	.00
2	514.2	514.54	.07
3	512.5	513.59	.21
4	510.5	510.99	.10
5	509.7	509.57	-.03
6	493.3	492.23	-.22
7	492.1	491.64	-.09
8	488.7	489.34	.13
9	484.5	483.07	-.30
10	482.3	479.47	-.59
11	482.3	481.10	-.25
12	479.8	479.78	.00
13	472.3	474.71	.51
14	462.8	460.86	-.42
15	458.0	452.93	-1.11
16	480.4	479.19	-.25
17	477.1	477.35	.05
18	466.8	470.05	.70
19	453.2	450.20	-.66
20	445.9	438.59	-1.64

VI. Conclusions

On the basis of the finite element analysis, the following conclusions can be made for cylindrical, composite panels subject to moisture exposure and elevated temperatures and loaded in axial compression.

1. The results of the STAGS-C1 finite element analysis, using modified flat plate elements, compare well with the STAGS-C finite difference analysis, using a curved surface representation, in predicting the bifurcation load of cylindrical panels using the linear pre-buckled displacement analysis mode.

2. The simpler 4 noded quadrilateral finite element (SH410) had better convergence characteristics, was more economical to use, and yielded results comparable to the 4 noded quadrilateral with 4 mid-side nodes (SH411) when calculating the panel's bifurcation load.

3. The bifurcation load of a composite panel, with a resin material whose elastic moduli are reduced by absorbed moisture and elevated temperatures, will degrade with increasing moisture concentrations and temperatures.

4. The extent of the degradation in the bifurcation load is influenced by the degree of moisture concentration, the temperature, and the panel's ply orientations. At 300 F and a moisture weight gain of 1.05 percent, the $[0.,45.,-45.,90.]_S$ panel experienced a 21.3 percent degradation, the $[90.,45.,-45.,0.]_S$ panel experienced a 24.5 percent degradation, and the $[45.,-45.]_{2S}$ panel experienced a 42.7

percent degradation.

5. A change in the rotational restraints of the vertical, straight sides, from fully fixed to simple-supported, did not significantly reduce the bifurcation load or change the moisture- and temperature-induced degradation characteristics for a panel aspect ratio of 1.

6. Increasing the cylindrical panel's radius decreased the panel's bifurcation load but did not significantly change the moisture- and temperature-induced degradation characteristics.

7. The bending-extension coupling resulting from the unsymmetric moisture concentration distributions, which resulted in an unsymmetric laminate, did not significantly influence the bifurcation load.

8. The cylindrical panel's bifurcation load is influenced by the ply orientations and the panel's pre-buckled displacements which vary with different ply orientations.

9. The reduction in the bifurcation load due to moisture and temperature was, in general, linearly related to the average reduction in the transverse, E_2, and shear, G_{12}, moduli. A linear relationship can be developed using the results of three STAGS-C1 runs for each ply orientation, panel aspect ratio, and boundary conditions from which the bifurcation load can be calculated from the average E_2 and G_{12} values for any moisture and temperature condition.

Bibliography

1. Wilkins, D. J. "Compression Buckling Tests of Laminated Graphite-Epoxy Curved Panels." AIAA paper no. 74-32. Presented at the AIAA 12th Aerospace Science Meeting: Washington, D. C., January 30 - February 1, 1974

2. Becker, M. L. Analytical/Experimental Investigation of the Instability of Composite Panels. MS Thesis. Wright-Patterson AFB, Ohio: Air Force Institute of Technology, December 1979.

3. Whitney, J. M. and Ashton, J. E. "Effect of Environment on the Elastic Response of Layered Composite Plates," AIAA Journal, 9: 1708-1712 (December 1971).

4. Bergmann, H. W. and Nitsch, J. Predictability of Moisture Absorption in Graphite/Epoxy Sandwich Panels, Institute for Structural Mechanics, German Aerospace Research Establishment (DFVLR), undated.

5. Crossman, F. W. and Flaggs, D. L. Viscoelastic Analysis of Hygrothermally Altered Laminate Stresses and Dimensions. LMSC-D633086, Applied Mechanics Laboratory, Lockheed Palo Alto Research Laboratory, November 1978.

6. Chi-Hung Shen and Springer, G. S. "Effects of Moisture and Temperature on the Tensile Strength of Composite Materials," Journal of Composite Materials, 11: 2-16 (January 1977).

7. The Effects of Relative Humidity and Elevated Temperature on Composite Structures, Transactions of the Workshop on, Sponsored by the Air Force Office of Scientific Research and the Center For Composite Materials, University of Delaware, March 30-31, 1976.

8. Chi-Hung Shen and Springer, G. S. "Environmental Effects on the Elastic Moduli of Composite Materials," Journal of Composite Materials, 11: 250-264 (July 1977).

9. Pipes, R. B., Vinson, J. R., and Tsu-Wei Chou. "On the Hygrothermal Response of Laminated Systems," Journal of Composite Materials, 10: 129-148 (April 1976).

10. McKague, E. L., Halkias, J. E., and Reynolds, J. D. "Moisture in Composites: The Effect of Supersonic Service on Diffusion," Journal of Composite Materials, 9: 2-9 (January 1975).

11. Chi-Hung Shen and Springer, G. S. "Moisture Absorption and Desorption of Composite Materials," Journal of Composite Materials, 10: 2-20 (January 1976).

12. Browning, C. E. "The Mechanisms of Elevated Temperature Property Losses in High Performance Structural Epoxy Matrix Materials After Exposures to High Humidity Environments," Polymer Engineering and Science, 18: 16-24 (January 1978).

13. Browning, C. E., Husman, G. E., and Whitney, J. M. "Moisture Effects in Epoxy Matrix Composites," Composite Materials: Testing and Design (Fourth Conference), ASTM STP 617: 481-496, American Society for Testing and Materials (1977).

14. Bueche, F. Physical Properties of Polymers. New York: Interscience, 1976.

15. Tsai, S. W. Introduction to Composite Materials. Westport, Connecticut: Technomic Publishing Company, 1980.

16. Donnell, L. H. Stability of Thin-walled Tubes under Torsion. NACA Report 479, 1933.

17. Thomas, K. and Sobel, L. H. Evaluation of the STAGS-C1 Shell Analysis Computer Program. Report No. WARD-10881, Westinghouse Electric Corporation, August 1981.

18. Almroth, B. O., Brogan, F. A., and Stanley, G. M. Structural Analysis of General Shells. Volume II, User Instructions For STAGS-C1. LMSC-D633873, Applied Mechanics Laboratory, Lockheed Palo Alto Research Laboratory, July 1979.

19. Almroth, B. O. and Brogan, F. A. Numerical Procedures for Analysis of Structural Shells. AFWAL-TR-80-3129, March 1981.

20. Users Manual for STAGS, Volume 1, Theory. Structural Mechanics Laboratory, Lockheed Palo Alto Research Laboratory, March 1978.

21. Jones, R. M. Mechanics of Composite Materials. New York: McGraw-Hill, 1975.

22. Flaggs, D. L. and Vinson, J. R. Elastic Stability of Generally Laminated Composite Plates Including Hygrothermal Effects. AFOSR-TR-78-1349, July 1977.

23. Crank, J. The Mathematics of Diffusion. Oxford: Clarendon Press, 1975.

Appendix A

Computer Program

```
      PROGRAM MCL (INPUT,OUTPUT,TA[illegible],TAPE7)
C
C JAMES M. S[illegible], [illegible], [illegible] INSTITUTE OF TECHNOLOGY
C THIS PROGRAM WAS DEVELOPED AS A PART OF MY AEROSPACE ENGINEERING
C MASTER'S THESIS.
C
C THIS PROGRAM CALCULATES THE MOISTURE CONCENTRATION THROUGH THE
C THICKNESS OF A COMPOSITE LAMINATE. THIS PROGRAM ALSO CALCULATES THE
C PLY STIFFNESSES [illegible] INVARIANT PROPERTIES, THE PLY'S REDUCED
C STIFFNESSES, AND THE LAMINATE'S [illegible], [illegible], AND [illegible].
C USING THE CALCULATED [illegible], INPUT FILES FOR THE STAGS
C FINITE ELEMENT [illegible] WRITTEN.
C
C     REF. "THE MATHEMATICS OF DIFFUSION" BY J. CRANK, SECOND EDITION,
C          CLARENDON PRESS, [illegible], 197[illegible]
C     REF. "INTRODUCTION TO COMPOSITE MATERIALS" BY STEPHEN W. TSAI AND
C          H. THOMAS HAHN, TECHNOMIC PUBLISHING CO., 19[illegible]
C     REF. "MECHANICS OF COMPOSITE MATERIALS" BY ROBERT M. JONES,
C          MCGRAW-HILL BOOK COMPANY, 19[illegible]
C
C     BASIC MOISTURE DIFFUSION EQUATION - FICK EQUATION (J. CRANK)
C
C                    K*S.D. OF C WRT Z = F.D. OF C WRT T
C              WHERE:
C                    K = MOISTURE DIFFUSION COEFFICIENT
C                    S.D. = SECOND PARTIAL DERIVATIVE
C                    F.D. = FIRST PARTIAL DERIVATIVE
C                    WRT = WITH RESPECT TO
C                    C = SPECIFIC MOISTURE CONCENTRATION IN LAMINAE
C                    Z = SPATIAL COORDINATE THROUGH LAMINATE THICKNESS
C                    T = TIME
C
C NOTES:
C     1. THIS PROGRAM IS SET UP FOR [illegible] GRAPHITE EPOXY USING
C        MATERIAL PROPERTIES FROM TSAI'S TEXT.
C     2. THE TEMPERATURES ARE IN UNITS OF DEGREES KELVIN.
C     3. THE TEMPERATURE DISTRIBUTION THROUGH THE THICKNESS IS ASSUMED
C        TO BE CONSTANT AND EQUAL TO [illegible] OF THE FOUR SPECIFIED
C        TEMPERATURES DEFINED AS [illegible](4).
C     4. TAPE[illegible] CONTAINS THE OUTPUT FILE AND TAPE7 CONTAINS THE INPUT
C        FILE FOR THE STAGS PROGRAM.
      REAL K
      COMMON/MAT/Z(20),T(10),[illegible](10), [illegible]TEMP(4),L,N,M,K,LL,LLL,TEMP,
     *C0,C1,C2,TEMPZ(20),[illegible](4,5,4),[illegible](4,5,4),G21(4,5,4),
     *G12(4,5,3),THETA(3),[illegible](4,5,5),[illegible](4,5,3),
     *Q22(4,5,3),Q66(4,5,3),U1(4,5,5),
     *U2(4,5,[illegible]),U3(4,5,8),U4(4,5,4),U5(4,5,4),
     *QP11(4,5,3),QP12(4,5,3),[illegible](4,5,3),[illegible]22(4,5,3),
     *QP26(4,[illegible]),[illegible]
     *A11(4,5),A12(4,5),[illegible](4,5),[illegible](4,5),[illegible](4,5),A[illegible](4,5),
     *B11(4,5),B12(4,5),B16(4,5),B22(4,5),B26(4,5),B66(4,5),
     *D11(4,5),D12(4,5),D16(4,5),[illegible](4,5),D26(4,5),D66(4,5)
```

```
C THESE ARE THE FOUR TEMPERATURES AT WHICH TEST DATA FOR AS/3501 IS
C AVAILABLE IN TSAI'S TEXT
      ELTEMP(1)=350.
      ELTEMP(2)=395.
      ELTEMP(3)=394.
      ELTEMP(4)=422.
C AS/3501 E1 ...
      E1=1...
C ZERO OUT THE ARRAYS
      DO 1 LLL=1,4
      DO 1 L=1,NTIM
      DO 1 LL=1,2
      Z(LL)=TH(LL)=0.
      Q11(LLL,L,LL)=Q12(LLL,L,LL)=Q22(LLL,L,LL)=...(LLL,L,LL)=0.
      U1(LLL,L,LL)=U2(LLL,L,LL)=U3(LLL,L,LL)=U4(LLL,L,LL)=U5(LLL,L,LL)=
     *.
      QR11(LLL,L,LL)=QR12(LLL,L,LL)=...(LLL,L,LL)=0.
      QR22(LLL,L,LL)=...(LLL,L,LL)=...(LLL,L,LL)=0.
    1 CONTINUE
      DO 4 L=1,15
    4 T(L)=TEMP(ELTEMP(L))
C INPUT BEGINNING CYCLE NO.(IB)
      PRINT *," INPUT CYCLE NO. (IB) "
      READ *,IB
C INPUT C0,C1,C2 IN UNITS OF PERCENT/100. (E.G. 1.0% = 0.01)
C  C1 IS THE CONCENTRATION IN THE INSIDE OF THE SHELL
C  C2 IS THE CONCENTRATION IN THE OUTSIDE OF THE SHELL
C  C0 IS THE INITIAL CONCENTRATION IN THE LAMINATE
      PRINT *," INPUT C0,C1,C2 "
      READ *,C0,C1,C2
C INPUT LAMINATE THICKNESS AND NUMBER OF PLIES
      PRINT *," INPUT LAMINATE THICKNESS AND NO. OF PLIES "
      READ *, HLAM,NO
C CALCULATE LAMINATE THICKNESS
      H=NO*HLAM
C CALCULATE THE CENTER OF EACH LAMINAE
      Z(1)=HLAM/2.
      DO 2 L=2,NO
    2 Z(L)=Z(L-1)+HLAM
C INPUT THE PLY ORIENTATIONS FROM INSIDE TO OUTSIDE
      PRINT *, "INPUT PLY ORIENTATIONS FROM INSIDE TO OUTSIDE "
      DO 5 L=1,NO
      READ *,THETA(L)
    5 CONTINUE
C DIFFUSION TEMPERATURE = 350 F (450 K)
      TEMP=350.
C REF. TSAI PAGE EQUATION 4.40 TO CALCULATE K FOR GRAPHITE/EPOXY
C         K=K0*EXP(-E0/RT)   (E.G.)
C         K=6.51*EXP(-5722/TEMP(DEG RANKINE))   (EQ. 4.7)
      K=6.51*EXP(-5722/(TEMP+459.67))*3600.
C INPUT NO. OF TIME INTERVALS AT WHICH MOISTURE DISTRIBUTION IN THE
C LAMINATE TO BE CALCULATED
      PRINT *," INPUT NO. OF TIME INTERVALS "
      READ *, NTIME
```

```
C INPUT NONDIM.SIGNAL TIME INTERVALS (K*T/H**2.)
      PRINT *, " INPUT TIME INTERVALS (K*T/H**2)  "
      DO 3 L=1,NTIM
      READ *,TNDTIM(L)
    3 T(L)=TNDTIM(L)*H**2./K

      ICASE=ICASE-1
      DO 1000 LLL=1,4
      DO 1000 L=1,NTIM
      ICASE=ICASE+1
      CALL H [illegible]
      CALL STAGE1
      DO 2000 LL=1,NL
      TEMP2(LL)=[illegible]TEMP(LL)
      C(LLL,L,LL)=0.
      IF(T(L). [illegible]) GO TO 12
      C(LLL,L,LL)=C1+(C2-C1)*Z(LL)/H
      CTEMP1=0.
      CTEMP2=0.
      PI=3.14159265358979
      N=0
   11 N=N+1
      IF(ABS(-K*N**2*PI**2*T(L)/H**2).[illegible]) GO TO 12
      CTEMP1=(2/PI)*(C2*COS(N*PI)-C1)/N*SIN(N*PI*Z(LL)/H)
      CTEMP1=CTEMP1*EXP(-K*N**2*PI**2*T(L)/H**2)
      C(LLL,L,LL)=C(LLL,L,LL)+CTEMP1
      M=(N-1)/2
      CTEMP2=(4*C0/PI)/(2*M+1)*SIN((2*M+1)*PI*Z(LL)/H)
      CTEMP2=CTEMP2*EXP(-K*(2*M+1)**2*PI**2*T(L)/H**2)
      C(LLL,L,LL)=C(LLL,L,LL)+CTEMP2
      N=N+1
      CTEMP3=(2/PI)*(C2*COS(N*PI)-C1)/N*SIN(N*PI*Z(LL)/H)
      CTEMP3=CTEMP3*EXP(-K*N**2*PI**2*T(L)/H**2)
      C(LLL,L,LL)=C(LLL,L,LL)+CTEMP3
      GO TO 11
   12 CONTINUE
      IF(C(LLL,L,LL).LT.0.0) C(LLL,L,LL)=0.0
      ZZ=Z(LL)/H
      CALL CALC1(C(LLL,L,LL),TEMP2(LL),E2(LLL,L,LL),U21(LLL,L,LL),G12(LL
     *L,L,LL))
  102 FORMAT(1H0,I2,T30,'SI-L [illegible] MATERIAL NO.')
      WRITE(7,102)LL
  100 FORMAT(4X,I2,2X,F6.4,2X,F[illegible].4,[illegible],F7.[illegible],1X,E11.5,1X,E[illegible].5,1X,E11.5,1X,
     *I3,1X,I3)
  101 FORMAT(T3,"[illegible]",F10.7,",",F10.1,",",[illegible],1.,",F10.1,",1. SI-2"
     *)
      WRITE(7,101)U21(LLL,L,LL),G12(LLL,L,LL),E2(LLL,L,LL)
      WRITE(6,100)LL,ZZ,Z(LL),C(LLL,L,LL),E2(LLL,L,LL),U21(LLL,L,LL),G12
     *(LLL,L,LL),N,M
```

```
2000 CONTINUE
     CALL CALC2
     CALL STRSS2
1000 CONTINUE

     STOP
     END
     SUBROUTINE [illegible]
     COMMON/MAT/Z(20),T(10),TNONDIM(10),[illegible](4),L,N,[illegible],M,K,LL,LLL,TEMP,
    *C0,C1,C2,TEMP[illegible](20),[illegible](4,5,4),[illegible](4,5,4),U21(4,5,4),
    *G12(4,5,4),THETA(4),[illegible]11(4,5,4),[illegible]12(4,5,4),
    *Q22(4,5,4),[illegible]66(4,5,4),[illegible](4,5,4),
    *U2(4,5,4),[illegible](4,5,4),[illegible](4,5,4),[illegible](4,5,4),
    *QR11(4,5,4),[illegible]12(4,5,4),[illegible]16(4,5,4),[illegible]22(4,5,4),
    *QR26(4,5,4),[illegible]66(4,5,4),[illegible],ICASE,[illegible],
    *A11(4,5),A12(4,5),A16(4,5),A22(4,5),A26(4,5),A66(4,5),
    *B11(4,5),B12(4,5),B16(4,5),B22(4,5),B26(4,5),B66(4,5),
    *D11(4,5),D12(4,5),D16(4,5),D22(4,5),D26(4,5),D66(4,5)
     REAL K
 100 FORMAT(1H1,//)
 101 FORMAT(T5,"PLY",T[illegible],"Z/H",T17,"[illegible]",T24,"[illegible]",T[illegible],"[illegible]",T44,"U21",
    *T53,"[illegible]",T[illegible],"[illegible]",T[illegible],"[illegible]",/,T17,"([illegible])",T3[illegible],"[illegible]",
    *T44,"[illegible]",T53,"[illegible]",/)
 103 FORMAT(//)
 104 FORMAT(T5,"CASE NO. ",I5,"   [illegible] ON [illegible]. SIDES"/
    *T5,"CALCULATION OF MOISTURE DISTRIBUTION IN ",I3,
    *" PLY LAMINATE",/,T5,"MOISTURE DIFFUSION COEFFICIENT = ",
    *E11.5,/,T5,"DIFFUSION TEMPERATURE = ",F7.2," (KELVIN)",
    */,T5,"PLY THICKNESS = 0.[illegible] I[illegible]",/,T5,"C0 = ",F9.5," C1 = ",
    *F9.5," C2 = ",F9.5,/," [illegible]ORIGINAL MODULI",/,T5,"E2 = 1.4137[illegible]",
    *" U21 = 0.02250  G12 = 0.[illegible] (PSI)",/,T5,
    *"NONDIMENSIONAL TIME = ",[illegible]11.5,[illegible],"TIME (SEC) = ",E11.5,/)
  10 WRITE(6,100)
     TNON=K*T/H**2
     WRITE(6,104)ICASE,[illegible],K,TEMP,C0,C1,C2,TNONDIM(L),T(L)
  30 CONTINUE
     WRITE(6,101)

     RETURN
     END

     SUBROUTINE CALC1(C,TEMP,E2,U21,G12)
     DIMENSION S(4,3),SS(4,3),C(3)
     N=0
     IF(TEMP.EQ.300.) N=1
     IF(TEMP.EQ.366.) N=2
     IF(TEMP.EQ.394.) N=3
     IF(TEMP.EQ.422.) N=4
     IF(N.EQ.0) PRINT *," ERROR IN CALC"
```

```
C  REF TSAT FOR AS/1501 02 AND G12 CALC
      S(1,1)=1.4137E04
      S(1,2)=1.335E05
      S(1,3)=1.2615E06
      S(2,1)=1.0347E04
      S(2,2)=.9135E05
      S(2,3)=.8611E06
      S(3,1)=1.01[illegible]
      S(3,2)=.8623E05
      S(3,3)=.8138E06
      S(4,1)=1.015E04
      S(4,2)=.9225E05
      S(4,3)=.8[illegible]
      SS(1,1)=.9557E04
      SS(1,2)=.8658E05
      SS(2,1)=.7833E04
      SS(2,2)=.7127E05
      SS(3,1)=.6815E04
      SS(3,2)=.6[illegible]
      SS(4,1)=.6525E04
      SS(4,2)=.5922E05
      X(1)=0.[illegible]
      X(2)=0.[illegible]105
      X(3)=0.[illegible]105
      U12=0.3[illegible]
      IF(0.0E.0.0336) GO TO 10
      SLOPE=(S(N,2)-S(N,1))/(X(2)-X(1))
      B=S(N,1)-SLOPE*X(1)
      E2=SLOPE*0+B
      U21=U12*E2/14.695E06
      GO TO 20
   10 CONTINUE
      SLOPE = (S(N,3)-S(N,2))/(X(3)-X(2))
      B=S(N,2)-SLOPE*X(2)
      E2=SLOPE*0+B
      U21=U12*E2/14.695E06
   20 CONTINUE
      SLOPE=(SS(N,2)-SS(N,1))/(X(3)-X(2))
      B=SS(N,1)-SLOPE*X(1)
      G12=SLOPE*0+B

      RETURN
      END
```

```
      SUBROUTINE STAGS1
      COMMON/DAT/Z(20),T(20),TMP(4,4),ELTEMP(4),L,M,N,LL,LLL,TE**2,
     *C0,C1,C2,EMP2(20),S(4,4),A(4,5),U21(4,5,5),
     *G12(4,5,4),THETA(8),S11(4,5,4),S12(4,5,4),
     *Q22(4,5,4),S66(4,5,4),Q11(4,5,4),
     *U2(4,5,5),U3(4,5,5),U4(4,5,5),U5(4,5,5),
     *QR11(4,5,5),QR12(4,5,5),QR16(4,5,5),QR22(4,5,5),
     *QR26(4,5,5),QR66(4,5,5),ELTEMP(4),ALL(4,5),
     *A11(4,5),A12(4,5),A16(4,5),A22(4,5),A26(4,5),A66(4,5),
     *B11(4,5),B12(4,5),B16(4,5),B22(4,5),B26(4,5),B66(4,5),
     *D11(4,5),D12(4,5),D16(4,5),D22(4,5),D26(4,5),D66(4,5)
      REAL K
  100 FORMAT("1MS.T60,I4,6X,3A4,6X,5A4,3X,"  =I=3-L,3X,A3,E15.5,5X
     *"I",
     *,/"DEL=1.0000.",/"LIMIT=4000.",/"ATTACH,STAGS1,ID=1.",
     */"ATTACH,STAGS2,ID=1."/"STAGS1.",/"REWIND,TAPE21.",
     */"REQUEST,TL,*T,GO,PE,S)=LGO7L5,P200.",/
     *"LISTPF,P=T1.",/
     *"REWIND,TAPE21,TAPE22.",/
     *"LABEL,T2,,P=T1,L=CASE",I4,"",P10.",/
     *"COPY,TAPE21,T2.",/
     *"LABEL,T3,,P=T1,L=CASE",I4,"3,,P10.",/
     *"COPY,TAPE22,T3.",/
     *"*EOR")
      WRITE(7,100)ICASE,10.0,ICASE,100

  101 FORMAT(T5," CASE NO. ",I5," - FIXED EDGE ON VERTICAL SIDES",/
     *"C  PLY ORIENTATIONS (",F5.1,","F5.1,","F5.1,","F5.1,",",
     *F5.1,",",F5.1,","F5.1,","F5.1,")",/
     *"C  BOUNDARY CONDITIONS - FIXED EDGE ON VERTICAL SIDES ",/
     *"C  PANEL RADIUS = 12.0 INCHES",/
     *"C  ELEMENT TYPE = 210",/
     *"C",/
     *"C  TRANSVERSE AND SHEAR MODULI REDUCED BY T1 MOISTURE AND TEMP",
     */"C  ORIGINAL MODULI FOR AS/3501 GRAPHITE/EPOXY IS",/
     *"C  E2 = 1.41375E06 U21=.0225 G12 = 0.85050E06 (PSI)",/
     *"C  MOISTURE DIFFUSION COEFFICIENT = ",E11.5," AT 300 DEG RELVIN"/
     *"C  C0 = ",E11.5," C1 = ",E11.5," C2 = ",E11.5,/
     *"C  C1 IS INSIDE SHELL; C2 IS OUTSIDE SHELL",/
     *"C  NON-DIMENSIONAL T1 = ",E11.5," T1 (DEG F) = ",E11.5,/
     *"C  LAMINATE TEMPERATURE = ",E11.5," (KELVIN)")
      WRITE(7,101)ICASE,THETA(1),THETA(2),THETA(3),THETA(4),THETA(5),
     *THETA(6),THETA(7),THETA(8),M,C0,C1,C2,T(N),Z(L),T(L),ELTEMP(LLL)

  102 FORMAT(T1,"1,1,1,,,0",T30,"1 =1 LINEAR BIFURCATION ANAL",/
     *T10,"1",T30,"1=2 1 SHELL UNIT LOAD ",/
     *T10,"3,0,1,0",T30,"2=3 1 MATERIAL; ; 1 SHELL WALL PROPERTY",/
```

```
     *T10,"1.[illegible],T30,"[illegible]C-1 STARTING [illegible] FACTOR",/
     *T10,"1.[illegible],10[illegible]",T30,"[illegible]-2 [illegible] EIGENVALUES;MAX NO. CPU SECS",/
     *T10,"1",T30,"[illegible]-3 EIGENVALUE [illegible] CLUSTER TO BE COMPUTED",/
     *T10,"15,15",T30,"[illegible]-1 [illegible] 15 COLUMNS",)
      WRITE(7,1[illegible])

      RETURN
      END

      SUBROUTINE STAGS2
      COMMON/[illegible]AT/Z(2[illegible]),[illegible](10),[illegible],LLL,T[illegible]MP,
     *C0,C1,C2,T[illegible]AP2(2[illegible]),[illegible],Q11(4,5,[illegible]),
     *G12(4,5,3),THETA(3),[illegible],
     *Q22(4,5,3),Q66(4,5,3),[illegible](4,[illegible]),
     *U2(4,5,[illegible]),U3(4,5,[illegible]),[illegible],
     *QR11(4,5,6),[illegible](4,5,[illegible]),[illegible],
     *QR26(4,5,3),[illegible]66(4,[illegible]),[illegible],
     *A11(4,5),A12(4,5),[illegible](4,5),[illegible](4,5),
     *B11(4,5),B12(4,5),[illegible](4,5),[illegible](4,5),
     *D11(4,5),D12(4,5),[illegible](4,5),[illegible](4,5)
  105 FORMAT(T10,"1,1,",I2,T2[illegible],"[illegible]-1 [illegible] OF [illegible] LAYER WALL."
     *I2," PLIES",/T10,"1,[illegible]","F[illegible].2,"   [illegible]-2")
      WRITE(7,105)N[illegible],THETA(1)
      NOTEMP=[illegible]-1
      DO 1 J=2,NOTEMP
    1 WRITE(7,106)J,THETA(J)
  106 FORMAT(T10,I2,",[illegible]",F[illegible].2)
  107 FORMAT(T10,I2,",[illegible]","F[illegible],"   [illegible]-2")
      WRITE(7,107)[illegible],THETA([illegible])
  108 FORMAT(T10,"[illegible]",T30,"[illegible]-1 CYLINDRICAL SHELL [illegible]",/
     *T5,"[illegible].,57.[illegible],12.   [illegible]-2[illegible]",/
     *T10,"1",T30,"[illegible]-5 SHELL WALL [illegible] NO. IN [illegible] TA[illegible]",/
     *T10,"4[illegible]",T30,"[illegible]-1 ELEMENT TYPE ",/
     *T10,"[illegible]",T30,"[illegible]-1 [illegible] Y CONSTRAINT [illegible] NEXT CA[illegible]"
     *,/T10,"[illegible]",T30,"[illegible]-2 TOP - [illegible]",/
     *T10,"1[illegible],0[illegible]",T30,"[illegible]-2 RIGHT SIDE - SAME AS TOP",/
     *T10,"0[illegible],00[illegible]",T30,"[illegible]-2 BOTTOM - ALL FIXED",/
     *T10,"1[illegible],0[illegible]",T30,"[illegible]-2 LEFT SIDE - SAME AS TOP",/
     *T10,"1",T30,"[illegible]-1 NO. OF LOAD SYSTEMS",/
     *T10,"1.1",T30,"[illegible]-2",/
     *T10,"1.,2,1.1",T30,"[illegible]-3",/
     *T10,"1,1,1.0     ",T30,"[illegible]-1 OUTPUT CONTROL",/
     *"*FOR")
      WRITE(7,108)

      RETURN
      END
```

```
      SUBROUTINE CALC2
C THIS SUBROUTINE CALCULATES THE PLY AND LAMINATE STIFFNESSES

      REAL K
      DIMENSION TTHETA(20),Z(20)
      COMMON/MAT/E(20),T(20),THICK(20),ELIMIT(20),L,NO,M,K,LL,LLL,TEMP,
     *C0,C1,C2,TEMP2(20),Q(4,5,4),S(4,5,4),Q11(4,5,5),
     *Q12(4,5,5),THETA(4),S11(4,5,5),S12(4,5,5),
     *Q22(4,5,5),Q66(4,5,5),QL(4,5,5),
     *U2(4,5,4),U3(4,5,5),U4(4,5,5),U5(4,5,5),
     *QR11(4,5,4),QR12(4,5,5),QR16(4,5,5),QR22(4,5,5),
     *QR26(4,5,5),QR66(4,5,5),T1,TSIST,ALA,
     *A11(4,5),A12(4,5),A16(4,5),A22(4,5),A26(4,5),A66(4,5),
     *B11(4,5),B12(4,5),B16(4,5),B22(4,5),B26(4,5),B66(4,5),
     *D11(4,5),D12(4,5),D16(4,5),D22(4,5),D26(4,5),D66(4,5)
C U12 FOR 1S/3501 GRAPHITE EPOXY
      U12=0.333
      DO 1 J=1,NO
C CALCULATING PLY STIFFNESSES
      S11(LLL,L,J)=E1/(1-U12**2*E1(LLL,L,J))
      Q12(LLL,L,J)=U12*S2(LLL,L,J)/(1-U12**2*E1(LLL,L,J))
      Q22(LLL,L,J)=S2(LLL,L,J)/(1-U12**2*E1(LLL,L,J))
    1 Q66(LLL,L,J)=G12(LLL,L,J)

C CALCULATING THE REDUCED PLY STIFFNESSES USING THE INVARIANT
C PROPERTIES APPROACH OF TSAI AND PAGANO (REF. JONES)
      DO 2 J=1,NO
      U1(LLL,L,J)=(3*Q11(LLL,L,J)+3*Q22(LLL,L,J)+2*Q12(LLL,L,J)+4*Q66(LL
     *L,L,J))/8.
      U2(LLL,L,J)=(Q11(LLL,L,J)-Q22(LLL,L,J))/2.
      U3(LLL,L,J)=(Q11(LLL,L,J)+Q22(LLL,L,J)-2*Q12(LLL,L,J)-4*Q66(LLL,L,
     *J))/8.
      U4(LLL,L,J)=(Q11(LLL,L,J)+Q22(LLL,L,J)+6*Q12(LLL,L,J)-4*Q66(LLL,L,
     *J))/8.
    2 U5(LLL,L,J)=(Q11(LLL,L,J)+Q22(LLL,L,J)-2*Q12(LLL,L,J)+4*Q66(LLL,L,
     *J))/4.

C CHANGING THE SIGN OF THETA TO BE CONSISTANT WITH THE TSAI/PAGANO
C FORMULATION AS SHOWN IN JONES
      DO 3 J=1,NO
    3 TTHETA(J)=-THETA(J)*3.14159265441/180.

C CALCULATING THE REDUCED STIFFNESSES
C
      DO 4 J=1,NO
      QR11(LLL,L,J)=U1(LLL,L,J)+U2(LLL,L,J)*COS(2*TTHETA(J))+U3(LLL,L,J)
     **COS(4*TTHETA(J))
      QR12(LLL,L,J)=U4(LLL,L,J)-U3(LLL,L,J)*COS(4*TTHETA(J))
```

```
      DR22(LLL,L,J)=U1(LLL,L,J)-U2(LLL,L,J)*COS(2*TTHETA(J))+U3(LLL,L,J)
     **COS(4*TTHETA(J))
      DR16(LLL,L,J)=-.5*U2(LLL,L,J)*SIN(2*TTHETA(J))-U3(LLL,L,J)*SIN(4*T
     *THETA(J))
      DR26(LLL,L,J)=-.5*U2(LLL,L,J)*SIN(2*TTHETA(J))+U3(LLL,L,J)*SIN(4*T
     *THETA(J))
    4 DR66(LLL,L,J)=U0(LLL,L,J)-U3(LLL,L,J)*COS(4*TTHETA(J))
C
C CALCULATING THE Z COORDINATE PER FIG. 4-5 IN JONES
C
      ZZ(1)=-THICK/2.
      NOTEMP=NPLY+1
      DO 5 J=2,NOTEMP
    5 ZZ(J)=ZZ(J-1)+THICK
C
C CALCULATING THE [A], [B], AND [D]
C
      A11(LLL,L)=A12(LLL,L)=A16(LL,L)=A22(LLL,L)=A26(LLL,L)=A66(LLL,L)=
     *0.
      DO 6 J=1,NPLY
      ZTEMP=ZZ(J+1)-ZZ(J)
      A11(LLL,L)=A11(LLL,L)+DR11(LLL,L,J)*ZTEMP
      A12(LLL,L)=A12(LLL,L)+DR12(LLL,L,J)*ZTEMP
      A16(LLL,L)=A16(LLL,L)+DR16(LLL,L,J)*ZTEMP
      A22(LLL,L)=A22(LLL,L)+DR22(LLL,L,J)*ZTEMP
      A26(LLL,L)=A26(LLL,L)+DR26(LLL,L,J)*ZTEMP
      A66(LLL,L)=A66(LLL,L)+DR66(LLL,L,J)*ZTEMP
    6 CONTINUE
      B11(LLL,L)=B12(LLL,L)=B16(LLL,L)=B22(LLL,L)=B26(LLL,L)=B66(LLL,L)=
     *0.
      DO 7 J=1,NPLY
      ZTEMP=ZZ(J+1)**2-ZZ(J)**2
      B11(LLL,L)=B11(LLL,L)+.5*DR11(LLL,L,J)*ZTEMP
      B12(LLL,L)=B12(LLL,L)+.5*DR12(LLL,L,J)*ZTEMP
      B16(LLL,L)=B16(LLL,L)+.5*DR16(LLL,L,J)*ZTEMP
      B22(LLL,L)=B22(LLL,L)+.5*DR22(LLL,L,J)*ZTEMP
      B26(LLL,L)=B26(LLL,L)+.5*DR26(LLL,L,J)*ZTEMP
      B66(LLL,L)=B66(LLL,L)+.5*DR66(LLL,L,J)*ZTEMP
    7 CONTINUE
      D11(LLL,L)=D12(LLL,L)=D16(LLL,L)=D22(LLL,L)=D26(LLL,L)=D66(LLL,L)=
     *0.
      DO 8 J=1,NPLY
      ZTEMP=ZZ(J+1)**3-ZZ(J)**3
      D11(LLL,L)=D11(LLL,L)+.3*DR11(LLL,L,J)*ZTEMP/3.
      D12(LLL,L)=D12(LLL,L)+.3*DR12(LLL,L,J)*ZTEMP/3.
      D16(LLL,L)=D16(LLL,L)+.3*DR16(LLL,L,J)*ZTEMP/3.
      D22(LLL,L)=D22(LLL,L)+.3*DR22(LLL,L,J)*ZTEMP/3.
      D26(LLL,L)=D26(LLL,L)+.3*DR26(LLL,L,J)*ZTEMP/3.
      D66(LLL,L)=D66(LLL,L)+.3*DR66(LLL,L,J)*ZTEMP/3.
    8 CONTINUE
```

```
  100 FORMAT(//,T6,"PLY",T17,"U11",T22,"U12",T34,"U22",T46,"U66",
     *T58,"THETA",T70,"PHI"/)
      WRITE(6,101)
  101 FORMAT(T6,I2,T10,E11.5,T22,E11.5,T34,E11.5,T46,E11.5,T58,
     *E11.5,T70,F7.2)
      DO 9 J=1,6
    9 WRITE(6,101)J,A1(LLL,L,J),A12(LLL,L,J),A22(LLL,L,J),A66(LLL,L,J),
     *THETA(J),PHI(J)
  102 FORMAT(//,T6,"PLY",T17,"U1",T22,"U2",T34,"U3",T46,"U4",T58,"U5"/)
      WRITE(6,103)
      DO 10 J=1,6
   10 WRITE(6,104)J,U1(LLL,L,J),U2(LLL,L,J),U3(LLL,L,J),U4(LLL,L,J),U5(L
     *LL,L,J)
  103 FORMAT(1H1//,T6,"PLY",T17,"A11",T22,"A12",T34,"A16",T46,"A22",
     *T58,"A26",T70,"A66"/)
      WRITE(6,104)
  104 FORMAT(T6,I2,T10,E11.5,T22,E11.5,T34,E11.5,T46,E11.5,T58,E11.5,
     *T70,E11.5)
      DO 11 J=1,6
   11 WRITE(6,104)J,A11(LLL,L,J),A12(LLL,L,J),A16(LLL,L,J),A22(LLL,L
     *,J),A26(LLL,L,J),A66(LLL,L,J)
  105 FORMAT(//,T6,"A11= ",E11.5,T30,"A11= ",E11.5,T54,"A11= ",E11.5,/
     *T6,"A12= ",E11.5,T30,"A12= ",E11.5,T54,"A12= ",E11.5,/
     *T6,"A16= ",E11.5,T30,"A16= ",E11.5,T54,"A16= ",E11.5,/
     *T6,"A22= ",E11.5,T30,"A22= ",E11.5,T54,"A22= ",E11.5,/
     *T6,"A26= ",E11.5,T30,"A26= ",E11.5,T54,"A26= ",E11.5,/
     *T6,"A66= ",E11.5,T30,"A66= ",E11.5,T54,"A66= ",E11.5)
      WRITE(6,105)A11(LLL,L),A12(LLL,L),A16(LLL,L),
     *A12(LLL,L),A22(LLL,L),A26(LLL,L),
     *A16(LLL,L),A26(LLL,L),A66(LLL,L),
     *A22(LLL,L),A26(LLL,L),A66(LLL,L),
     *A26(LLL,L),A66(LLL,L),A66(LLL,L)
      RETURN
      END
```

Appendix B

Summary of STAGS-C1 Runs

Case No. 1-20 [0.,45.,-45.,90.]S

Laminate Temperature (Deg. F)	Nondimensional Time 0.00	0.001	0.01	0.1	0.5
80.0	514.8	514.2	512.5	510.5	509.7
	1	.9988345	.9955322	.9916472	.9900932
200.0	493.3	492.1	488.7	484.5	482.3
	.9582362	.9559052	.9493007	.9411422	.9368687
250.0	482.3	479.8	472.3	462.8	458
	.9368687	.9320124	.9174437	.8989899	.8896659
300.0	480.4	477.1	466.8	453.2	445.9
	.9331779	.9267677	.9067599	.8803419	.8661616

Case No. 21-40 [90.,45.,-45.,0.]S

Laminate Temperature (Deg. F)	Nondimensional Time 0.00	0.001	0.01	0.1	0.5
80.0	446	445.1	442.9	440.9	440.1
	1	.9979821	.9930493	.9885650	.9867713
200.0	422.2	420.8	417	412.9	410.6
	.9466368	.9434978	.9349776	.9257848	.9206278
250.0	412	409	400.5	392.1	386.7
	.9237668	.9170404	.8979821	.8791480	.8670404
300.0	410.5	406.8	395.4	382.7	375.3
	.9204036	.9121076	.8865471	.8580717	.8414798

Case No. 41-60 [45.,-45]2S

Laminate Temperature (Deg. F)	Nondimensional Time 0.00	0.001	0.01	0.1	0.5
80.0	428.9	428.6	427.7	426.7	426.4
	1	.9993005	.9972021	.9948706	.9941711
200.0	408.4	407.8	406.1	401.4	397.7
	.9522033	.9508044	.9468408	.9358825	.9272558
250.0	387.4	386.3	382.5	371.4	362.2
	.9032408	.9004761	.8918163	.8659361	.8444859
300.0	381.7	380.3	375	355.6	340.4
	.8899510	.8866869	.8743297	.8314292	.7936582

Case No. 101-120 [0.,45.,-45.,90.]S

Laminate Temperature (Deg. F)	Nondimensional Time 0.00	0.001	0.01	0.1	0.5
80.0	502.8	502.2	500.5	498.5	497.6
	1	.9988067	.9954256	.9914479	.9896579
200.0	481.2	480	476.6	472.4	470.3
	.9570406	.9546539	.9478918	.9395386	.9353620
250.0	470.3	467.8	460.3	451	446.3
	.9353620	.9303899	.9154733	.8969769	.8876293
300.0	468.5	465.2	455	441.7	434.6
	.9317820	.9252188	.9049324	.8784805	.8643596

Case No. 121-140 [90.,45.,-45.,0.]S

Laminate Temperature (Deg. F)	Nondimensional Time 0.00	0.001	0.01	0.1	0.5
80.0	444.1	443.3	441.2	439.2	438.4
	1	.9981986	.9934699	.9889664	.9871651
200.0	420.6	419.3	415.5	411.5	409.2
	.9470840	.9441567	.9356001	.9265931	.9214141
250.0	410.5	407.7	399	389.9	385
	.9243414	.9180365	.8984463	.8779554	.8669219
300.0	409	405.5	393.8	380.9	373.5
	.9209637	.9130826	.8867372	.8576897	.8410268

Case No. 141-160 [45.,-45.]2S

Laminate Temperature (Deg. F)	Nondimensional Time 0.00	0.001	0.01	0.1	0.5
80.0	421.6	421.3	420.5	419.6	419.2
	1	.9992884	.9973909	.9952562	.9943074
200.0	401	400.5	398.6	393.6	389.8
	.9511385	.9499526	.9454459	.9335863	.9245731
250.0	379.7	378.5	374.3	362.3	352.9
	.9006167	.8977704	.8878083	.8593454	.8370493
300.0	373.9	372.3	366	345.8	328.9
	.8868596	.8830645	.8681214	.8202087	.7801233

Case No. 201-220 [0.,45.,-45.,90.]S

Laminate Temperature (Deg. F)	Nondimensional Time 0.00	0.001	0.01	0.1	0.5
80.0	514.8	514.4	513.3	511.7	510.7
	1	.9992230	.9970862	.9939782	.9920357
200.0	493.3	491.9	487.5	482.7	480.3
	.9582362	.9555167	.9469697	.9376457	.9329837
250.0	482.3	479.2	468.9	458	452.6
	.9368687	.9308469	.9108392	.8896659	.8791764
300.0	480.4	475.6	460	443.1	435.1
	.9331779	.9238539	.8935509	.8607226	.8451826

Case No. 221-240 [90.,45.,-45.,0.]S

Laminate Temperature (Deg. F)	Nondimensional Time 0.00	0.001	0.01	0.1	0.5
80.0	445.9	445.1	443.2	441.9	440.9
	1	.9982059	.9939448	.9910294	.9887867
200.0	422.1	420.8	416.7	411.7	409.1
	.9466248	.9437094	.9345145	.9233012	.9174703
250.0	411.9	409	399.7	388.4	382.6
	.9237497	.9172460	.8963893	.8710473	.8580399
300.0	410.5	406.7	393.7	375.5	366.9
	.9206100	.9120879	.8829334	.8421171	.8228302

Case No. 241-260 [45.,-45.]2S

Laminate Temperature (Deg. F)	Nondimensional Time 0.00	0.001	0.01	0.1	0.5
80.0	428.9	428.7	428.3	427.7	427.3
	1	.9995337	.9986011	.9972021	.9962695
200.0	408.4	407	402	393.5	389.5
	.9522033	.9489391	.9372814	.9174633	.9081371
250.0	397.4	384.2	372.1	351.1	341.1
	.9032408	.8957799	.8675662	.8186057	.7952903
300.0	381.7	376.5	355.9	319	300.9
	.8699510	.8778270	.8295640	.7437631	.7015621

Case No. 401-420 (0.,45.,-45.,90.)S

Laminate Temperature (Deg. F)	Nondimensional Time 0.00	0.001	0.01	0.1	0.5
80.0	514.8	513.8	511	507.8	506.8
	1	.9980575	.9926185	.9864025	.9844600
200.0	493.3	490.8	482.9	474.5	471.4
	.9582362	.9533800	.9380342	.9217172	.9156954
250.0	482.3	476.6	458.7	439.8	432.6
	.9368687	.9257964	.8910256	.8543124	.8403263
250.0	480.4	472.3	445.9	417.1	405
	.9331779	.9174437	.8661616	.8102176	.7867133

Case No. 421-440 (90.,45.,-45.,0.)S

Laminate Temperature (Deg. F)	Nondimensional Time 0.00	0.001	0.01	0.1	0.5
80.0	445.9	444.3	440.3	437.3	436.3
	1	.9964118	.9874411	.9807132	.9784705
200.0	422.1	419.4	411.4	403	399.7
	.9466248	.9405696	.9226284	.9037901	.8963893
250.0	411.9	406	387.8	369	361.2
	.9237497	.9105191	.8697017	.8275398	.8100471
250.0	410.5	403	378	349.6	336.6
	.9206100	.9037901	.8477237	.7840323	.7548778

Case No. 441-460 (45.,-45.)2S

Laminate Temperature (Deg. F)	Nondimensional Time 0.00	0.001	0.01	0.1	0.5
80.0	428.9	428.4	427.2	425.8	425.4
	1	.9988342	.9960364	.9927722	.9919396
200.0	408.4	406.5	399.7	386.8	379.5
	.9522033	.9477734	.9319189	.9018419	.8848216
250.0	387.4	383.1	367.3	335.2	316
	.9032408	.8932152	.8563768	.7815342	.7367685
250.0	381.7	375.1	349.1	290.7	245.7
	.8899510	.8745628	.8139426	.6777804	.5728608

Case No. 601-620 (0.,45.,-45.,90.)S
Radius = 24 in.

Laminate Temperature (Deg. F)	Nondimensional Time 0.00	0.001	0.01	0.1	0.5
80.0	290.8	290.5	289.6	288.5	288.1
	1	.998968	.995873	.992091	.990715
200.0	279.3	278.7	276.8	274.5	273.4
	.960454	.958391	.951857	.943948	.940165
250.0	273.5	272.1	268	262.9	260.4
	.940509	.935695	.921596	.904059	.895461
300.0	272.5	270.7	265	257.7	254
	.937070	.930880	.911279	.886176	.873453

Case No. 701-720 (0.,45.,-45.,90.)S
Radius = 48 in.

Laminate Temperature (Deg. F)	Nondimensional Time 0.00	0.001	0.01	0.1	0.5
80.0	170.3	170.2	169.7	169.1	168.9
	1	.999413	.996477	.992954	.991779
200.0	164.5	164.2	163.2	162	161.4
	.965942	.964181	.958309	.951262	.947739
250.0	161.5	160.8	158.6	156	154.7
	.948326	.944216	.931298	.916031	.908397
300.0	160.7	160	157.1	153.3	151.4
	.944803	.939518	.922490	.900176	.889019

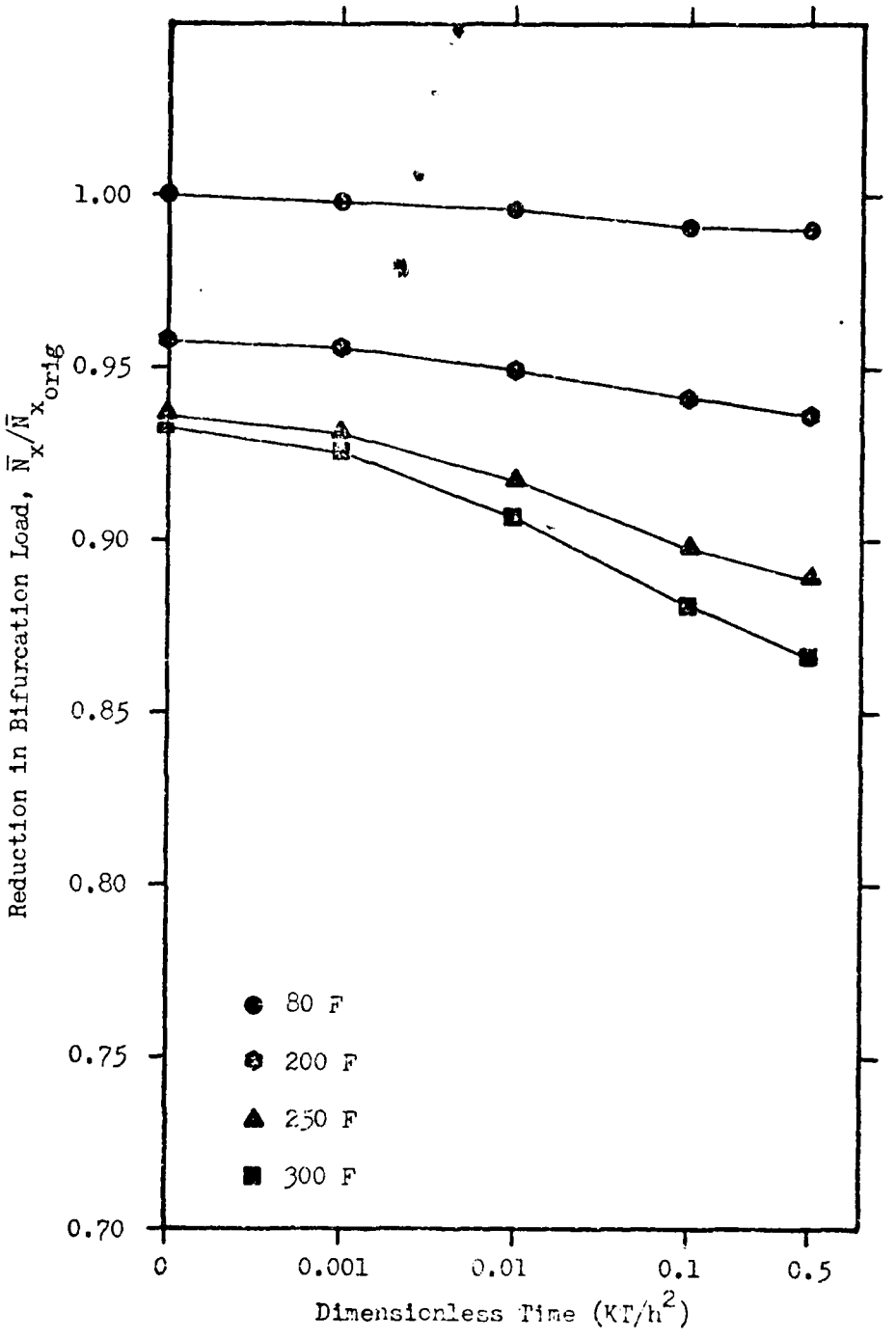

Figure 38. Case No. 1-20; $(0.,+45.,-45.,90.)_S$

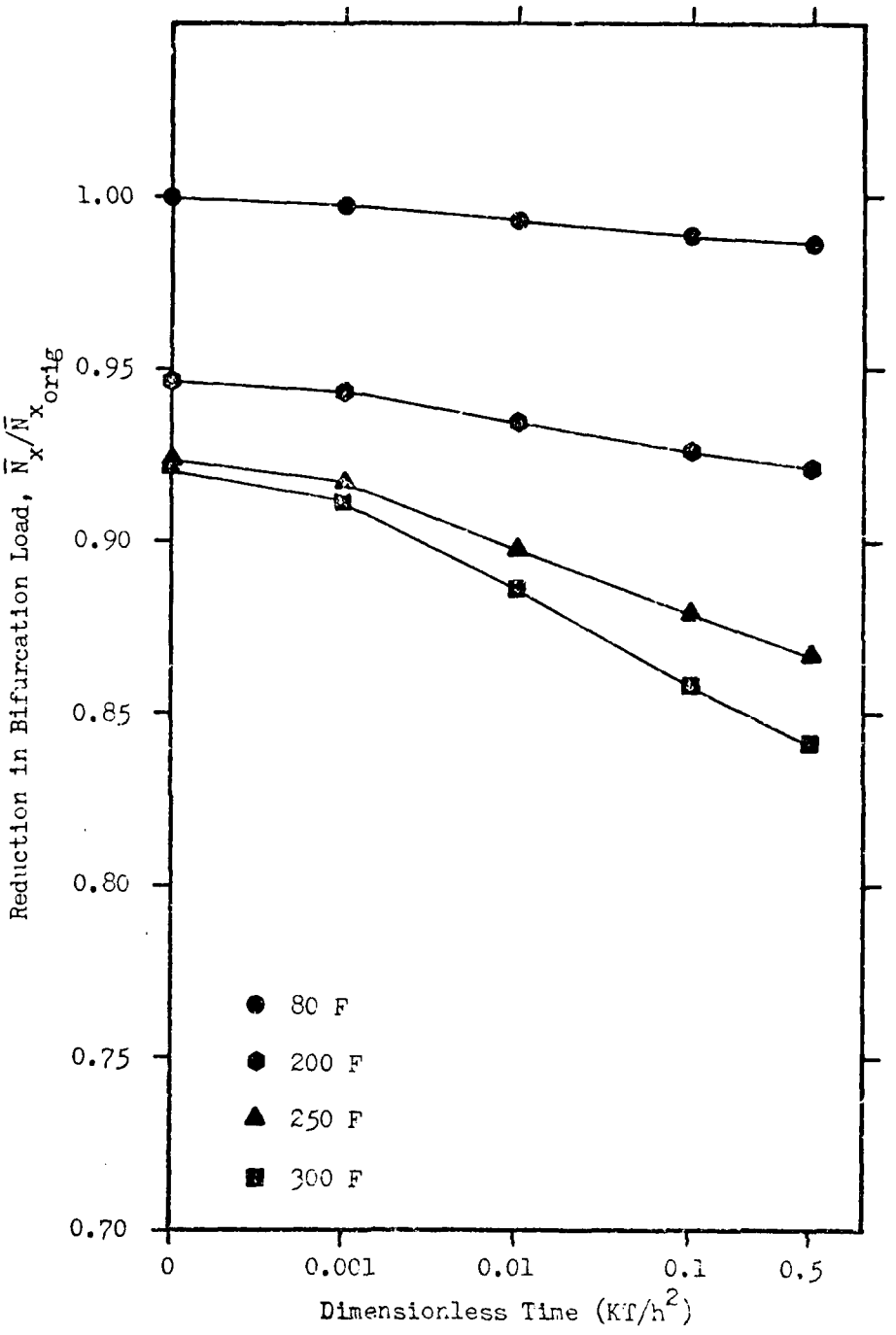

Figure 39. Case No. 21-40; $(90.,+45.,-45.,0.)_S$

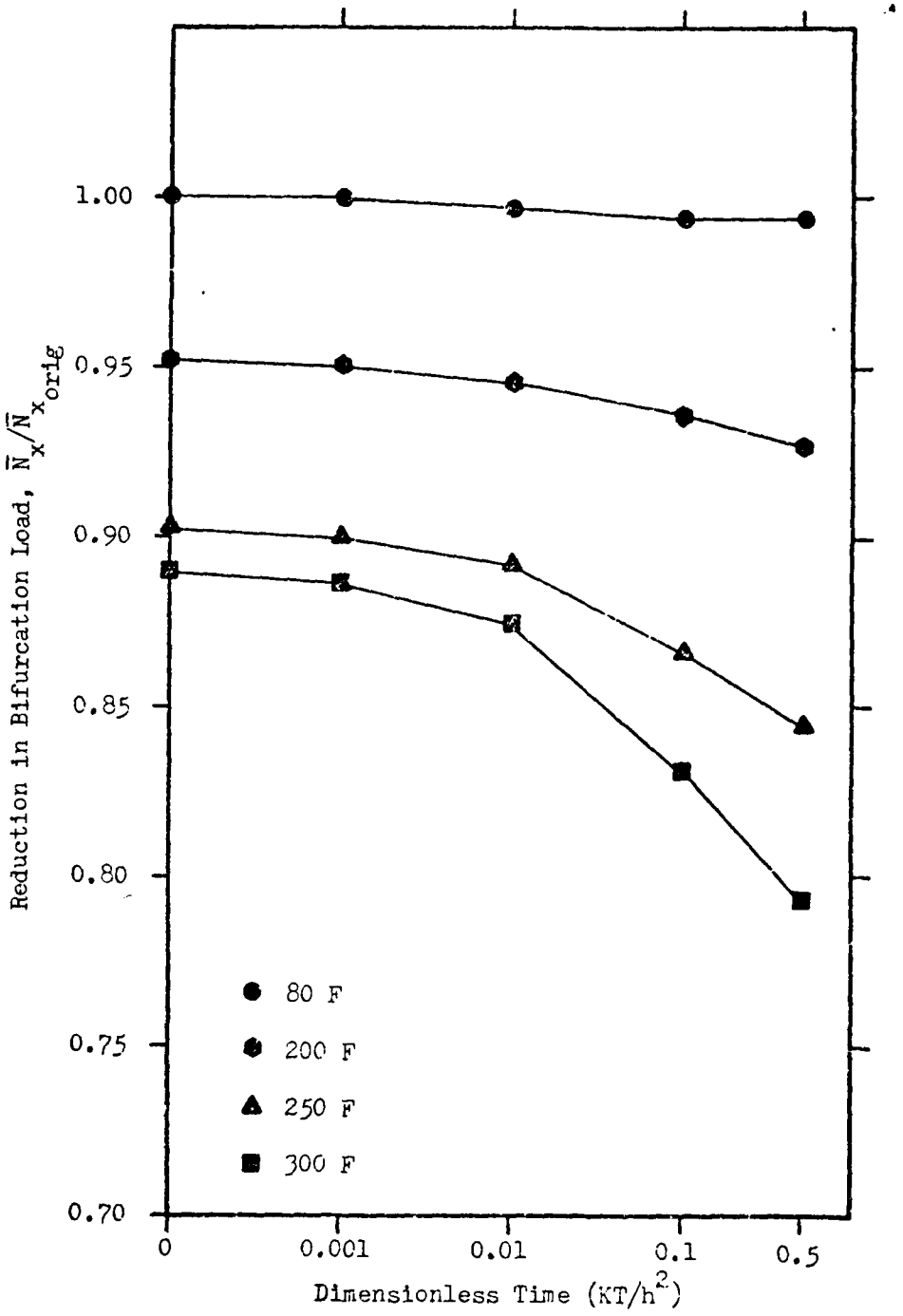

Figure 40. Case No. 41-60; $(45.,-45.)_{2S}$

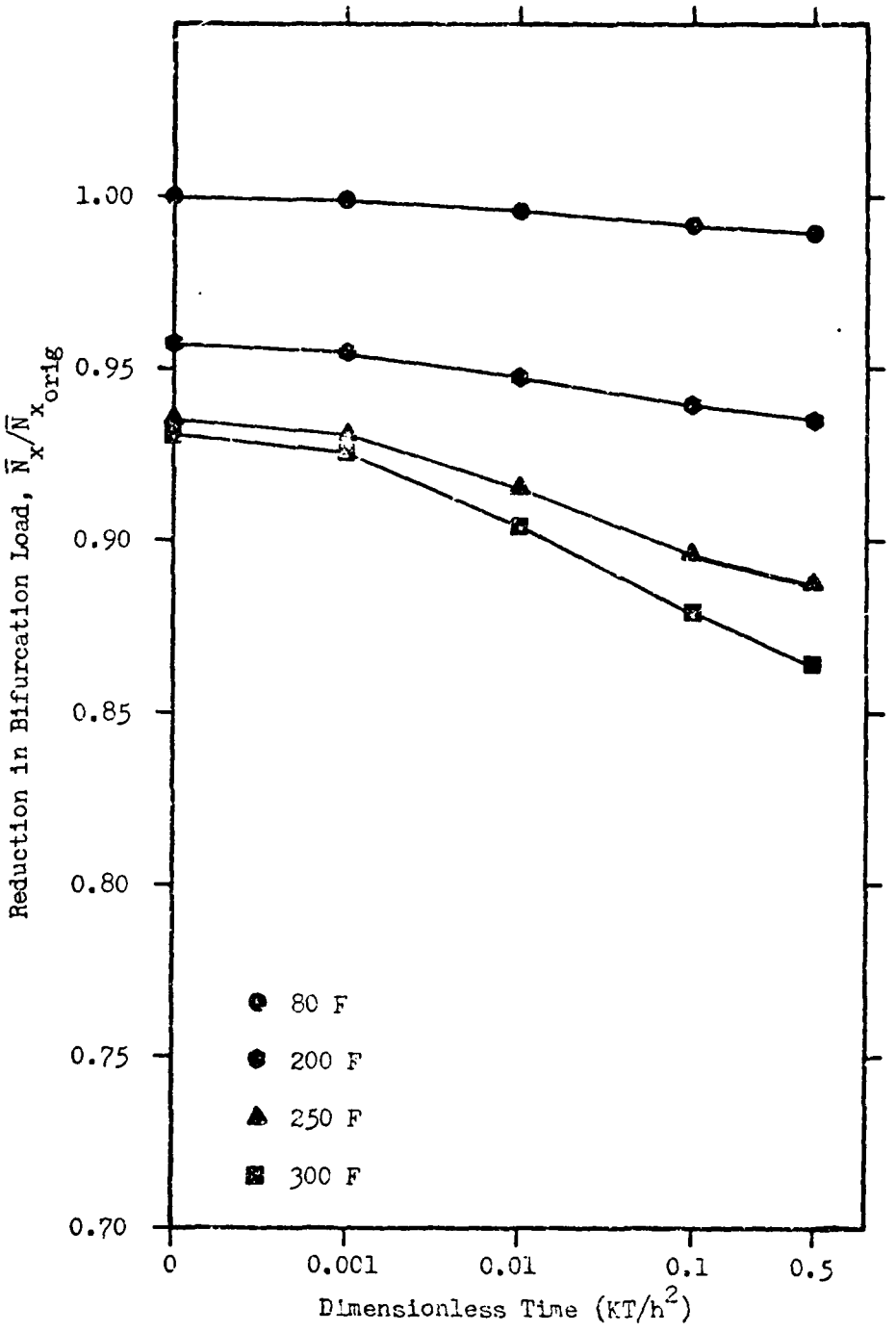

Figure 41. Case No. 101-120; $(0.,+45.,-45.,90.)_S$

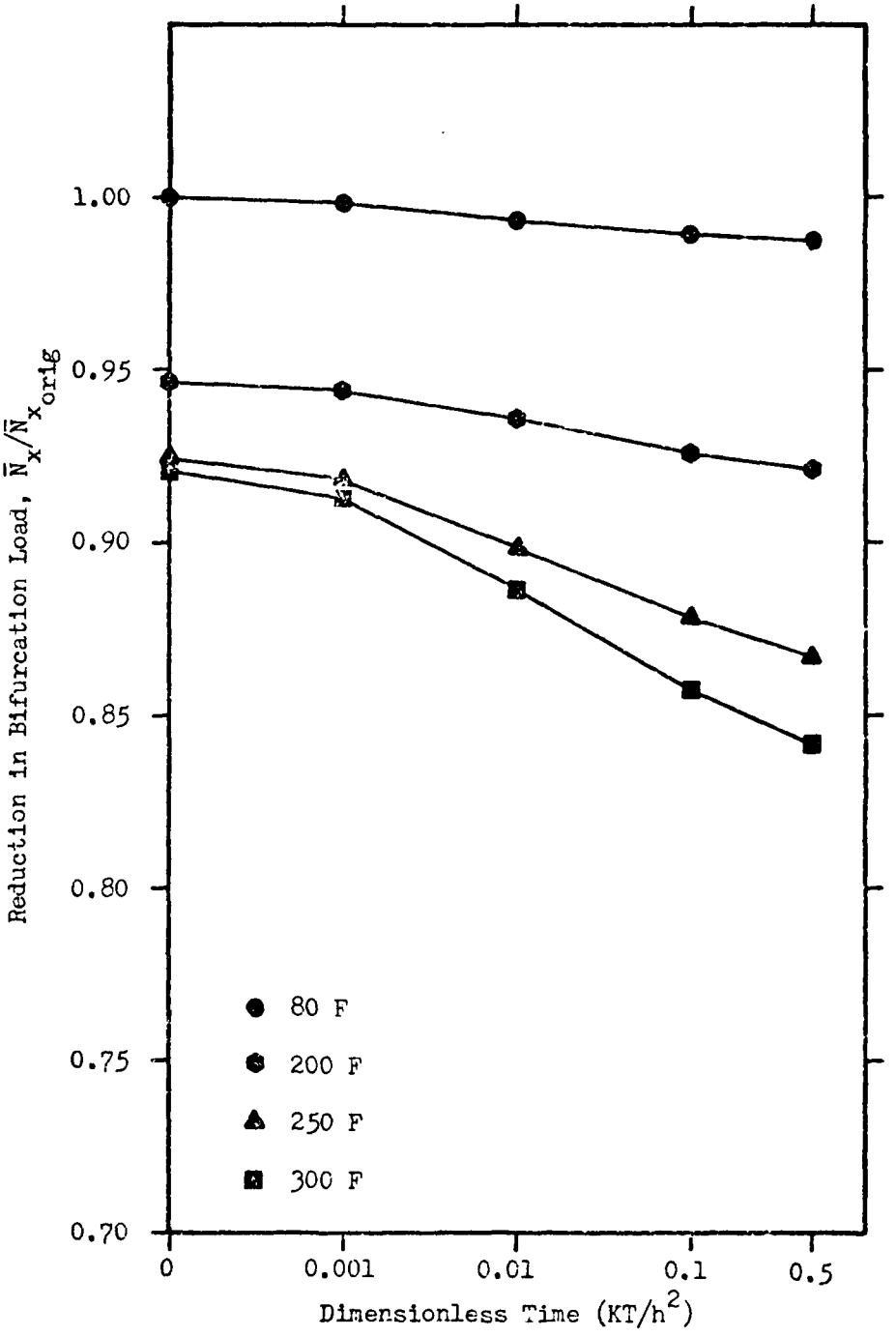

Figure 42. Case No. 121-140; $(90.,+45.,-45.,0.)_S$

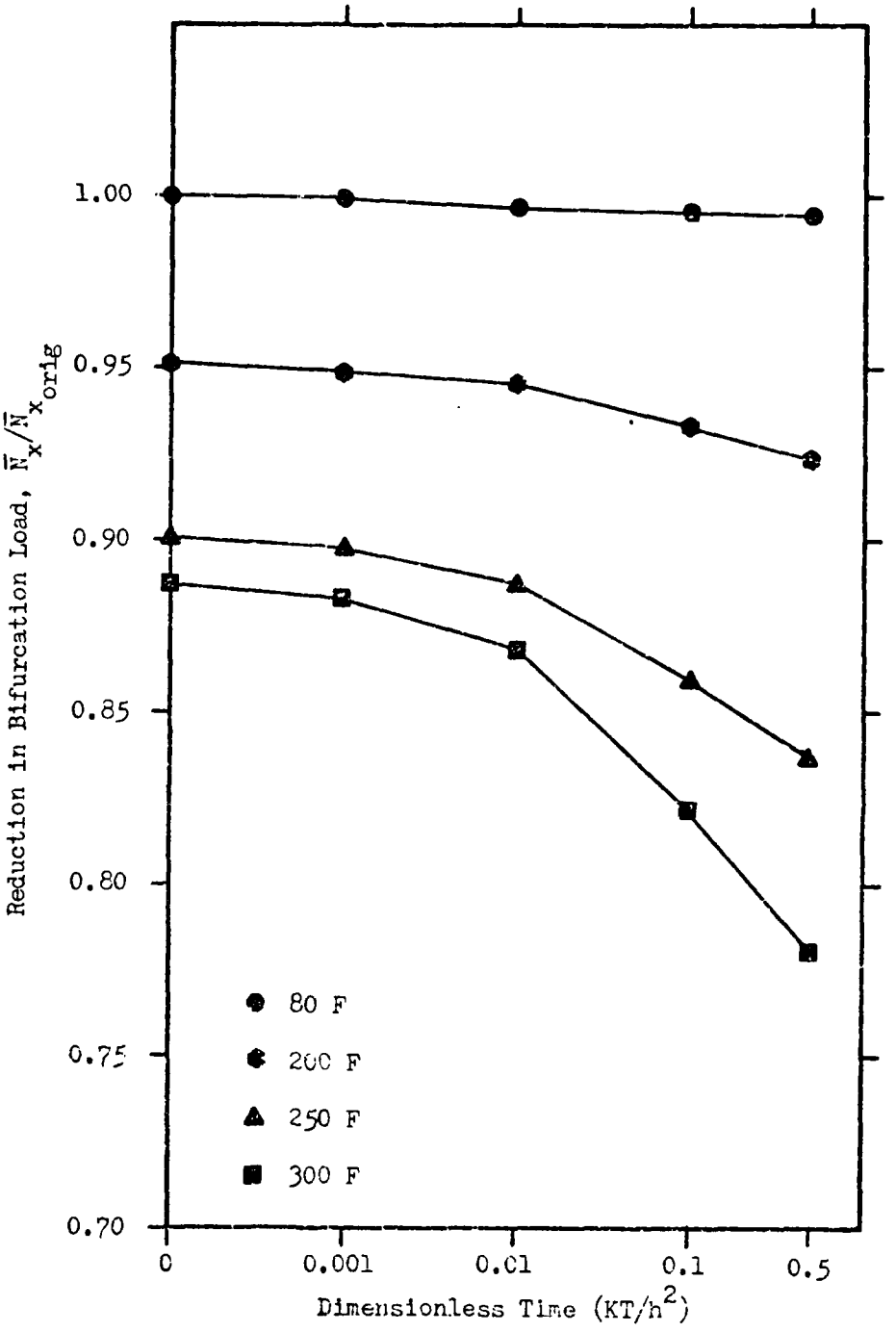

Figure 43. Case No. 141-160; $(45.,-45.)_{2S}$

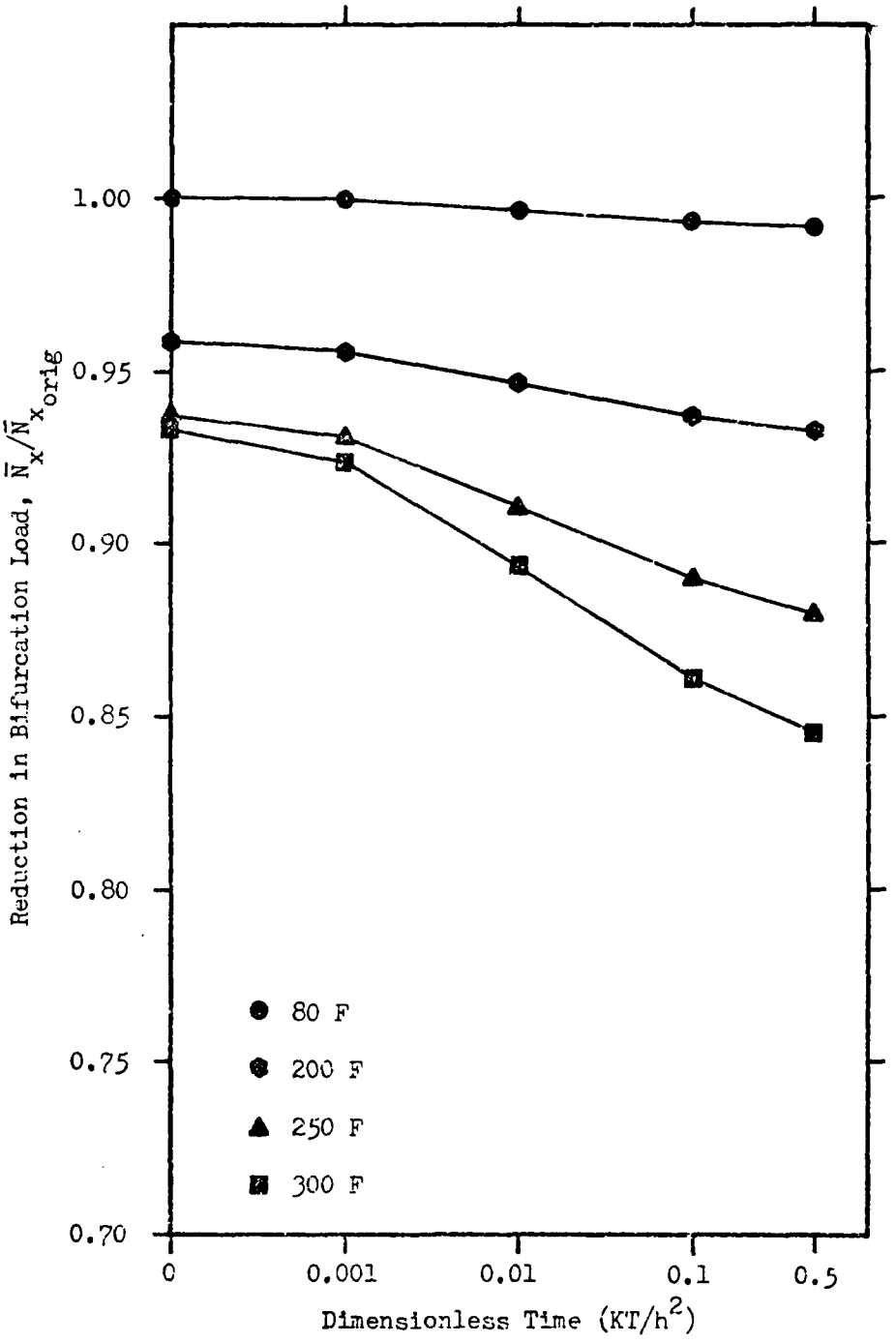

Figure 44. Case No. 201-220; $(0.,+45.,-45.,90.)_S$

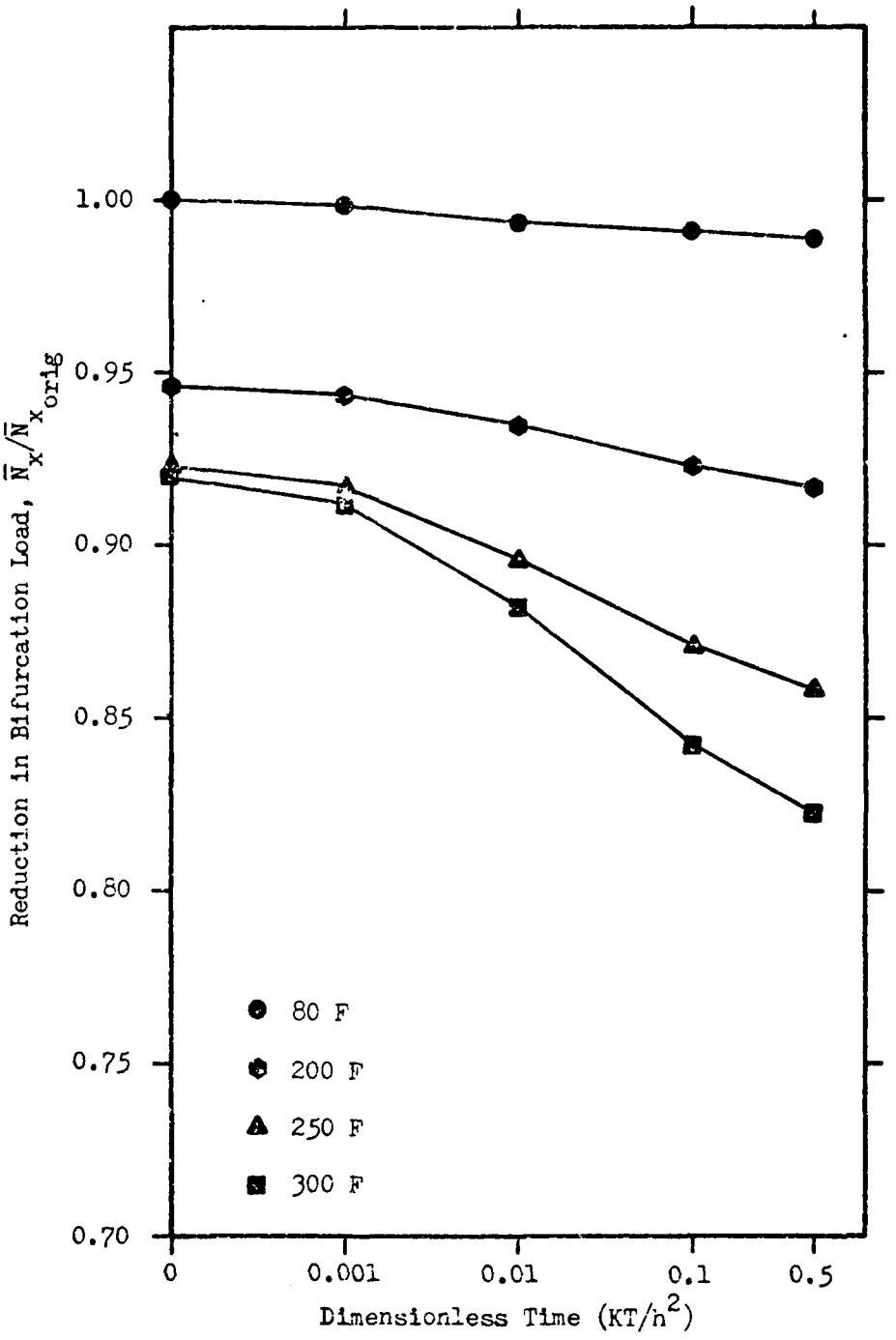

Figure 45. Case No. 221-240; $(90.,+45.,-45.,0.)_S$

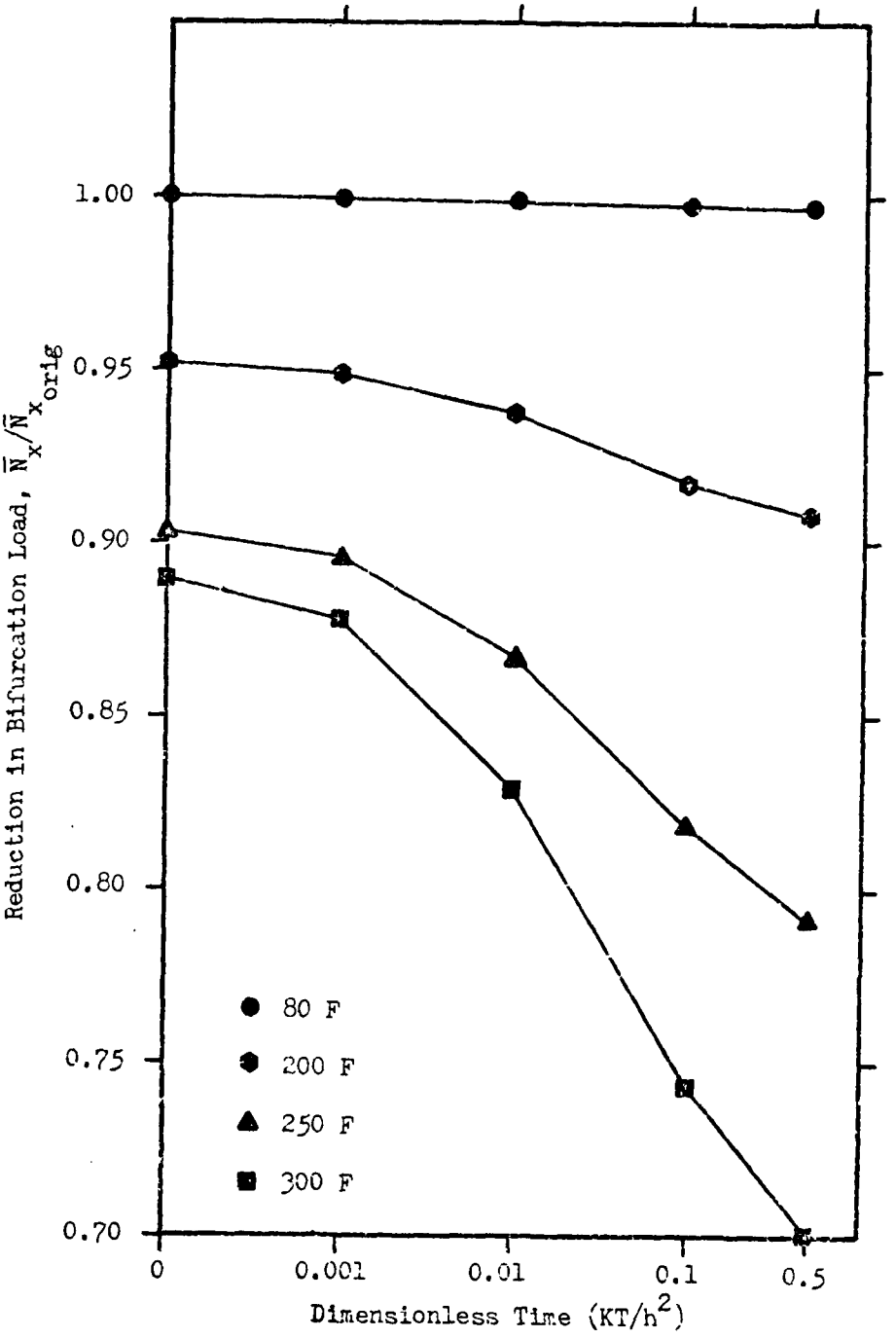

Figure 46. Case No. 241-260; $(45.-45.)_{2S}$

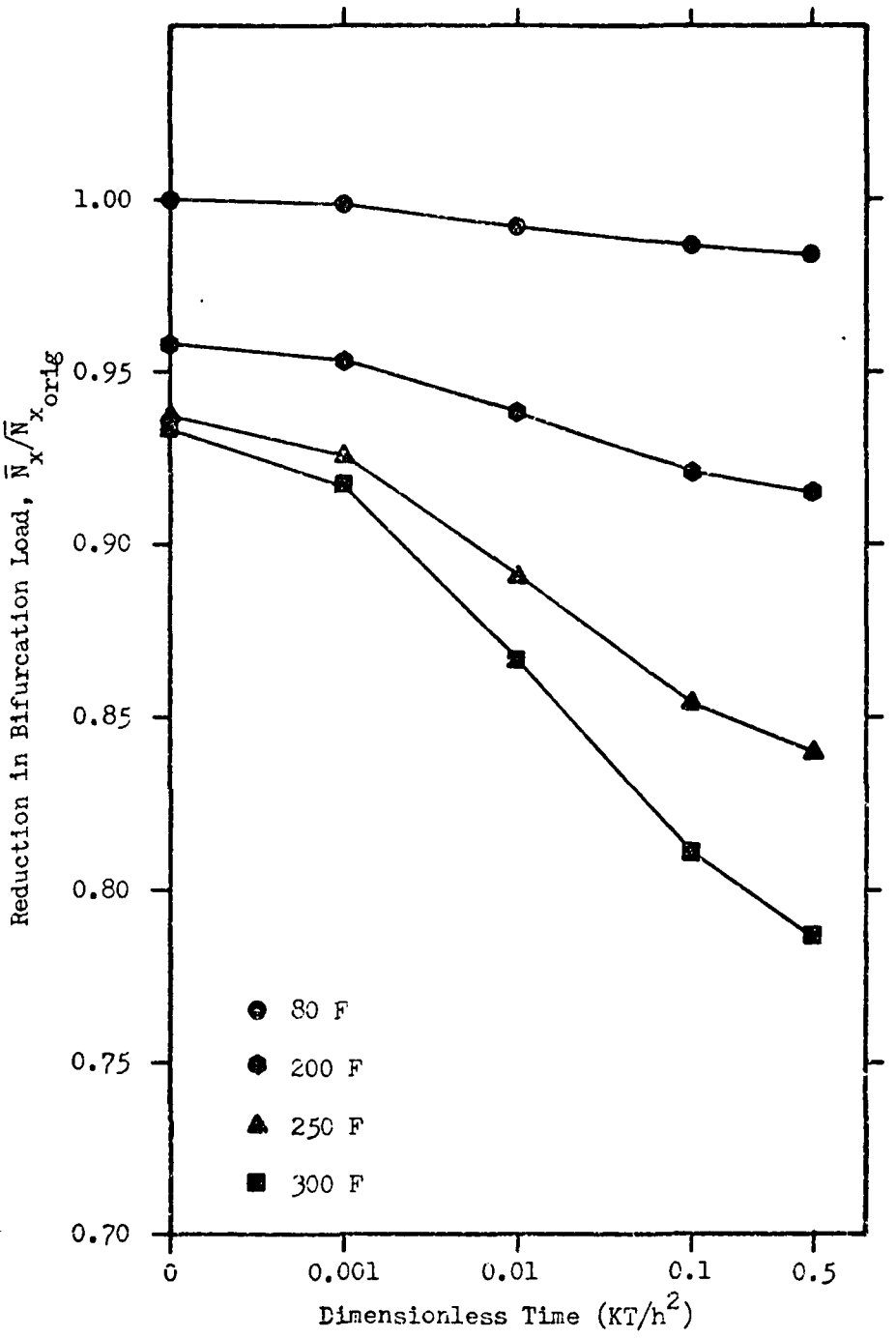

Figure 47. Case No. 401-420; $(0.,+45.,-45.,90.)_S$

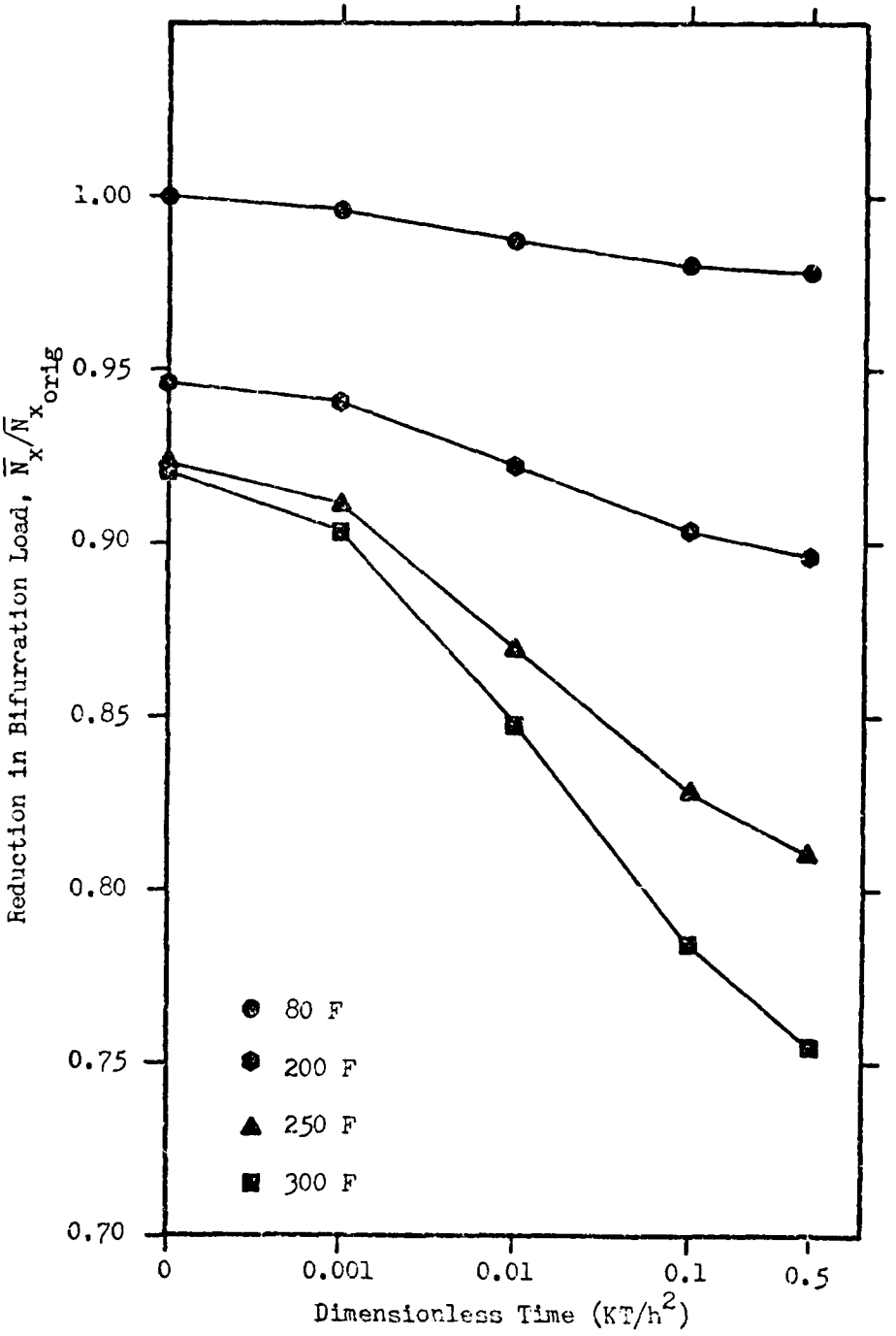

Figure 48. Case No. 421-440; $(90.,+45.,-45.,0.)_S$

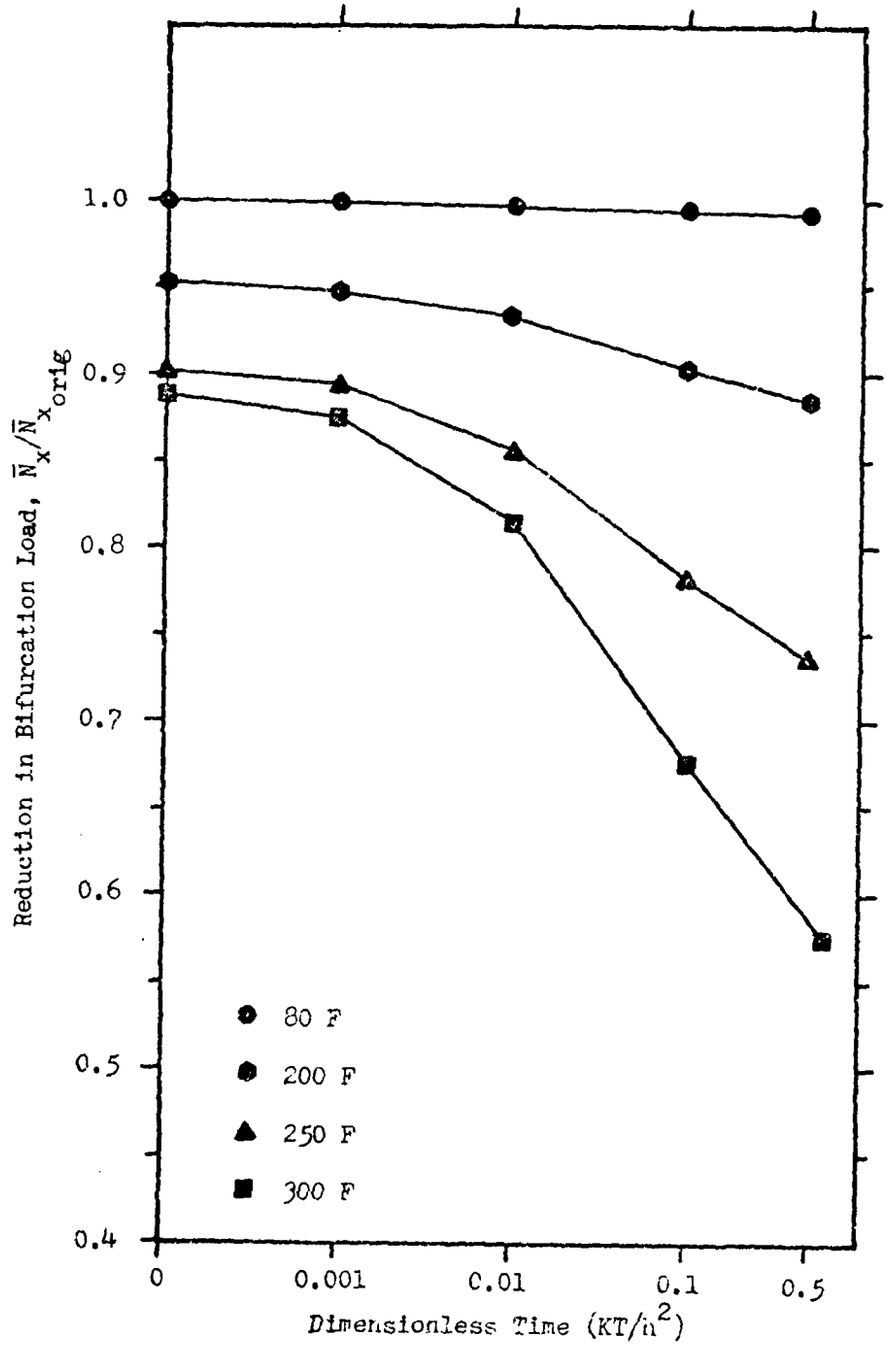

Figure 49. Case No. 441-460; $(45.,-45.)_{2S}$

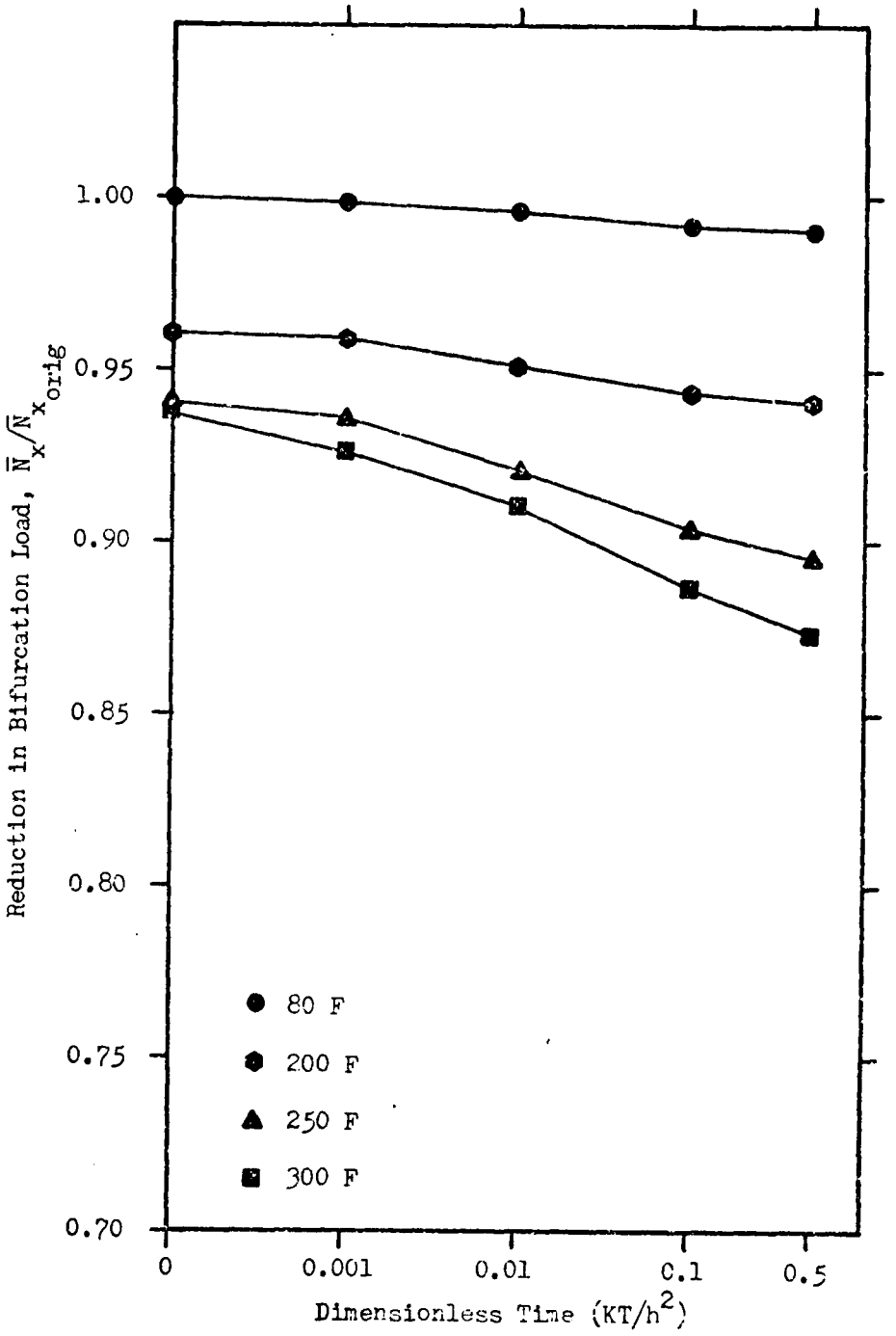

Figure 50. Case No. 601-620; $(0.,+45.,-45.,90.)_S$

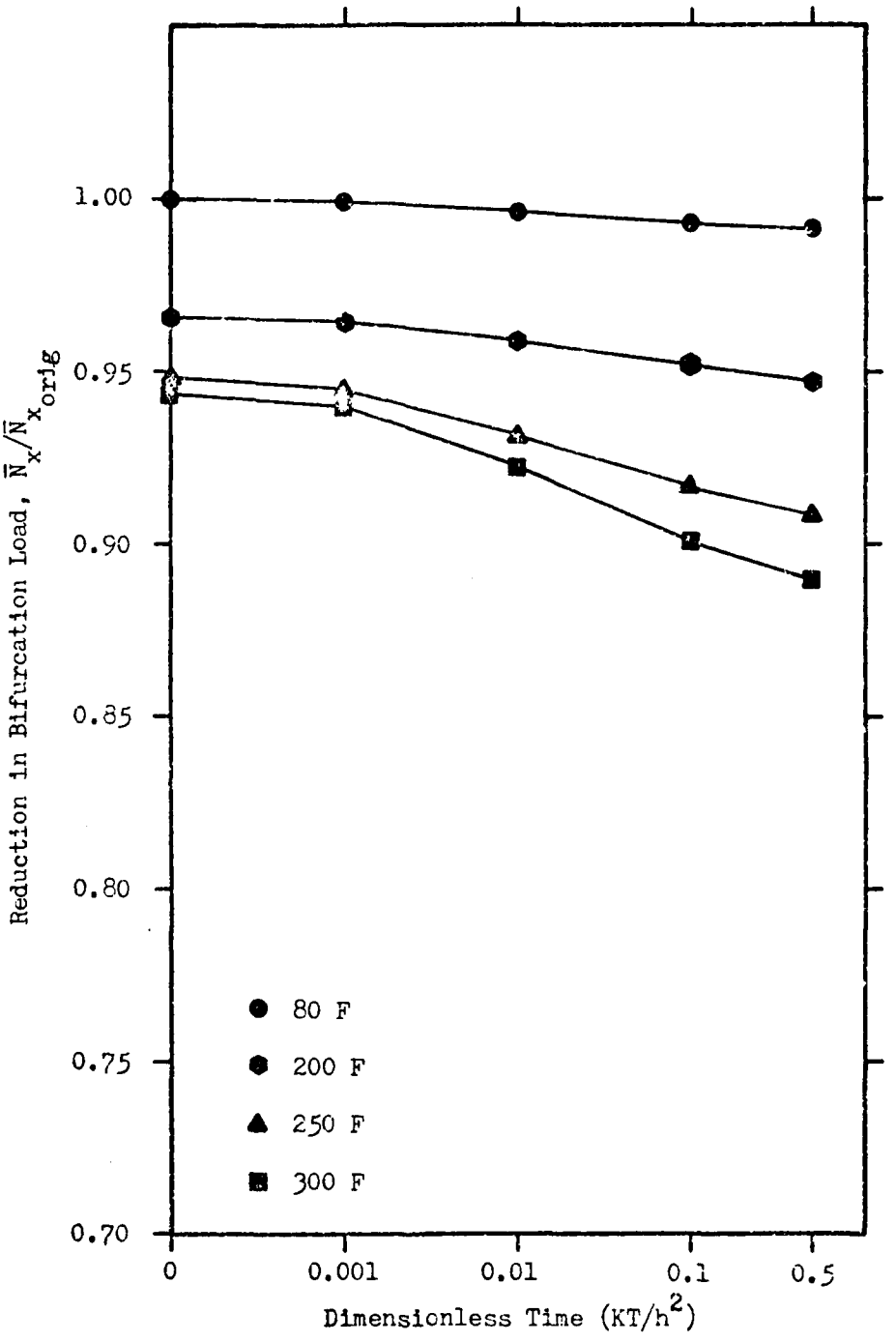

Figure 51. Case No. 701-720; $(0.,+45.,-45.,90.)_S$

Appendix C

Pre-Buckled and Eigenvector Displacement and Contour Plots

CASE NO. 40
PLOT NO. 1, UNIT 0, STEP 0
DISPLACEMENT GEOMETRY
UVW COMPONENT

MODEL SCALE = .5000E-00, ORIENT. = 0.00, 60.00,
SOLUTION SCALE = .2000E-05

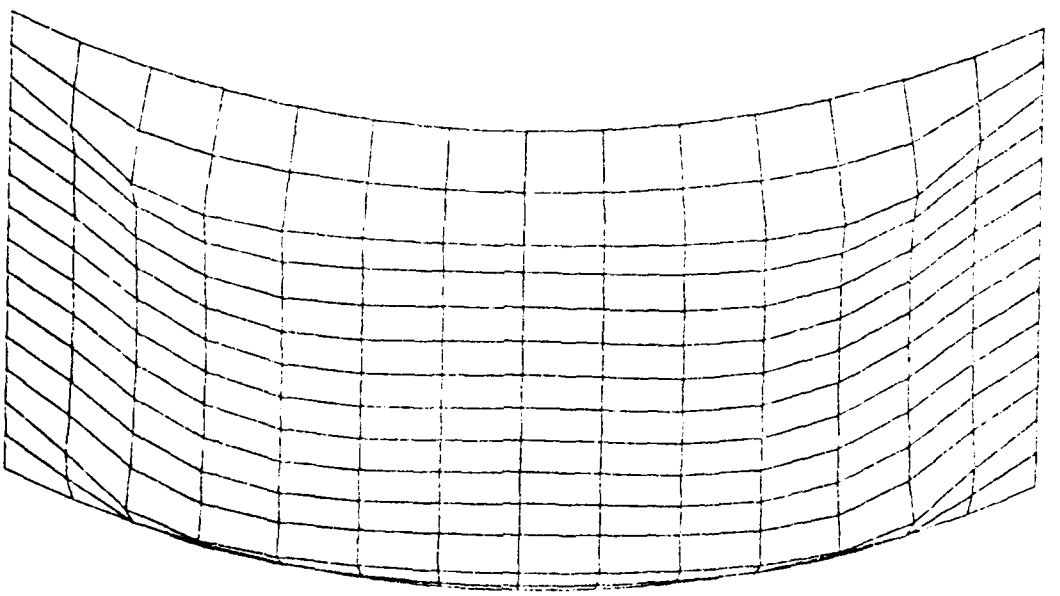

Figure 52. Case 40, UVW Displacement Component

CASE NO. 40
PLOT NO. 4. UNIT 1. STEP 0
DISPLACEMENT CONTOURS
V COMPONENT

MODEL SCALE = .5000E+00. ORIENT. = 0.00. 0.00.
SOLUTION SCALE = .7733E+05

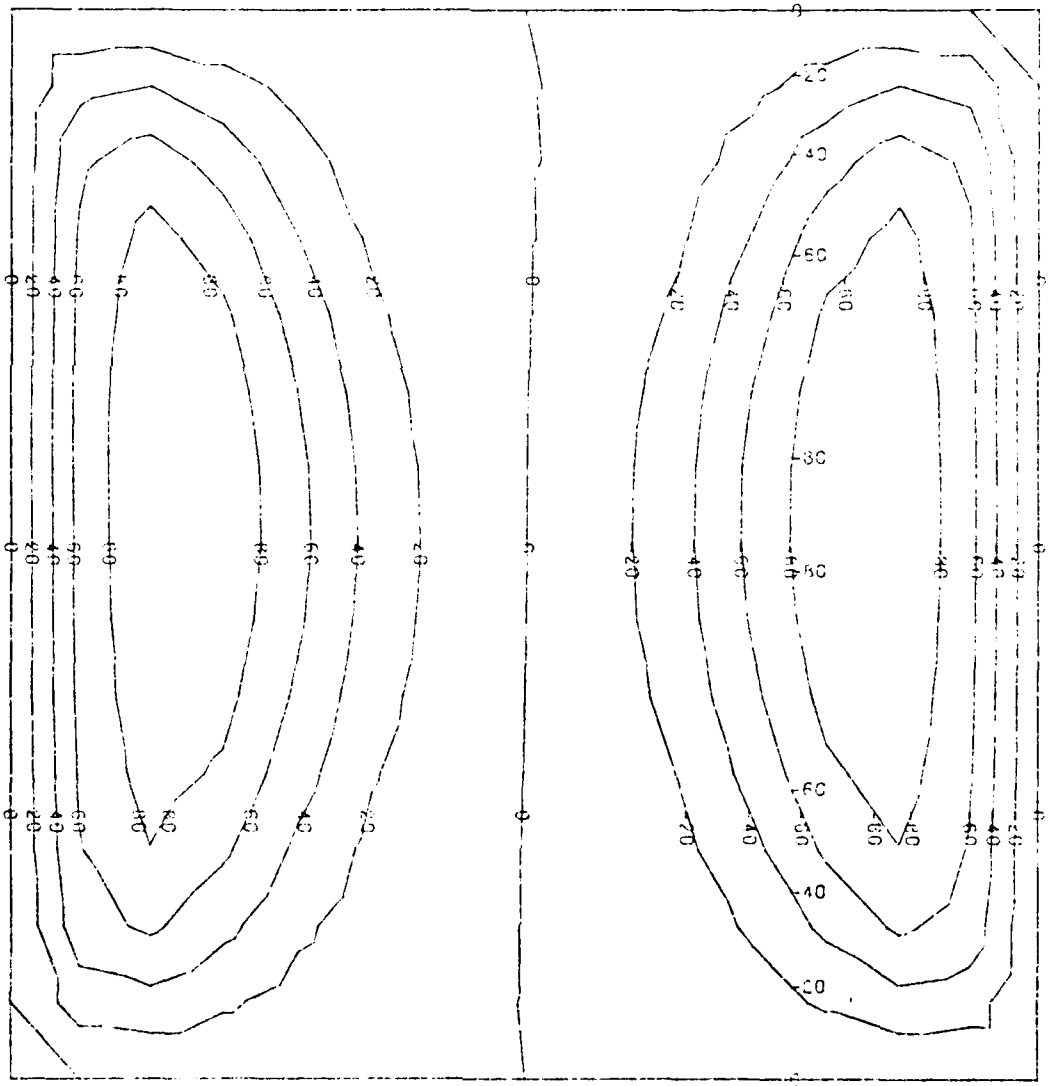

Figure 53. Case 40, V Displacement Component

CASE NO. 40
PLOT NO. 5. UNIT 1. STEP 0
DISPLACEMENT CONTOURS
W COMPONENT

MODEL SCALE = .5000E+00. ORIENT. = 0.00. 0.00.
SOLUTION SCALE = .4943E+07

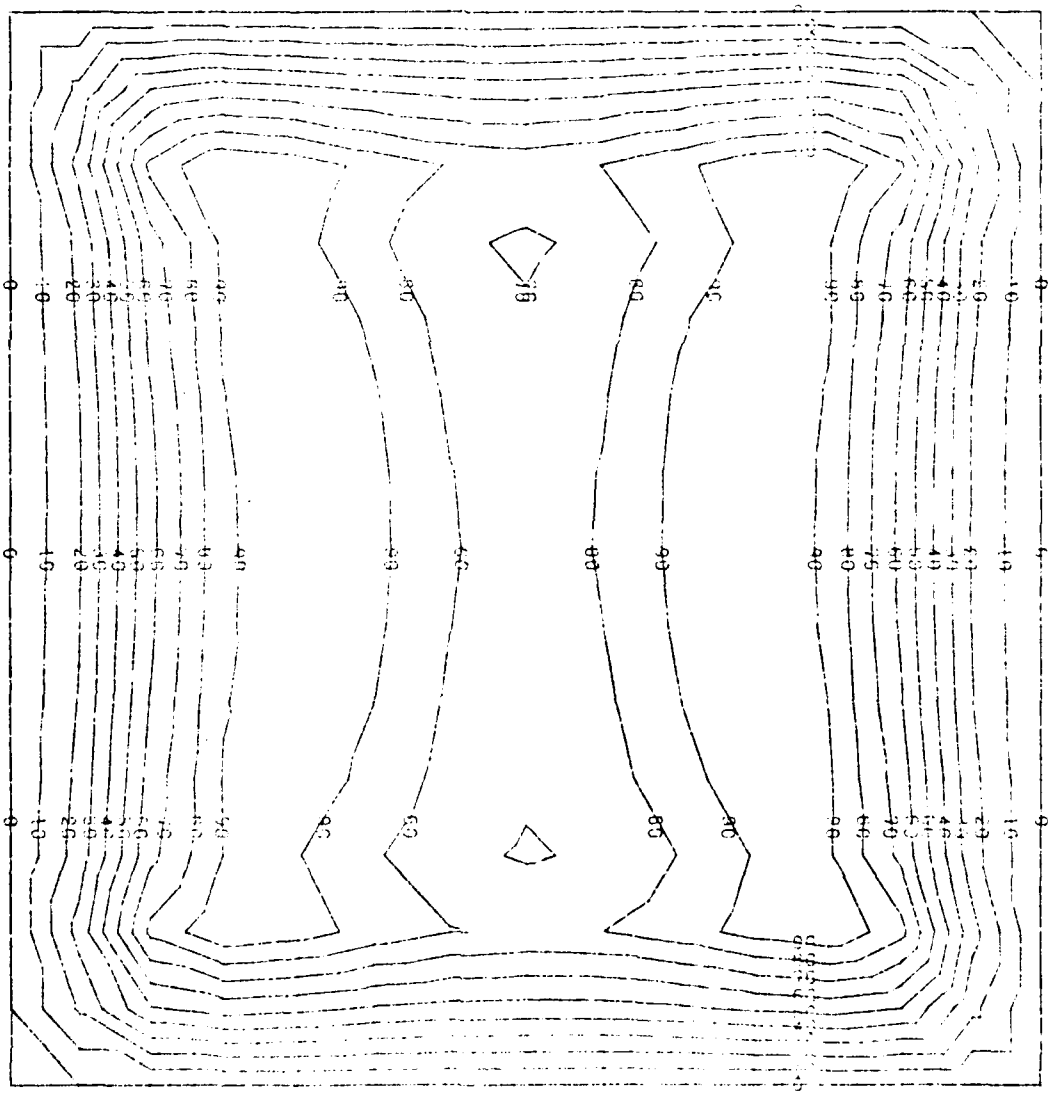

Figure 54. Case 40, W Displacement Component

CASE NO. 40
PLOT NO. 6, UNIT 1, STEP 0
DISPLACEMENT CONTOURS
RU COMPONENT

MODEL SCALE = .5000E+00, ORIENT. = 0.00, 0.00.
SOLUTION SCALE = .6343E+07

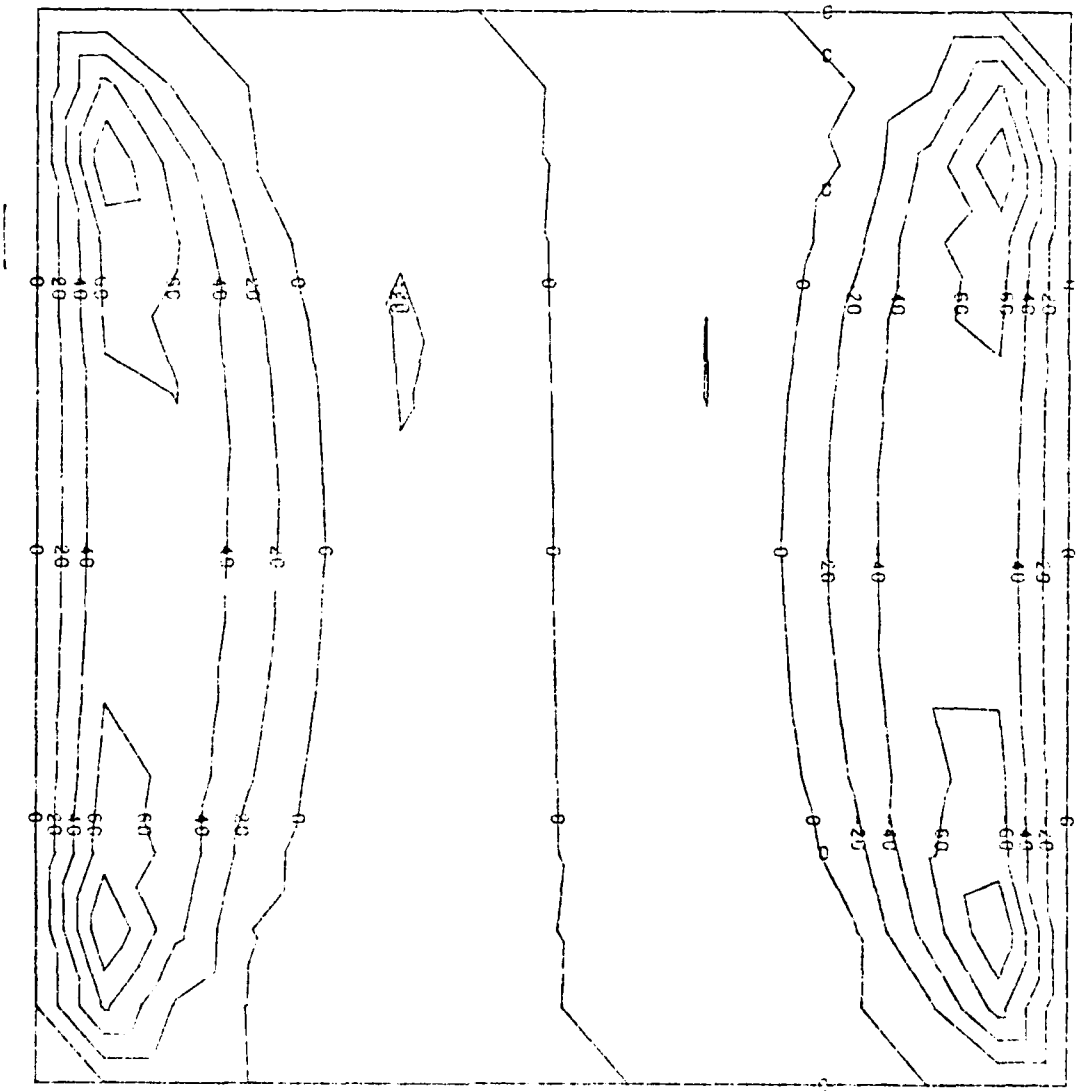

Figure 55. Case 40, RU Displacement Component

CASE NO. 40
PLOT NO. 7. UNIT 1. STEP 0
DISPLACEMENT CONTOURS
RV COMPONENT

MODEL SCALE = .5000E+00. ORIENT. = 0.00. 0.00.
SOLUTION SCALE = .3946E+07

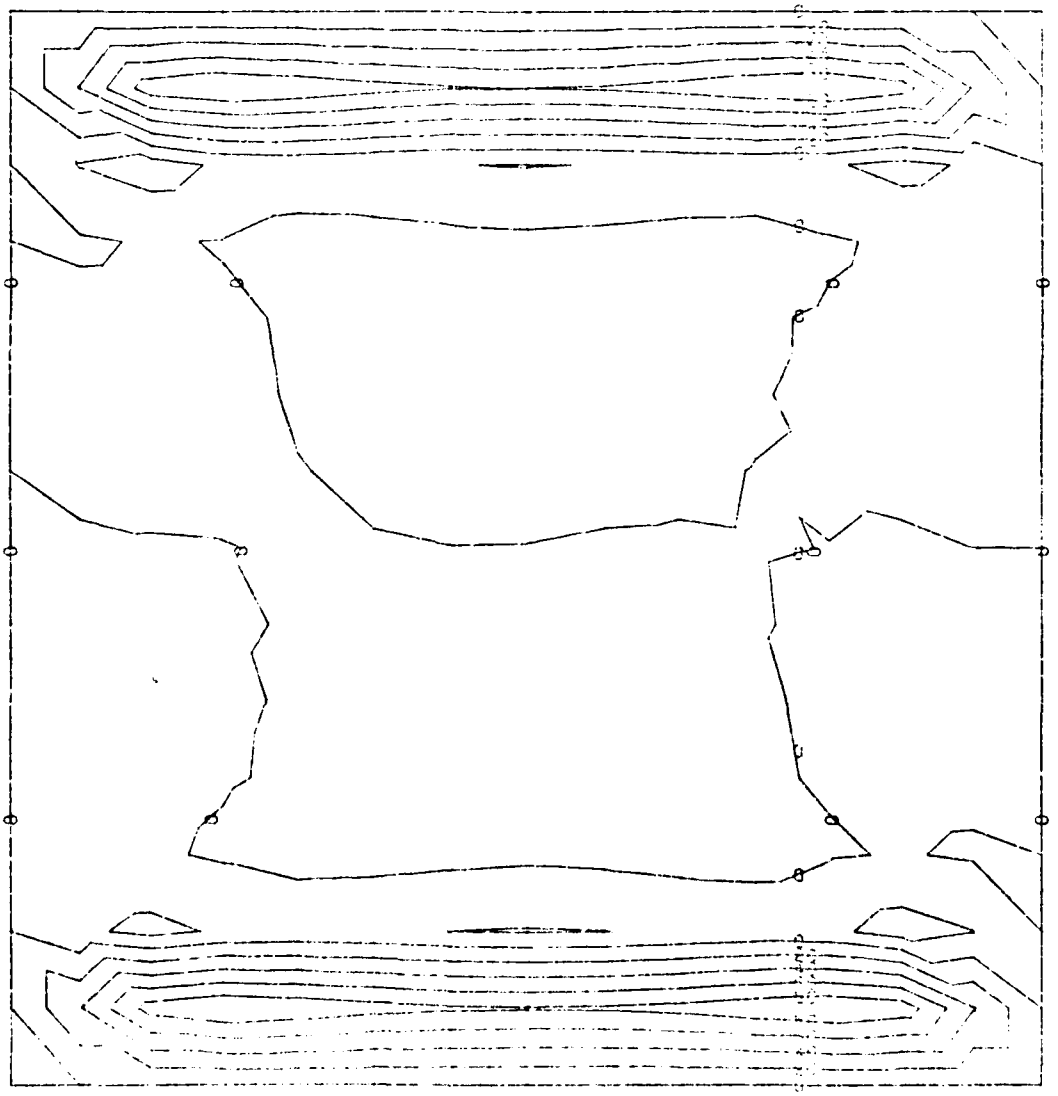

Figure 56. Case 40, RV Displacement Component

CASE NO. 60
PLOT NO. 1, UNIT U, STEP 0
DISPLACEMENT GEOMETRY
UVW COMPONENT
MODEL SCALE = .5000E+00, ORIENT. = 0.00. 60.00.
SOLUTION SCALE = .1000E+04

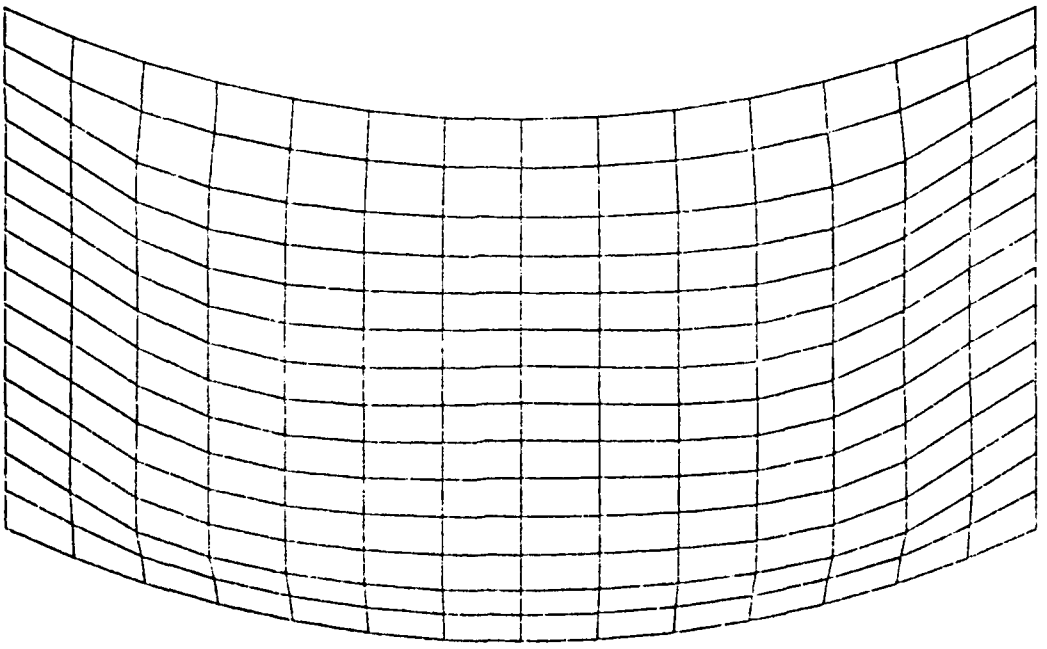

Figure 57. Case 60, UVW Displacement Component

CASE NO. 60
PLOT NO. 2. UNIT 0. STEP 0
EIGENVECTOR GEOMETRY
UVW COMPONENT , MODE 1
MODEL SCALE = .5000E+00. ORIENT. = 0.00. 60.00.
SOLUTION SCALE = .8000E+00

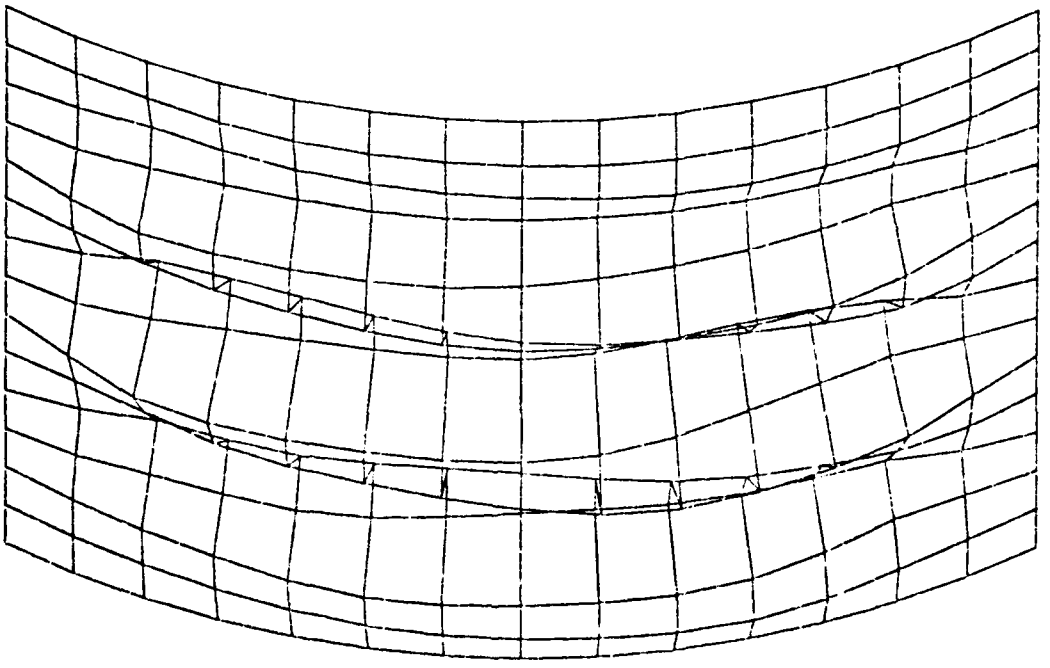

Figure 58. Case 60, UVW Eigenvector Component

CASE NO. 60
PLOT NO. 3, UNIT 1, STEP 0
DISPLACEMENT CONTOURS
U COMPONENT

MODEL SCALE = .5000E+00. ORIENT. = 0.00. 0.00.
SOLUTION SCALE = .5518E+05

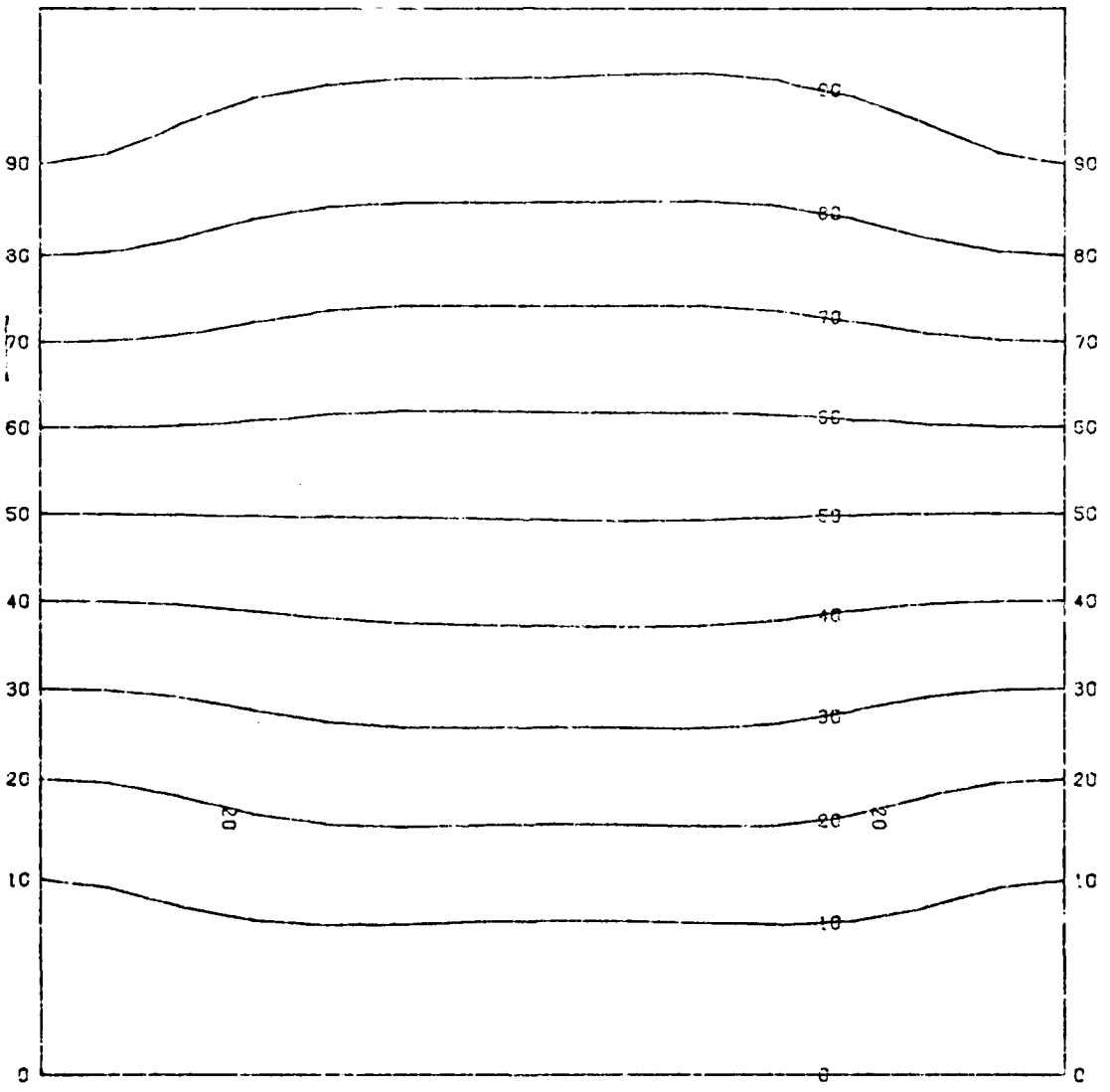

Figure 59. Case 60, U Displacement Component

CASE NO. 60
PLOT NO. 4, UNIT 1, STEP 0
DISPLACEMENT CONTOURS
V COMPONENT

MODEL SCALE = .6000E+00. ORIENT. = 0.00. 0.00.
SOLUTION SCALE = .5935E-07

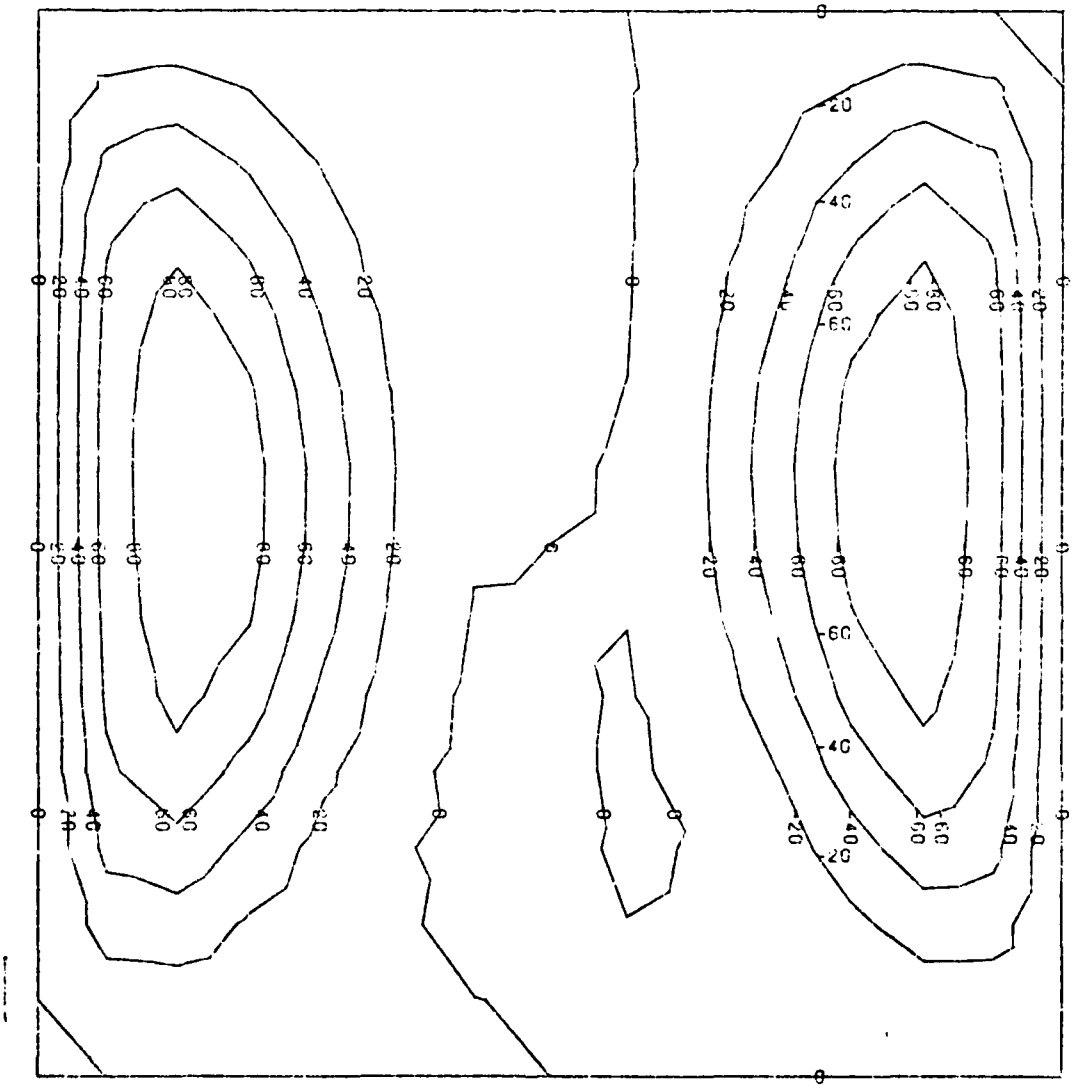

Figure 60. Case 60, V Displacement Component

CASE NO. 60
PLOT NO. 5, UNIT 1, STEP 0
DISPLACEMENT CONTOURS
W COMPONENT

MODEL SCALE = .5000E+00. ORIENT. = 0.00. 0.00.
SOLUTION SCALE = .3911E+06

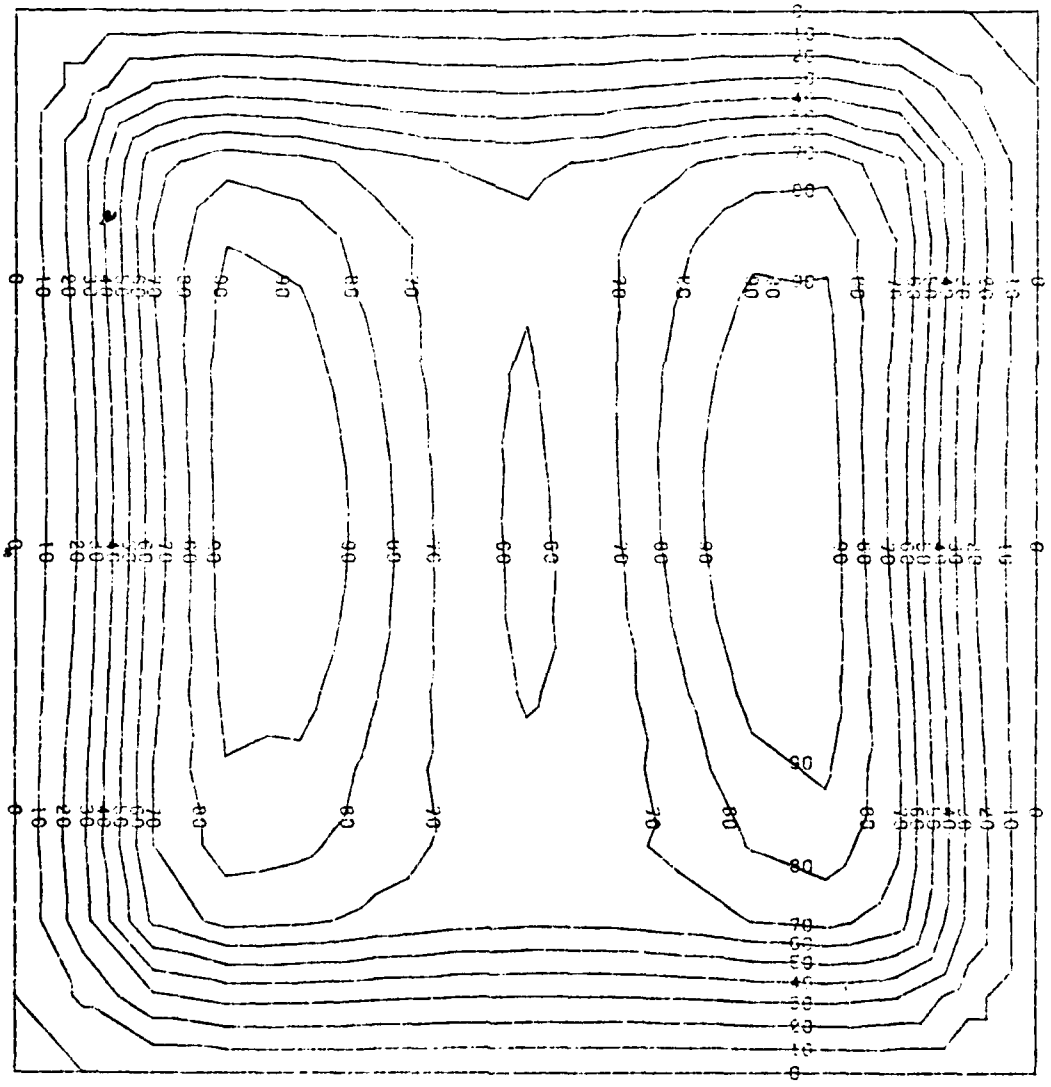

Figure 61. Case 60, W Displacement Component

CASE NO. 60
PLOT NO. 6. UNIT 1. STEP 0
DISPLACEMENT CONTOURS
RU COMPONENT

MODEL SCALE = .5000E+00. ORIENT. = 0.00. 0.00.
SOLUTION SCALE = .5963E+06

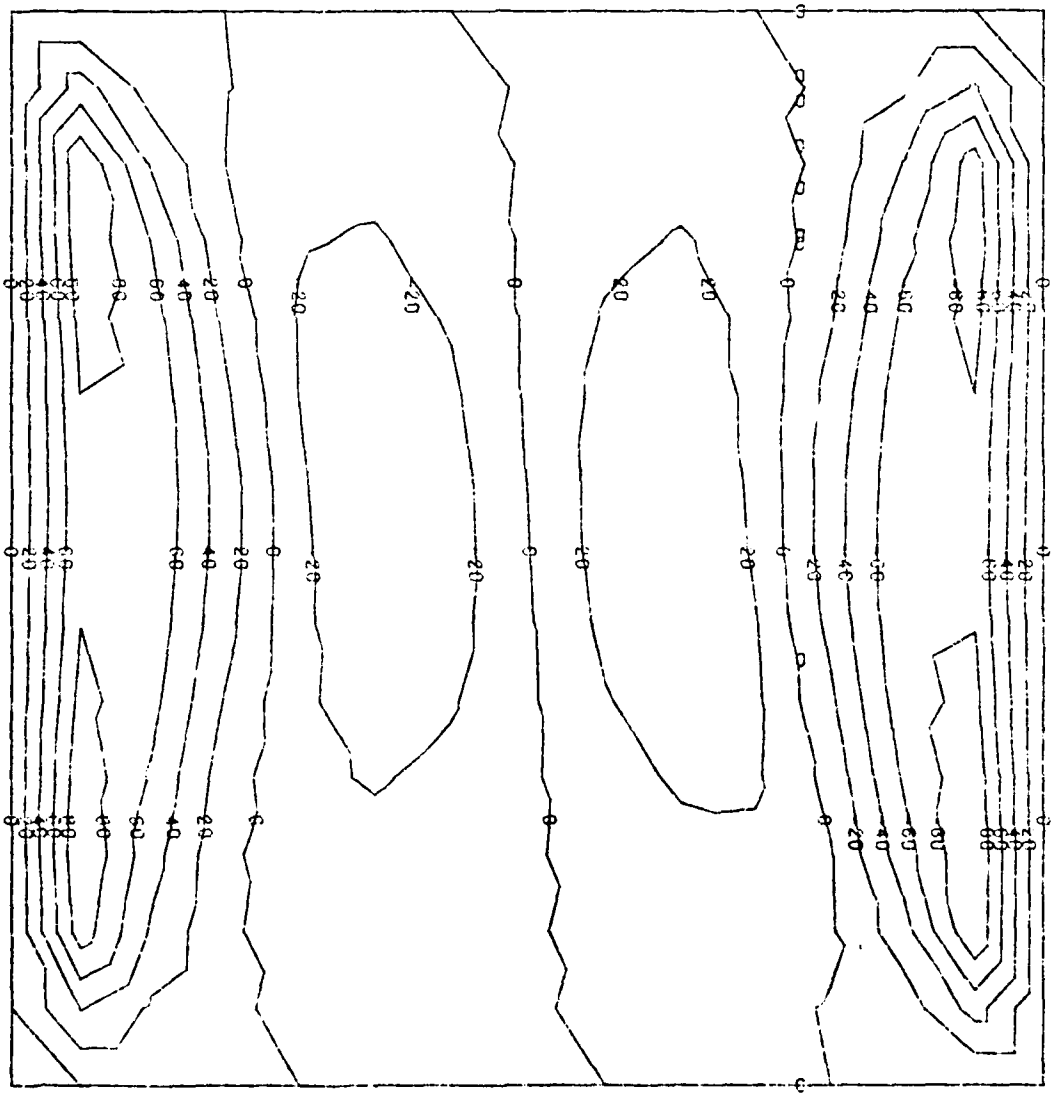

Figure 62. Case 60, RU Displacement Component

CASE NO. 60
PLOT NO. 7, UNIT 1, STEP 0
DISPLACEMENT CONTOURS
RV COMPONENT

MODEL SCALE = .5000E+00. ORIENT. = 0.00. 0.00.
SOLUTION SCALE = .5079E+06

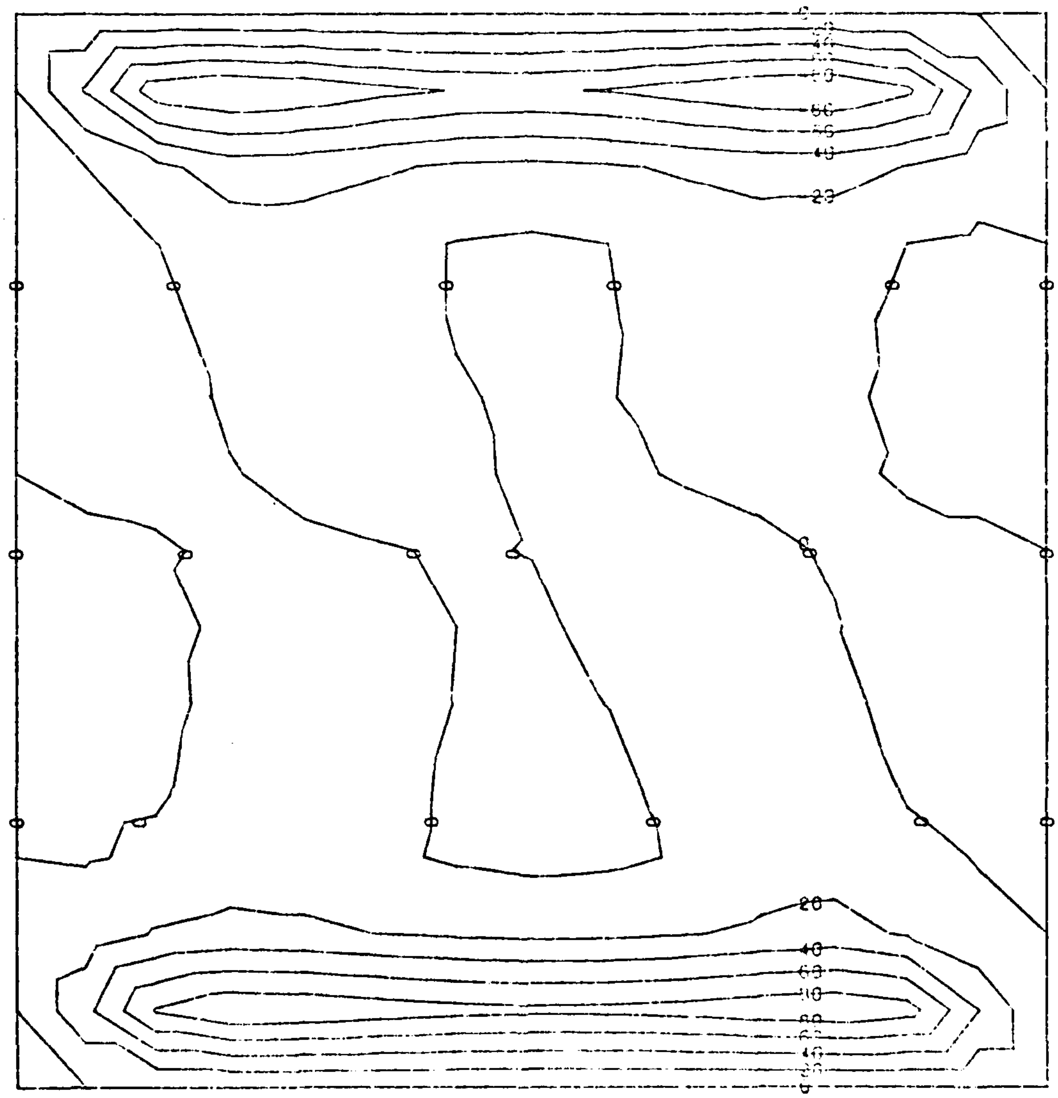

Figure 63. Case 60, RV Displacement Component

CASE NO. 120
PLOT NO. 1, UNIT 0, STEP 0
DISPLACEMENT GEOMETRY
UVW COMPONENT

MODEL SCALE = .5000E+00. ORIENT. = 0.00, 60.00.
SOLUTION SCALE = .2000E+05

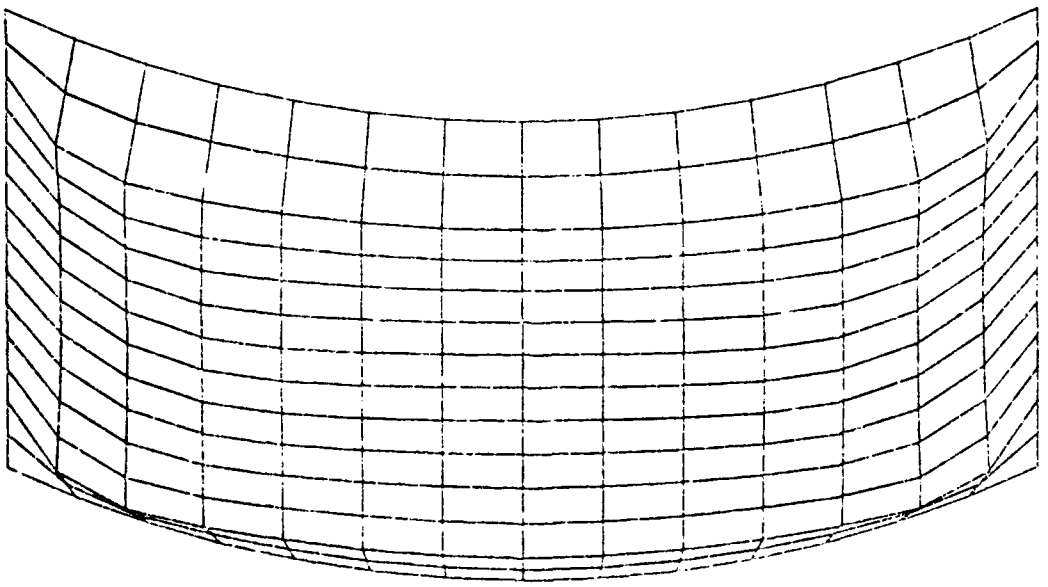

Figure 64. Case 120, UVW Displacement Component

CASE NO. 120
PLOT NO. 2, UNIT 0, STEP 3
EIGENVECTOR GEOMETRY
UVW COMPONENT , MODE 1

MODEL SCALE = .5000E+00, ORIENT. = 0.00, 60.00.
SOLUTION SCALE = .5000E+00

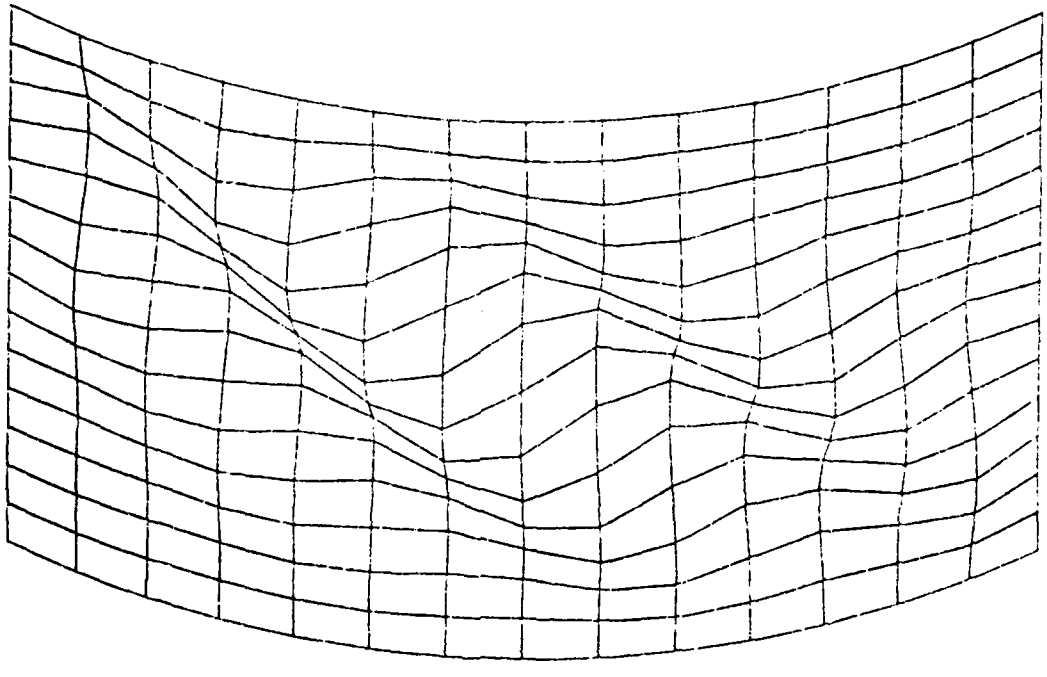

Figure 65. Case 120, UVW Eigenvector Component

CASE NO. 120
PLOT NO. 4, UNIT 1, STEP 0
DISPLACEMENT CONTOURS
V COMPONENT

MODEL SCALE = .5000E+00. ORIENT. = 0.00. 0.00.
SOLUTION SCALE = .1674E+09

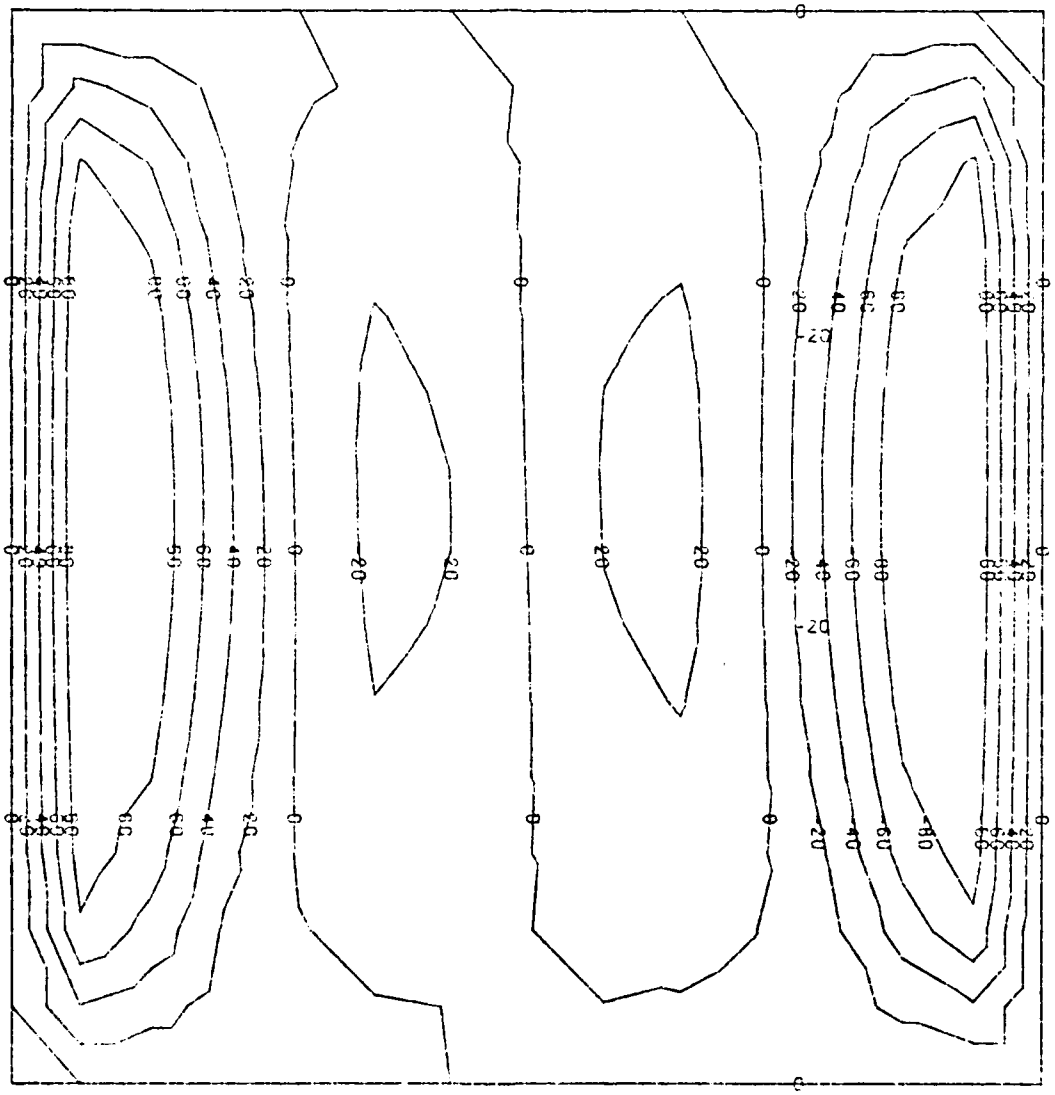

Figure 66. Case 120, V Displacement Component

CASE NO. 120
PLOT NO. 5, UNIT 1, STEP 0
DISPLACEMENT CONTOURS
W COMPONENT

MODEL SCALE = .5000E+00. ORIENT. = 0.00. 0.00.
SOLUTION SCALE = .5348E+07

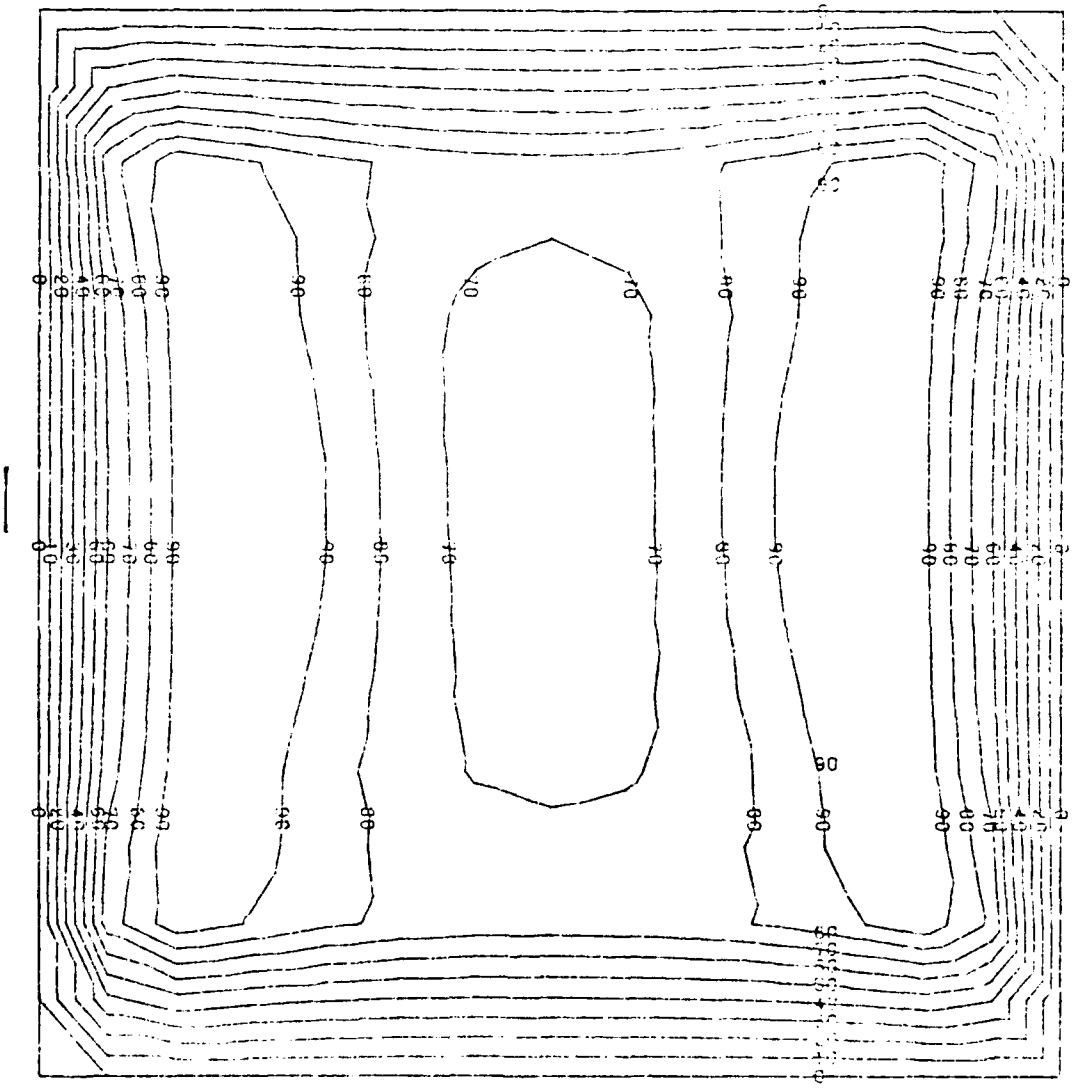

Figure 67. Case 120, W Displacement Component

CASE NO. 120
PLOT NO. 6, UNIT 1, STEP 0
DISPLACEMENT CONTOURS
RU COMPONENT

MODEL SCALE = .5000E+00, ORIENT. = 0.00, 0.00,
SOLUTION SCALE = .4200E+07

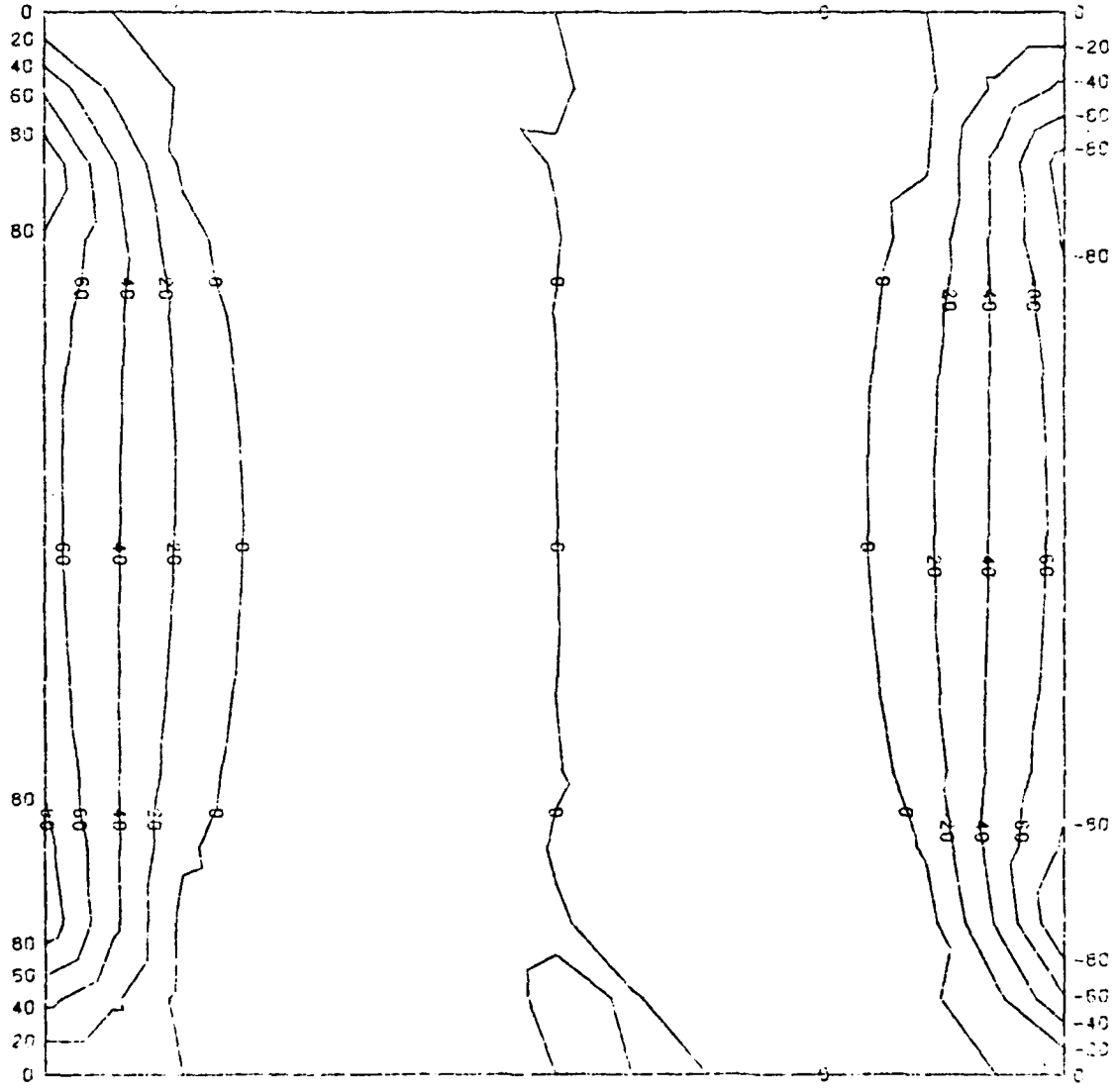

Figure 68. Case 120, RU Displacement Component

CASE NO. 120
PLOT NO. 7, UNIT 1, STEP 0
DISPLACEMENT CONTOURS
RV COMPONENT

MODEL SCALE = .5000E+00. ORIENT. = 0.00, 0.00,
SOLUTION SCALE = .5028E+07

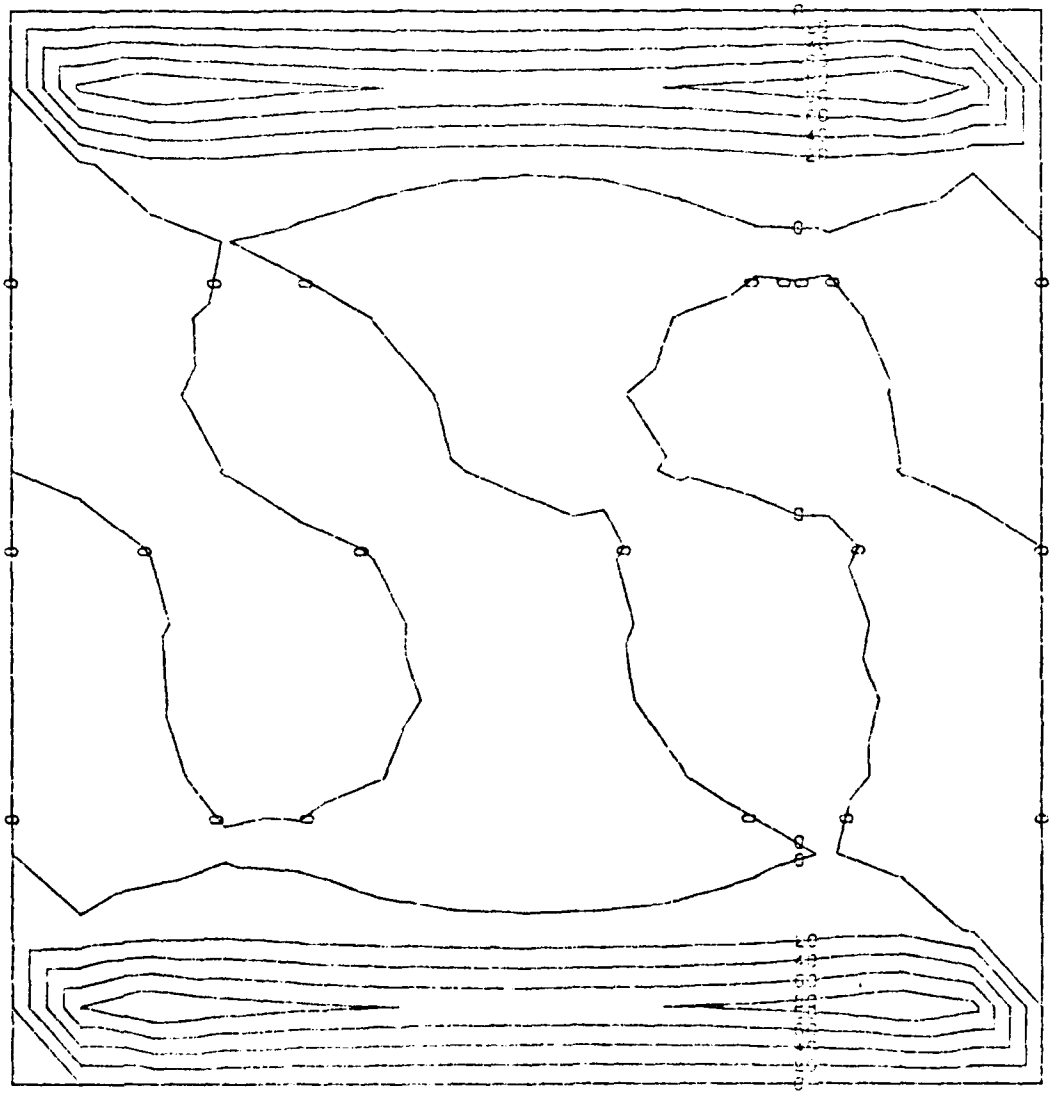

Figure 69. Case 120, RV Displacement Component

CASE NO. 140
PLOT NO. 1, UNIT 0, STEP 0
DISPLACEMENT GEOMETRY
UVW COMPONENT

MODEL SCALE = .6000E-00, ORIENT. = 0.00, 60.00,
SOLUTION SCALE = .2000E-05

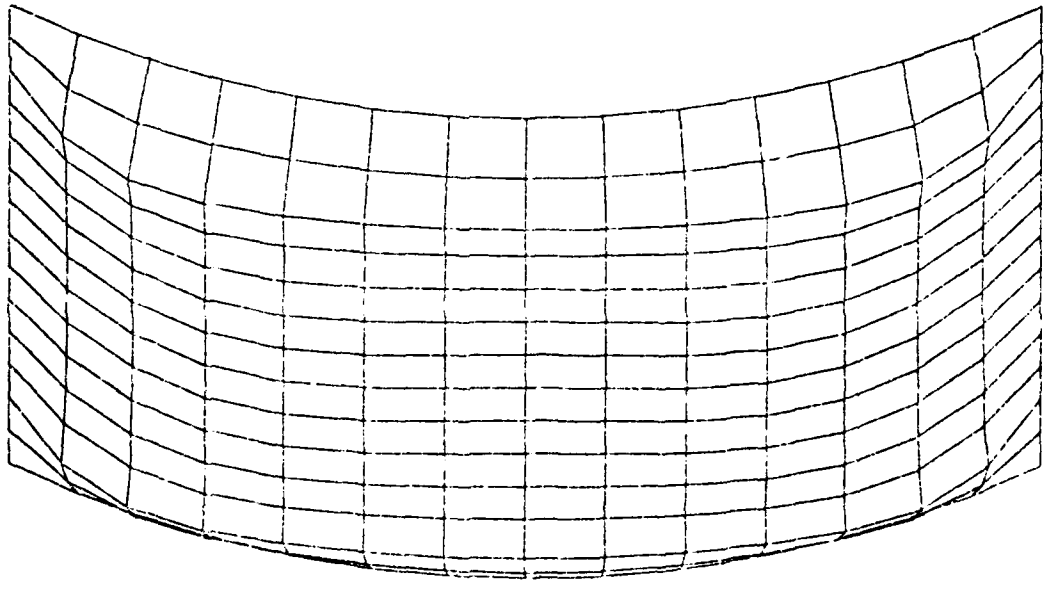

Figure 70. Case 140, UVW Displacement Component

CASE NO. 140
PLOT NO. 4. UNIT 1. STEP 0
DISPLACEMENT CONTOURS
V COMPONENT

MODEL SCALE = .5000E+00. ORIENT. = 0.00. 0.00.
SOLUTION SCALE = .1228E+03

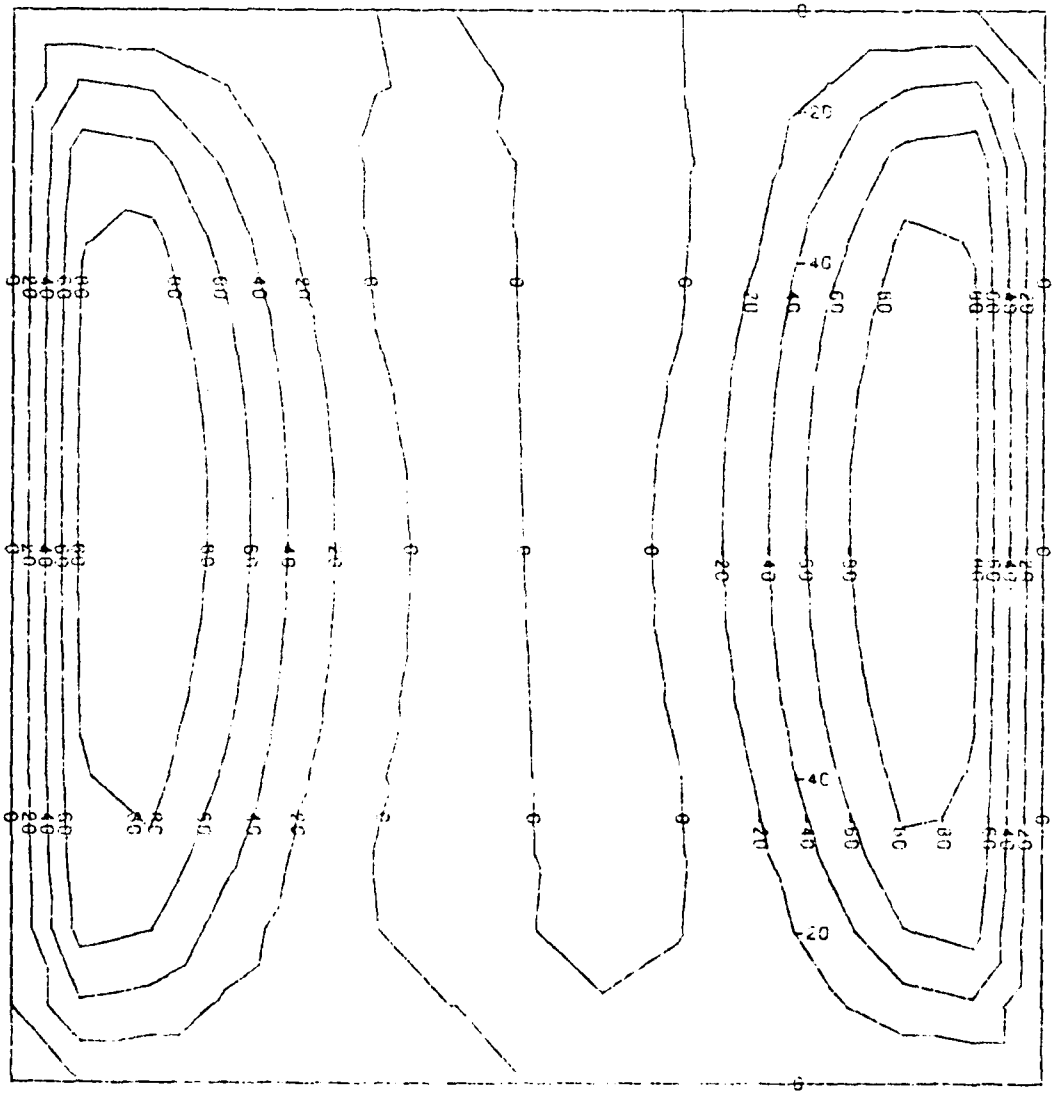

Figure 71. Case 140, V Displacement Component

CASE NO. 140
PLOT NO. 5. UNIT 1. STEP 0
DISPLACEMENT CONTOURS
W COMPONENT

MODEL SCALE = .5000E+00. ORIENT. = 0.00. 0.00.
SOLUTION SCALE = .5204E+07

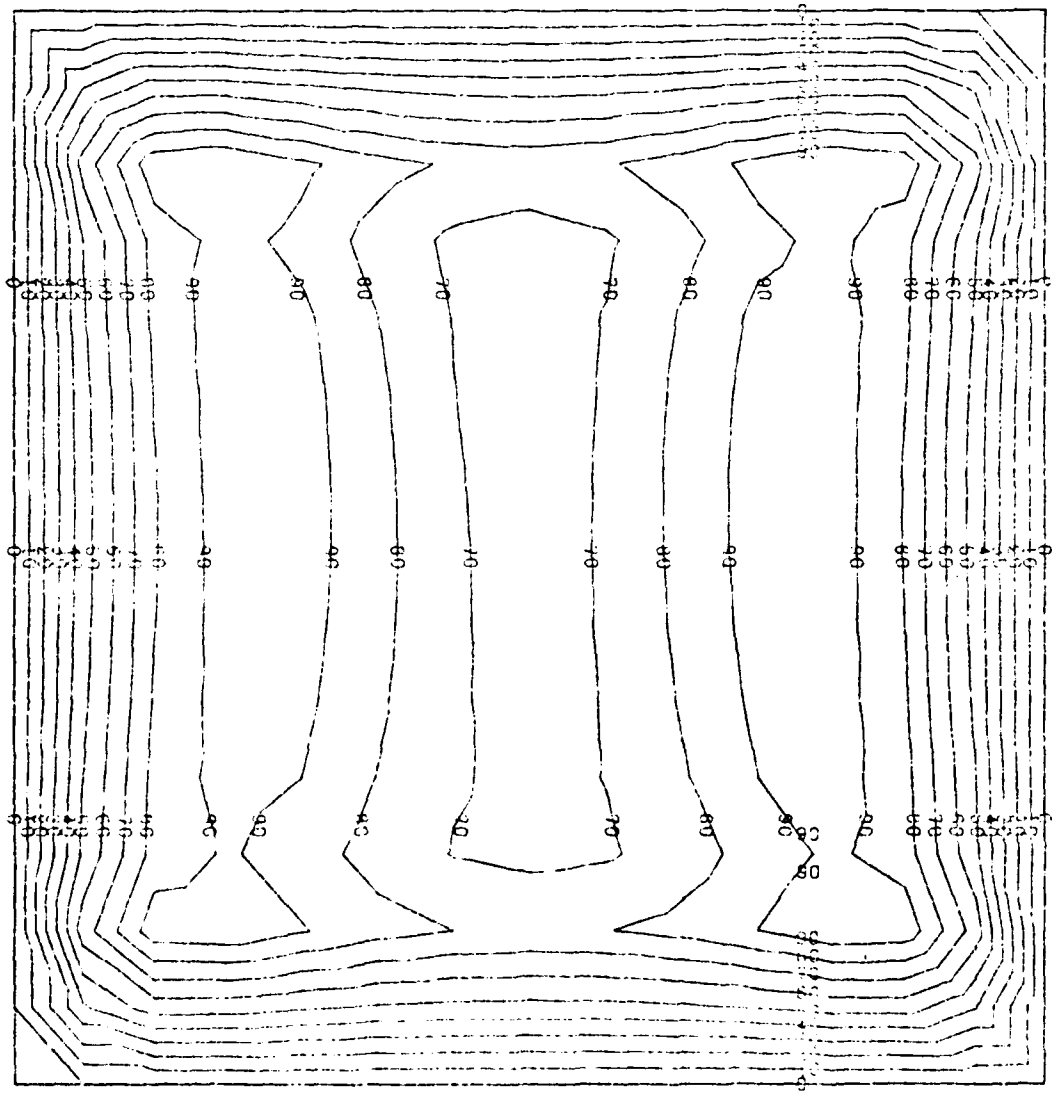

Figure 72. Case 140, W Displacement Component

CASE NO. 140
PLOT NO. 6, UNIT 1, STEP 0
DISPLACEMENT CONTOURS
RU COMPONENT

MODEL SCALE = .5000E+00. ORIENT. = 0.00. 0.00.
SOLUTION SCALE = .5662E+07

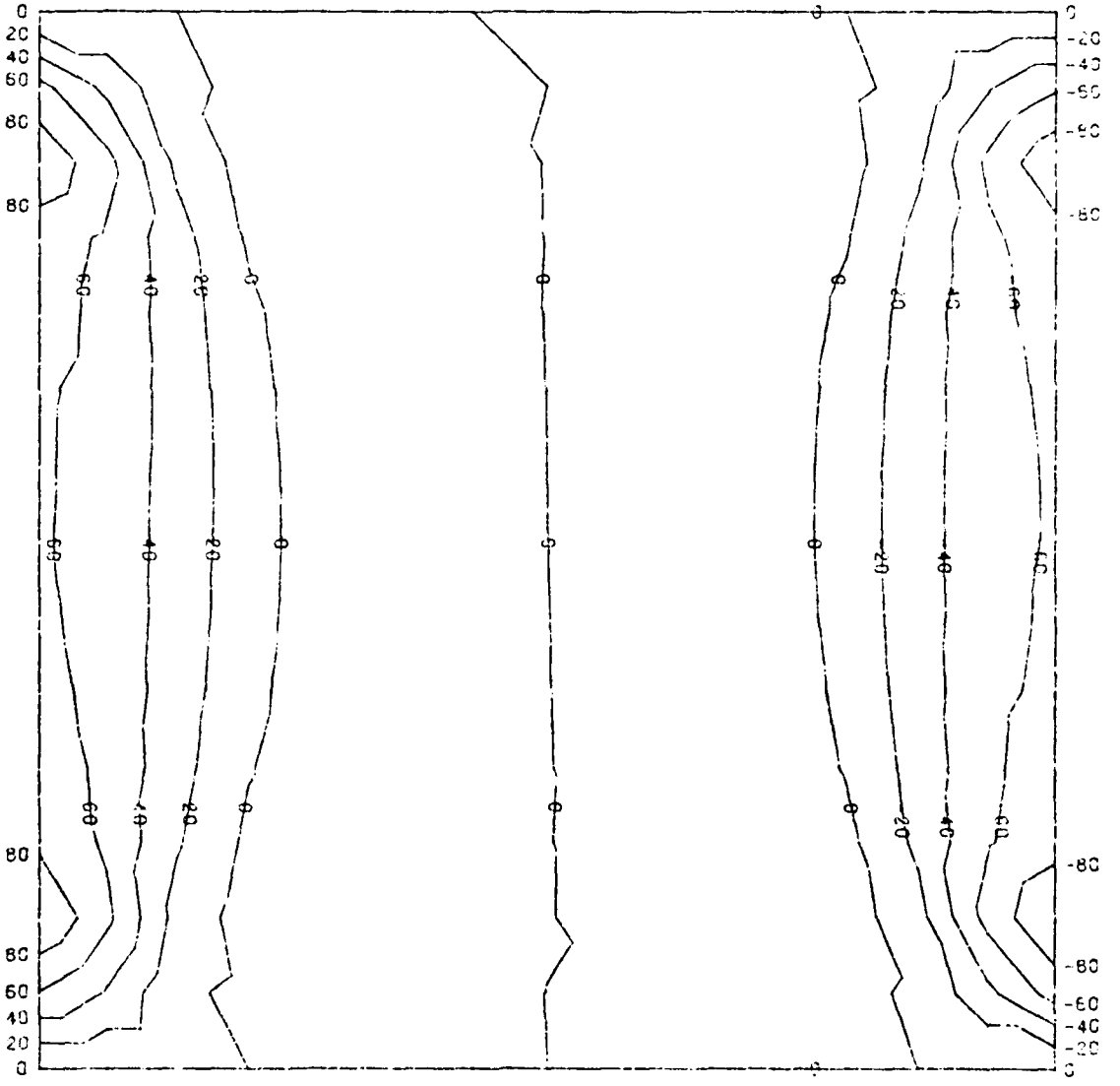

Figure 73. Case 140, RU Displacement Component

CASE NO. 140
PLOT NO. 7. UNIT 1. STEP 0
DISPLACEMENT CONTOURS
RV COMPONENT

MODEL SCALE = .5000E+00. ORIENT. = 0.00. 0.00.
SOLUTION SCALE = .4120E+07

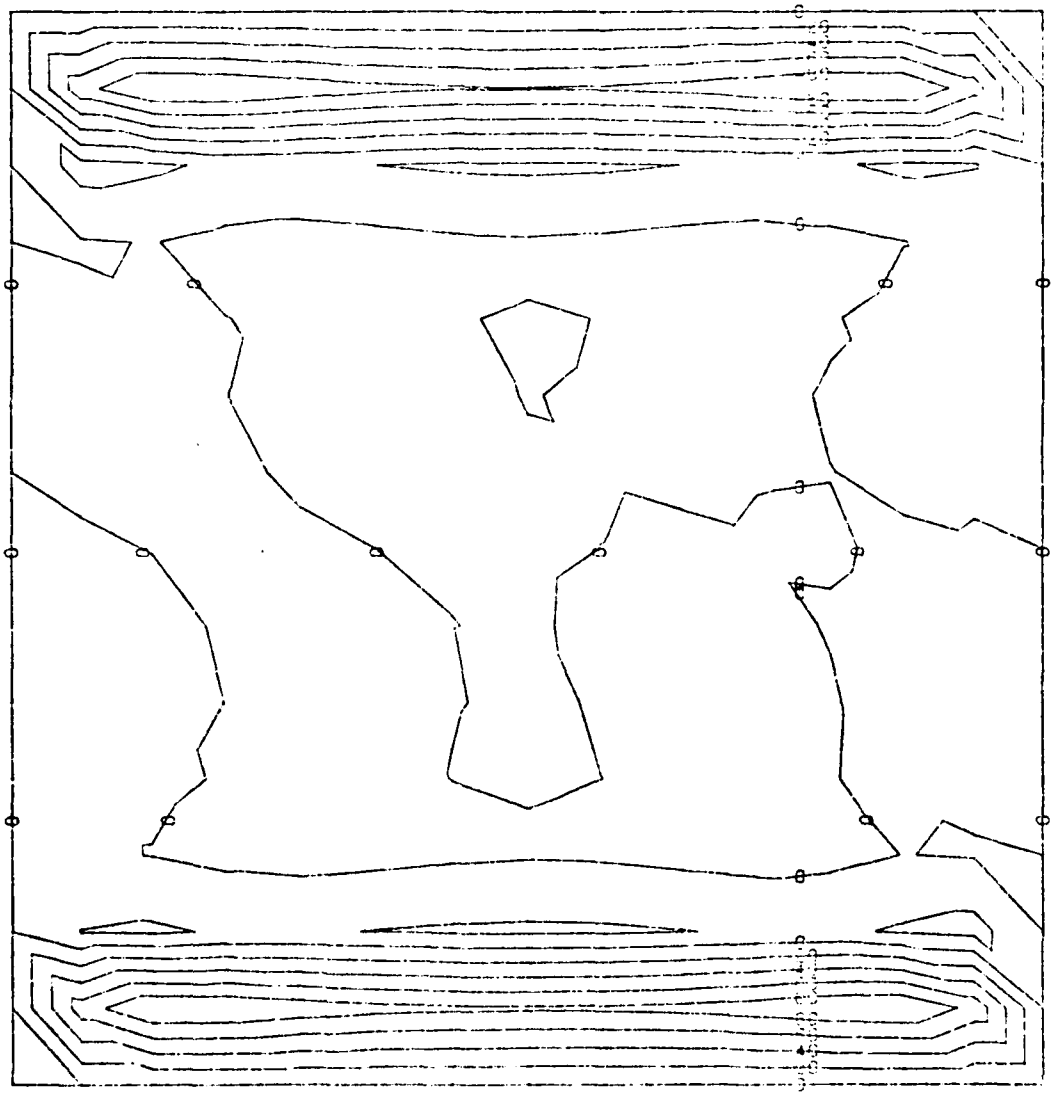

Figure 74. Case 140, RV Displacement Component

CASE NO. 160
PLOT NO. 1. UNIT 0. STEP 0
DISPLACEMENT GEOMETRY
UVW COMPONENT

MODEL SCALE = .5000E+00. ORIENT. = 0.00. 60.00.
SOLUTION SCALE = .1000E+04

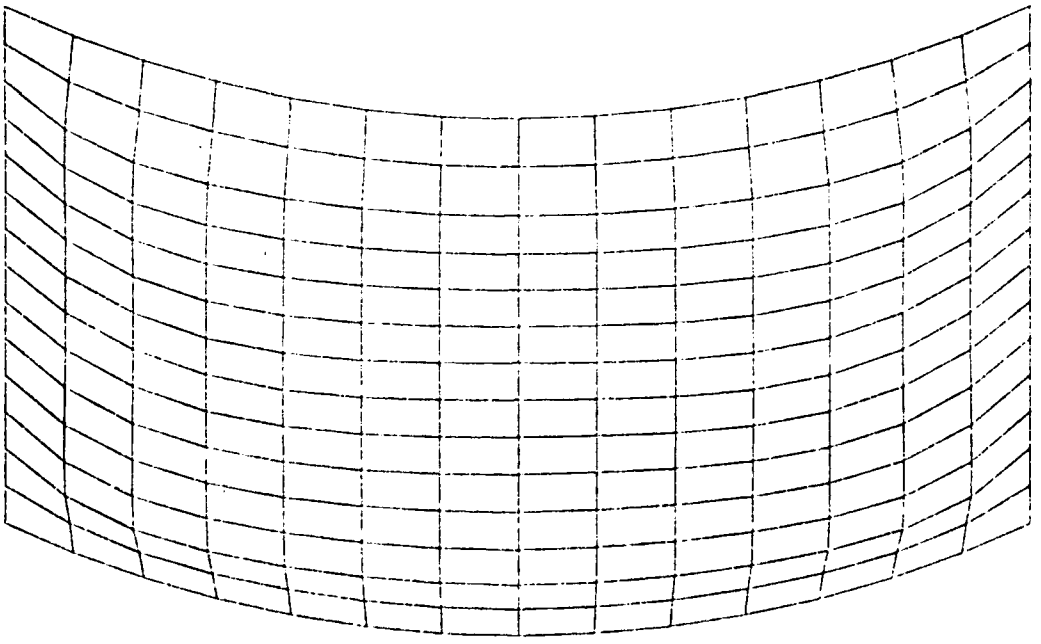

Figure 75. Case 160, UVW Displacement Component

CASE NO. 160
PLOT NO. 2, UNIT 0, STEP 0
EIGENVECTOR GEOMETRY
UVW COMPONENT , MODE 1
MODEL SCALE = .8000E+00, ORIENT. = 0.00, 30.00.
SOLUTION SCALE = .8000E+00

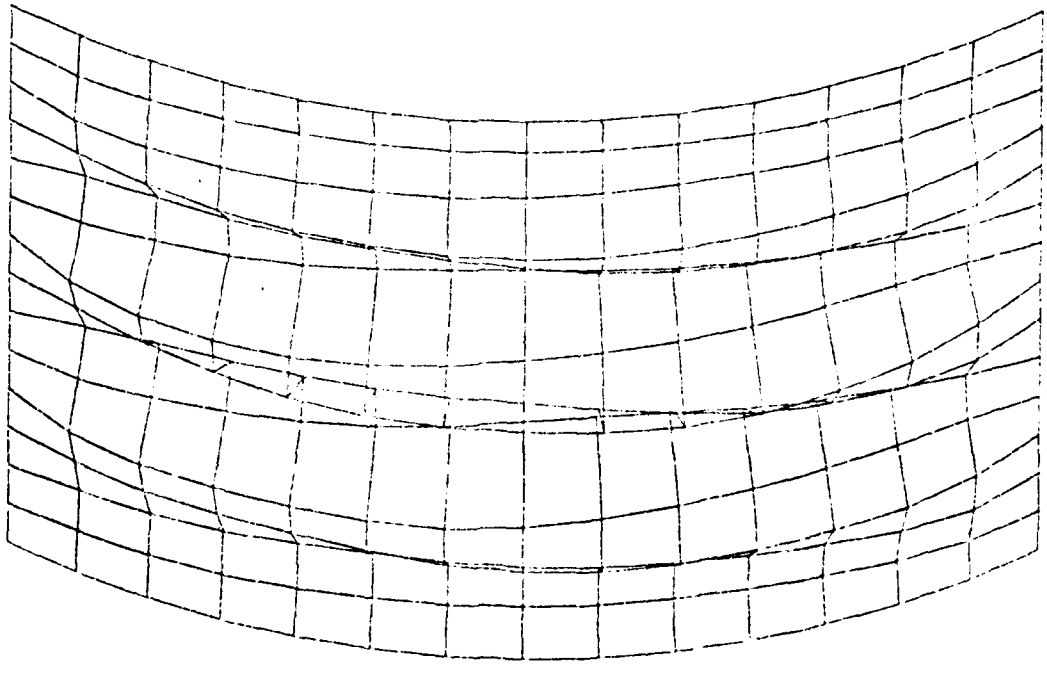

Figure 76. Case 160, UVW Eigenvector Component

CASE NO. 160.
PLOT NO. 3. UNIT 1. STEP 0
DISPLACEMENT CONTOURS
U COMPONENT

MODEL SCALE = .5000E+00. ORIENT. = 0.00, 0.00.
SOLUTION SCALE = .5504E+06

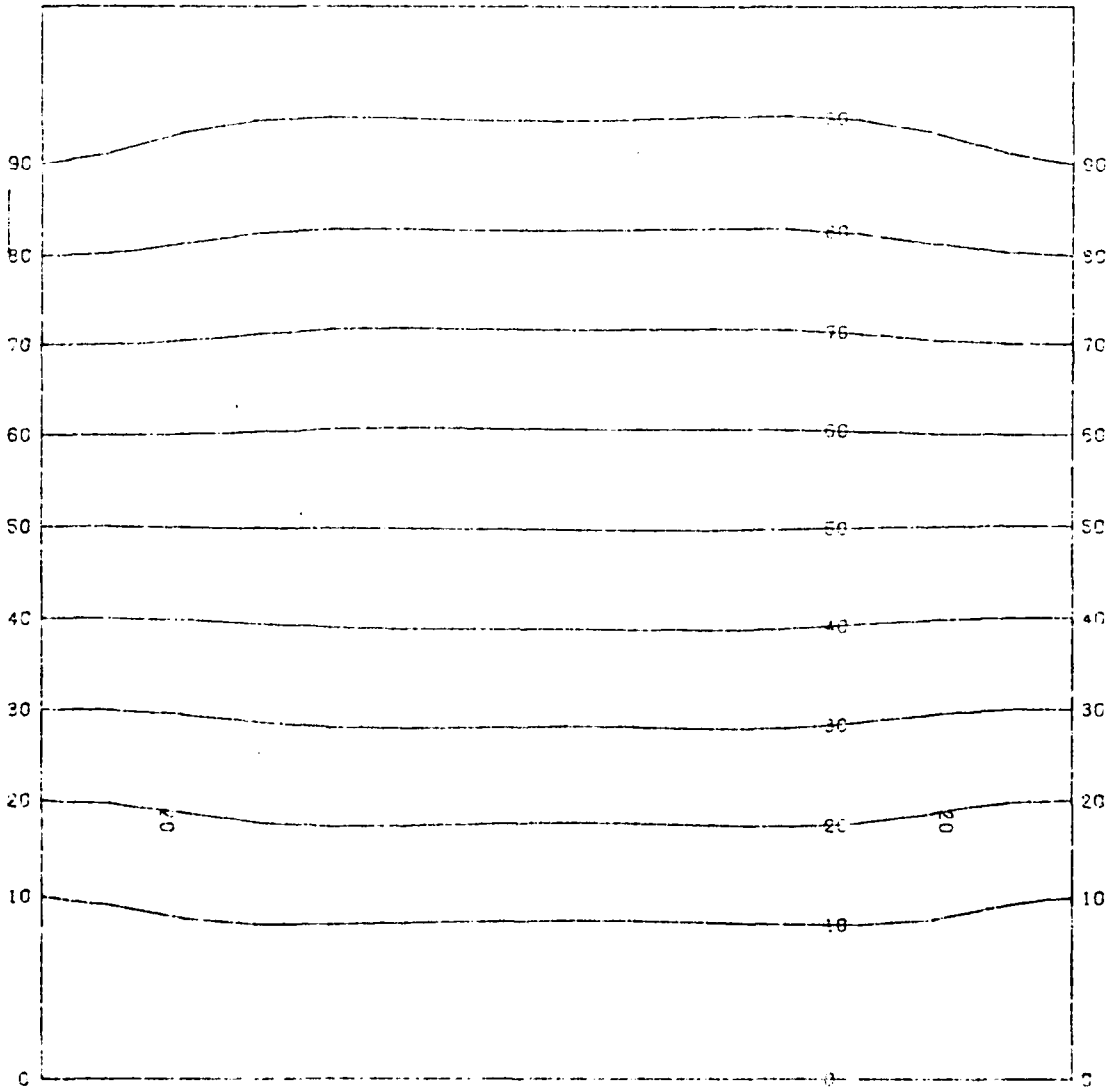

Figure 77. Case 160, U Displacement Component

CASE NO. 160
PLOT NO. 4. UNIT 1. STEP 0
DISPLACEMENT CONTOURS
V COMPONENT

MODEL SCALE = .5000E+00. ORIENT. = 0.00. 0.00.
SOLUTION SCALE = .1042E-08

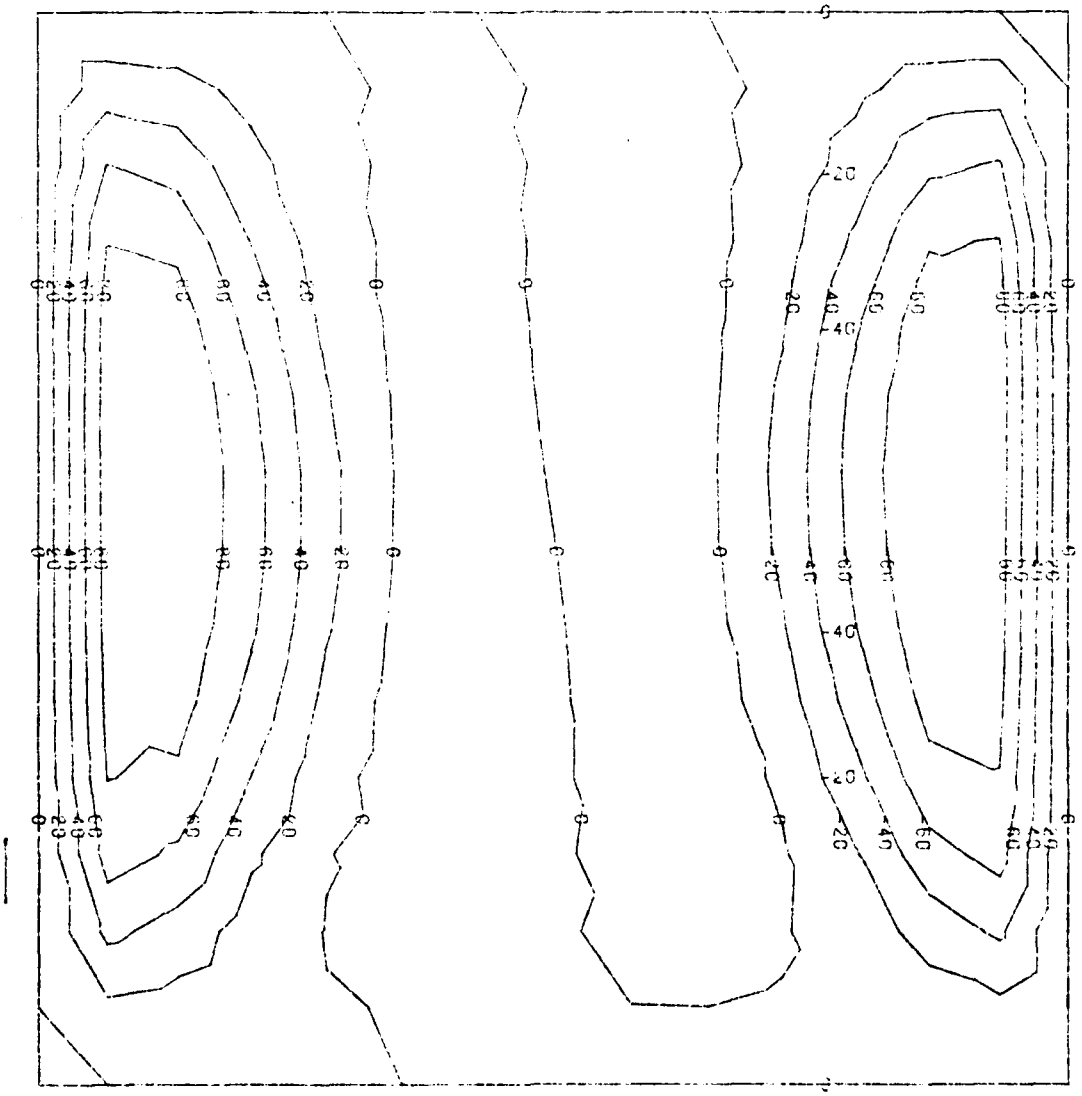

Figure 78. Case 160, V Displacement Component

CASE NO. 160
PLOT NO. 5. UNIT 1. STEP 0
DISPLACEMENT CONTOURS
W COMPONENT

MODEL SCALE = .50000E+00. ORIENT. = 0.00. 0.00
SOLUTION SCALE = .43000E+00

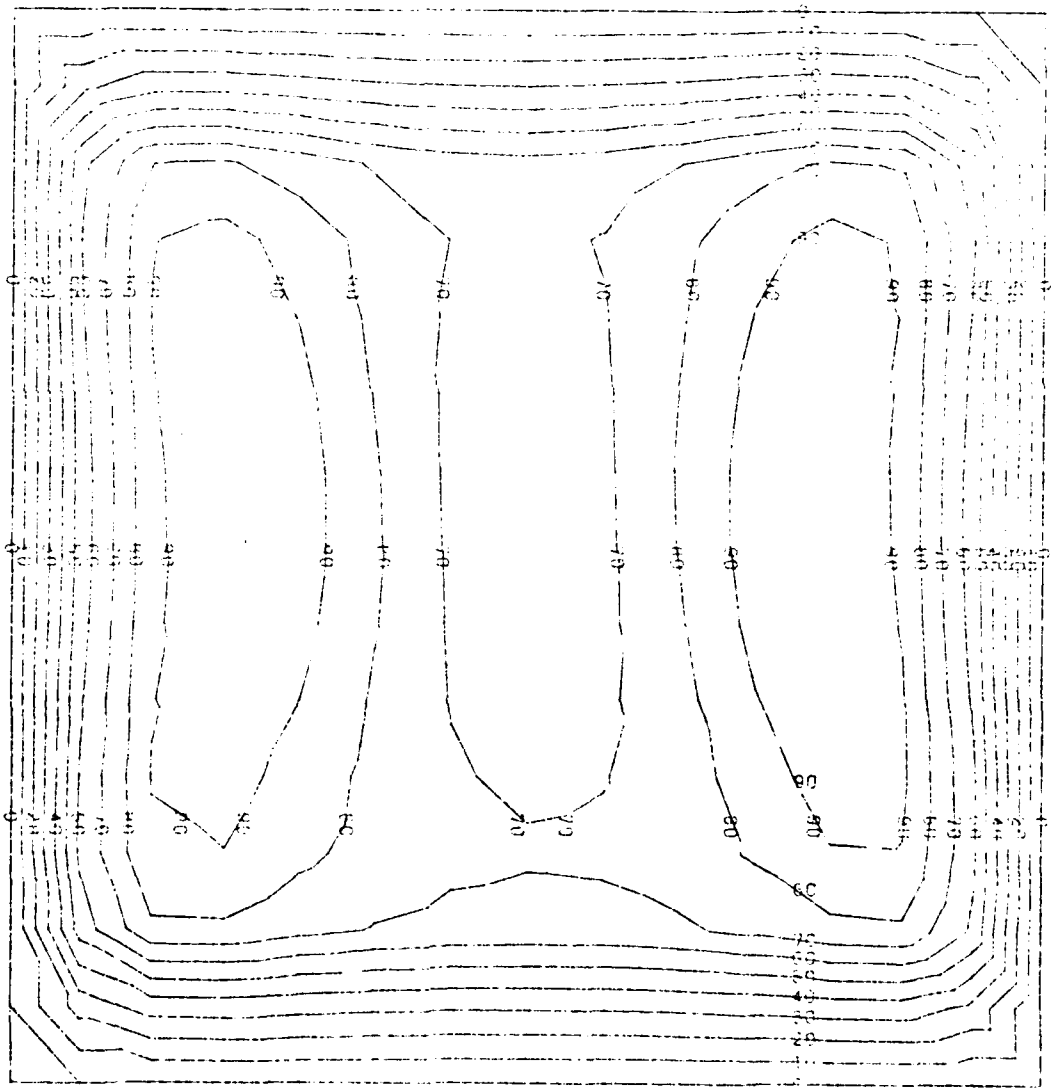

Figure 79. Case 160, W Displacement Component

CASE NO. 160
PLOT NO. 6. UNIT 1. STEP 0
DISPLACEMENT CONTOURS
RU COMPONENT

MODEL SCALE = .5000E+00. ORIENT. = 0.00. 0.00.
SOLUTION SCALE. = .4672E+06

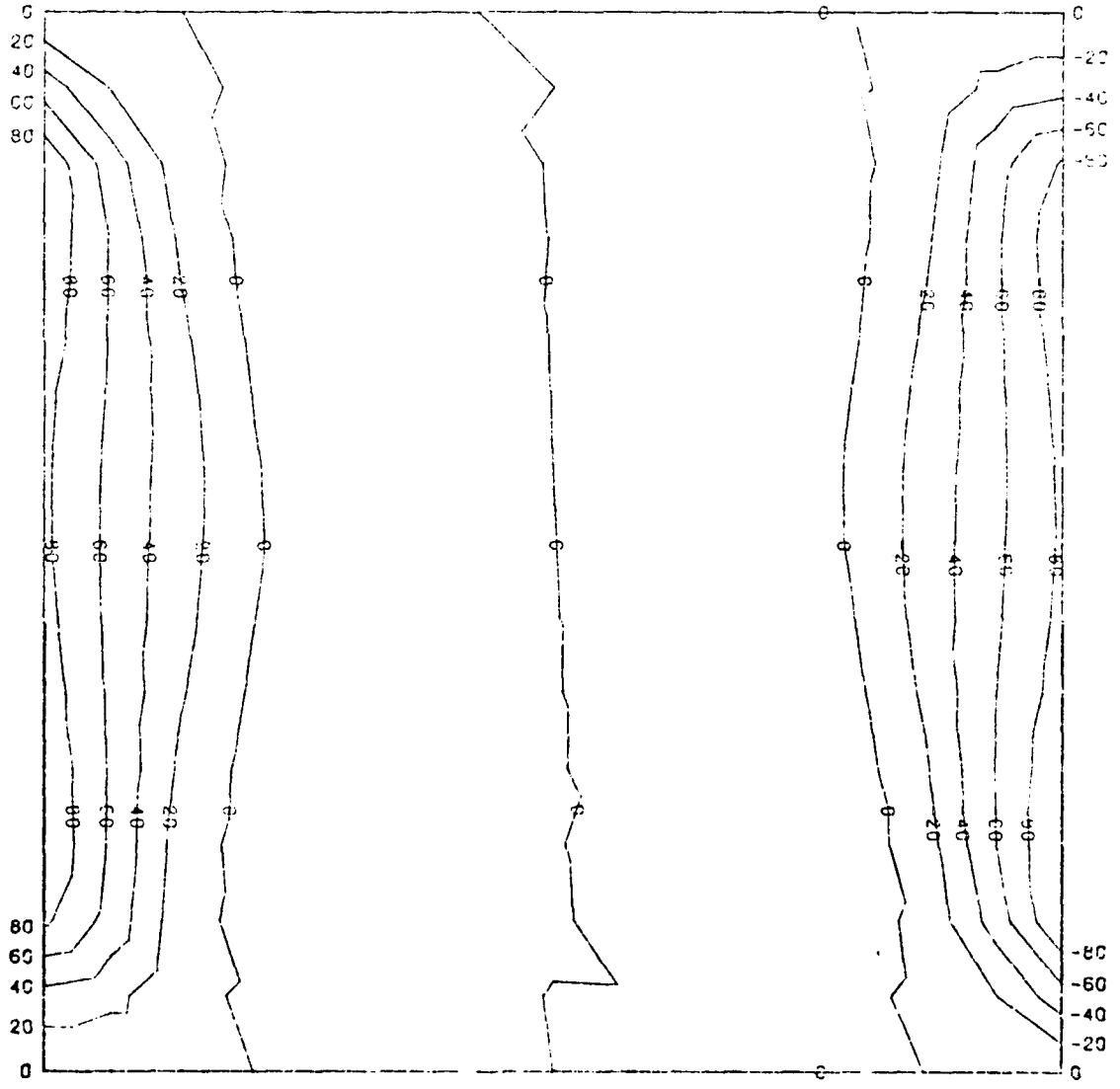

Figure 80. Case 160, RU Displacement Component

CASE NO. 160
PLOT NO. 7, UNIT 1, STEP 0
DISPLACEMENT CONTOURS
RV COMPONENT

MODEL SCALE = .5000E+00. ORIENT. = 0.00. 0.00.
SOLUTION SCALE = .5202E+06

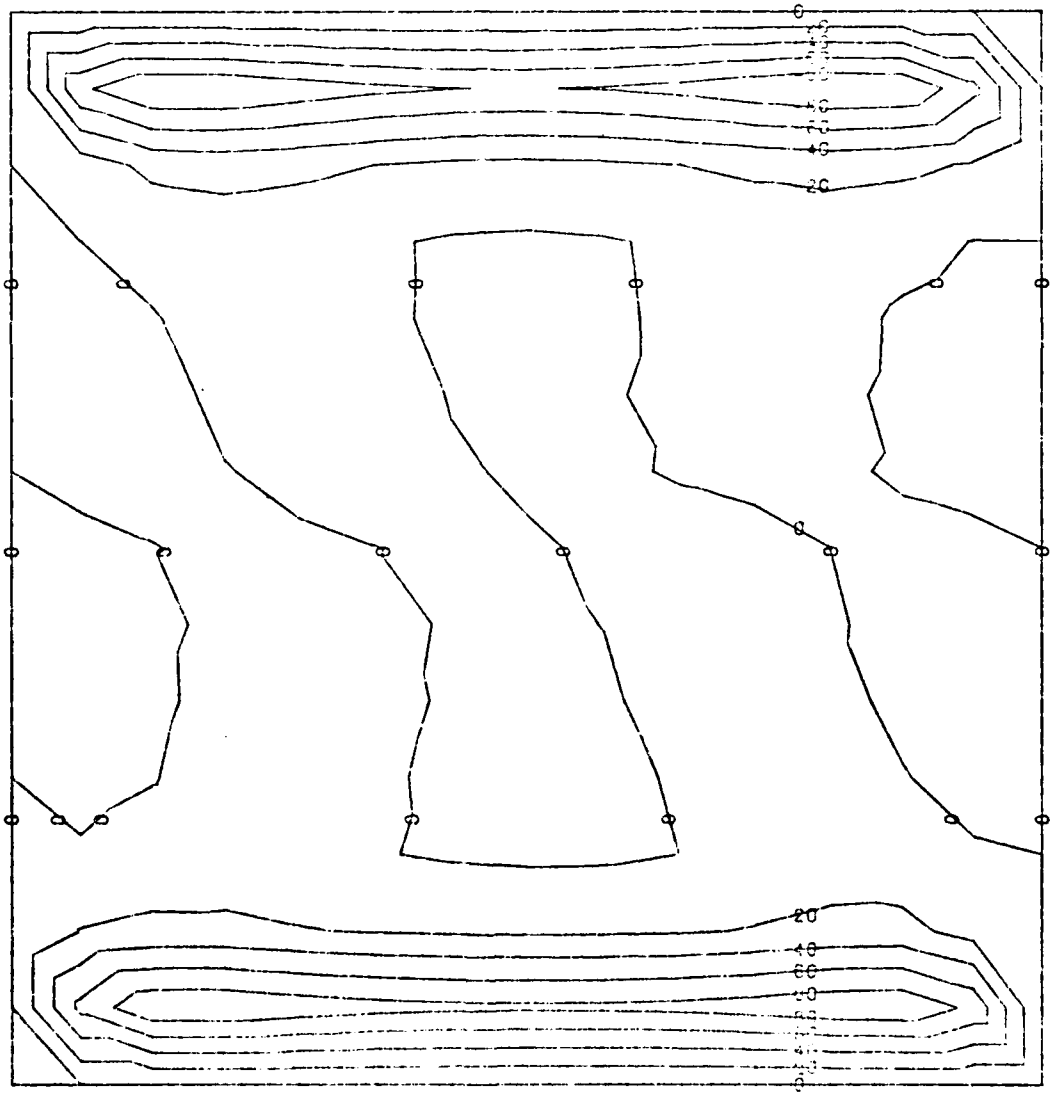

Figure 81. Case 160, RV Displacement Component

Appendix D

Comparisons of Calculated and Predicted Bifurcation Loads

Case No.	STAGS-C1 $\bar{N}_x$ Value	Predicted $\bar{N}_x$ Value	Percent Error
21	446.0	446.00	.00
22	445.1	445.69	.13
23	442.9	444.57	.38
24	440.9	441.48	.13
25	440.1	439.79	-.07
26	422.2	420.98	-.29
27	420.8	420.34	-.11
28	417.0	417.87	.21
29	412.9	411.15	-.42
30	410.6	407.33	-.80
31	412.0	410.24	-.43
32	409.0	408.82	-.04
33	400.5	403.43	.73
34	392.1	389.67	-.87
35	386.7	380.33	-1.65
36	410.5	408.68	-.44
37	406.8	406.75	-.01
38	395.4	399.17	.95
39	382.7	378.51	-1.09
40	375.3	366.56	-2.33
41	428.9	428.90	.00
42	428.6	428.79	.04
43	427.7	428.39	.16
44	426.7	427.30	.14
45	426.4	426.70	.07
46	408.4	404.65	-.92
47	407.8	403.89	-.96
48	406.1	400.70	-1.33
49	401.4	392.06	-2.33
50	397.7	386.81	-2.74
51	387.4	379.29	-2.09
52	386.3	377.54	-2.27
53	382.5	370.16	-3.22
54	371.4	350.23	-5.70
55	362.2	338.09	-6.66
56	381.7	372.58	-2.39
57	380.3	369.74	-2.78
58	375.0	357.63	-4.63
59	356.6	324.94	-8.88
60	340.4	304.86	-10.44

Case No.	STAGS-C1 $\bar{N}_x$ Value	Predicted $\bar{N}_x$ Value	Percent Error
101	502.80	502.80	.00
102	502.20	502.54	.07
103	500.50	501.61	.22
104	498.50	499.03	.11
105	497.60	497.62	.00
106	481.20	480.49	-.15
107	480.00	479.90	-.02
108	476.60	477.63	.22
109	472.40	471.43	-.20
110	470.30	467.89	-.51
111	470.30	469.52	-.17
112	467.80	468.22	.09
113	460.30	463.21	.63
114	451.00	449.53	-.33
115	446.30	441.71	-1.03
116	468.50	467.65	-.18
117	465.20	465.83	.14
118	455.00	458.63	.80
119	441.70	439.03	-.60
120	434.60	427.58	-1.61
121	444.10	444.10	.00
122	443.30	443.79	.11
123	441.20	442.68	.33
124	439.20	439.61	.09
125	438.40	437.92	-.11
126	420.60	419.16	-.34
127	419.30	418.51	-.19
128	415.50	416.06	.13
129	411.50	409.34	-.52
130	409.20	405.54	-.90
131	410.50	408.40	-.51
132	407.70	406.99	-.18
133	399.00	401.60	.65
134	389.90	386.87	-.78
135	385.00	378.54	-1.68
136	409.00	406.83	-.53
137	405.50	404.90	-.15
138	393.80	397.33	.90
139	380.90	376.69	-1.11
140	373.50	364.74	-2.34

Case No.	STAGS-C1 $\bar{N}_x$ Value	Predicted $\bar{N}_x$ Value	Percent Error
141	421.6	421.60	.00
142	421.3	421.50	.05
143	420.5	421.11	.15
144	419.6	420.06	.11
145	419.2	419.48	.07
146	401.0	397.32	-.92
147	400.5	396.55	-.99
148	398.6	393.34	-1.32
149	393.6	384.65	-2.27
150	389.8	379.36	-2.68
151	379.7	371.62	-2.13
152	378.5	369.86	-2.28
153	374.3	362.43	-3.17
154	362.3	342.35	-5.51
155	352.9	330.11	-6.46
156	373.9	364.80	-2.44
157	372.3	361.93	-2.79
158	366.0	349.70	-4.45
159	345.8	316.71	-8.41
160	328.9	296.44	-9.87
401	514.80	514.80	.00
402	513.80	514.28	.09
403	511.00	512.39	.27
404	507.80	507.72	-.02
405	506.80	506.33	-.09
406	493.30	492.23	-.22
407	490.80	491.04	.05
408	482.90	486.45	.73
409	474.50	474.78	.06
410	471.40	470.05	-.29
411	482.30	481.10	-.25
412	476.60	478.47	.39
413	458.70	468.32	2.10
414	439.80	442.58	.63
415	432.60	432.28	-.07
416	480.40	479.19	-.25
417	472.30	475.51	.68
418	445.90	460.91	3.37
419	417.10	423.34	1.50
420	405.00	406.15	.28

Case No.	STAGS-C1 $\bar{N}_x$ Value	Predicted $\bar{N}_x$ Value	Percent Error
421	445.90	445.90	.00
422	444.30	445.29	.22
423	440.30	443.04	.62
424	437.30	437.49	.04
425	436.30	435.85	-.10
426	422.10	420.89	-.29
427	419.40	419.59	.05
428	411.40	414.67	.80
429	403.00	402.26	-.18
430	399.70	397.56	-.54
431	411.90	410.15	-.42
432	406.00	407.31	.32
433	387.80	396.52	2.25
434	369.00	369.36	.10
435	361.20	359.25	-.54
436	410.50	408.59	-.46
437	403.00	404.72	.43
438	378.00	389.56	3.06
439	349.60	350.80	.34
440	336.60	334.04	-.76
441	428.90	428.90	.00
442	428.40	428.68	.07
443	427.20	427.89	.16
444	425.80	425.93	.03
445	425.40	425.34	-.01
446	408.40	404.65	-.92
447	406.50	403.13	-.83
448	399.70	396.74	-.74
449	386.80	379.84	-1.80
450	379.50	370.37	-2.41
451	387.40	379.29	-2.09
452	383.10	375.79	-1.91
453	367.30	361.04	-1.71
454	335.20	321.99	-3.94
455	316.00	300.05	-5.05
456	381.70	372.58	-2.39
457	375.10	366.90	-2.19
458	349.10	342.67	-1.84
459	290.70	278.19	-4.30
460	245.70	240.57	-2.09

Case No.	STAGS-C1 $\bar{N}$ Value x	Predicted $\bar{N}$ Value x	Percent Error
601	290.80	290.80	.00
602	290.50	290.65	.05
603	289.60	290.12	.18
604	288.50	288.65	.05
605	288.10	287.84	-.09
606	279.30	278.05	-.45
607	278.70	277.72	-.35
608	276.80	276.42	-.14
609	274.50	272.87	-.59
610	273.40	270.85	-.93
611	273.50	271.76	-.63
612	272.10	271.02	-.40
613	268.00	268.15	.06
614	262.90	260.33	-.98
615	260.40	255.85	-1.75
616	272.50	270.69	-.67
617	270.70	269.65	-.39
618	265.00	265.52	.20
619	257.70	254.31	-1.32
620	254.00	247.75	-2.46
701	170.30	170.30	.00
702	170.20	170.21	.01
703	169.70	169.90	.12
704	169.10	169.04	-.03
705	168.90	168.57	-.20
706	164.50	162.84	-1.01
707	164.20	162.64	-.95
708	163.20	161.88	-.81
709	162.00	159.80	-1.36
710	161.40	158.61	-1.73
711	161.50	159.15	-1.45
712	160.80	158.72	-1.30
713	158.60	157.04	-.99
714	156.00	152.45	-2.27
715	154.70	149.83	-3.15
716	160.90	158.52	-1.48
717	160.00	157.91	-1.31
718	157.10	155.50	-1.02
719	153.30	148.93	-2.85
720	151.40	145.09	-4.17

Vita

James M. Snead was born on 14 July 1951 in Dayton, Ohio. He attended high school at Fairmont West High School in Kettering, Ohio. After graduating from high school, he attended the University of Cincinnati, graduating with a Bachelor of Science degree in Aerospace Engineering in 1974. Upon graduation, he returned to full time employment with the U.S. Air Force at Wright-Patterson AFB, Ohio. He had previously co-oped with the Air Force at Wright-Patterson. He works in the Aeronautical Systems Division, Deputy for Engineering, Directorate of Flight Systems Engineering. In 1980, he was accepted into the Graduate Aeronautical Engineering Program at the AFIT School of Engineering.

UNCLASSIFIED

SECURITY CLASSIFICATION OF THIS PAGE (When Data Entered)

REPORT DOCUMENTATION PAGE		READ INSTRUCTIONS BEFORE COMPLETING FORM
1. REPORT NUMBER AFIT/GAE/AA/81D-29	2. GOVT ACCESSION NO. AD-A111 127	3. RECIPIENT'S CATALOG NUMBER
4. TITLE (and Subtitle) MOISTURE AND TEMPERATURE EFFECTS ON THE INSTABILITY OF CYLINDRICAL COMPOSITE PANELS		5. TYPE OF REPORT & PERIOD COVERED MS THESIS 6. PERFORMING ORG. REPORT NUMBER
7. AUTHOR(s) James M. Snead		8. CONTRACT OR GRANT NUMBER(s)
9. PERFORMING ORGANIZATION NAME AND ADDRESS Air Force Institute of Technology (AFIT/EN) Wright-Patterson AFB, Ohio 45433		10. PROGRAM ELEMENT, PROJECT, TASK AREA & WORK UNIT NUMBERS
11. CONTROLLING OFFICE NAME AND ADDRESS		12. REPORT DATE December 1981 13. NUMBER OF PAGES 155
14. MONITORING AGENCY NAME & ADDRESS(if different from Controlling Office)		15. SECURITY CLASS. (of this report) Unclassified 15a. DECLASSIFICATION/DOWNGRADING SCHEDULE

16. DISTRIBUTION STATEMENT (of this Report)

Approved for public release; distribution unlimited.

17. DISTRIBUTION STATEMENT (of the abstract entered in Block 20, if different from Report)

28 JAN 1982

18. SUPPLEMENTARY NOTES

Approved for public release; IAW AFR 190-17
Frederic C. Lynch
Major, USAF
Director of Public Affairs

19. KEY WORDS (Continue on reverse side if necessary and identify by block number)

Moisture
Temperature
Bifurcation Analysis
Laminated Composite Panels
Axial Compression
Hygrothermal Effects
Instability Analysis

20. ABSTRACT (Continue on reverse side if necessary and identify by block number)

An analytical investigation was performed to evaluate the influences of moisture and temperature on the bifurcation load of cylindrical, composite panels subject to axial loading. The composite panels were 8-ply graphite/epoxy (AS/3501-5) laminates. The laminate ply orientations considered were $(0.,45.,-45.,90.)_S$, $(90.,45.,-45.,0.)_S$, and $(45.,-45.)_{2S}$. The analysis included several different panel radii, two sets of boundary conditions, and three sets of initial moisture conditions. To evaluate the influences of moisture and temperature, the

DD FORM 1 JAN 73 1473 EDITION OF 1 NOV 65 IS OBSOLETE

UNCLASSIFIED

SECURITY CLASSIFICATION OF THIS PAGE (When Data Entered)

transverse moduli, E_2, and shear moduli, G_{12}, were degraded based on test data for the AS/3501-5 system. Each ply orientation was evaluated at 20 time/temperature conditions that ranged from 80 F to 300 F and moisture concentrations ranging from zero moisture content to an equilibrium moisture concentration distribution. The bifurcation loads were determined using the STAGS-C1 finite element shell analysis program. The bifurcation analysis mode with a pre-buckled linear displacement option was used for the analysis. Moisture and temperature were found to cause a reduction in the panels' bifurcation load ranging from 20.6 percent for the $(0.,45.,-45.,90.)_S$ laminate to 42.7 percent for the $(45.,-45.)_{2S}$ laminate.

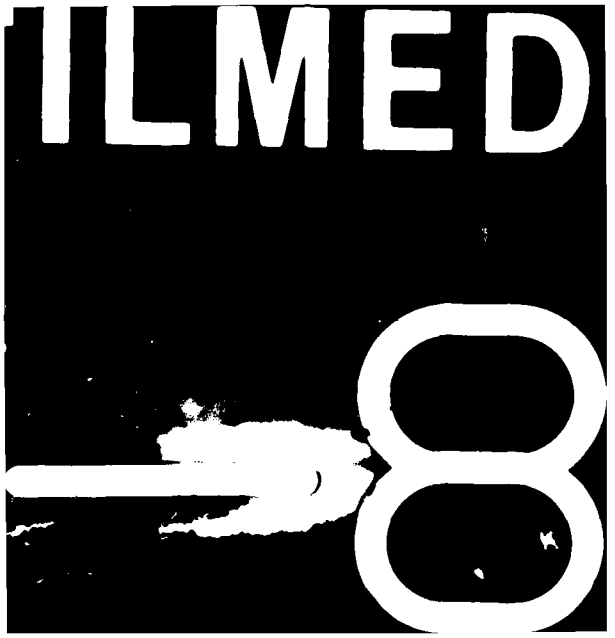
ILMED
8